Development and Application of Metabolomics Techniques to Improve Understanding of Glucose and Fatty Acid Metabolism in β-cells and their Role in Insulin Secretion.

By

Mahmoud El Azzouny

A dissertation submitted in partial fulfillment
of the requirements for the degree of
Doctor of Philosophy
(Chemistry)
In The University of Michigan
2014

Doctoral Committee:

Professor Robert T. Kennedy, Chair
Professor Charles F. Burant
Professor Kristina I. Håkansson
Assistant Professor: Brandon T. Ruotolo

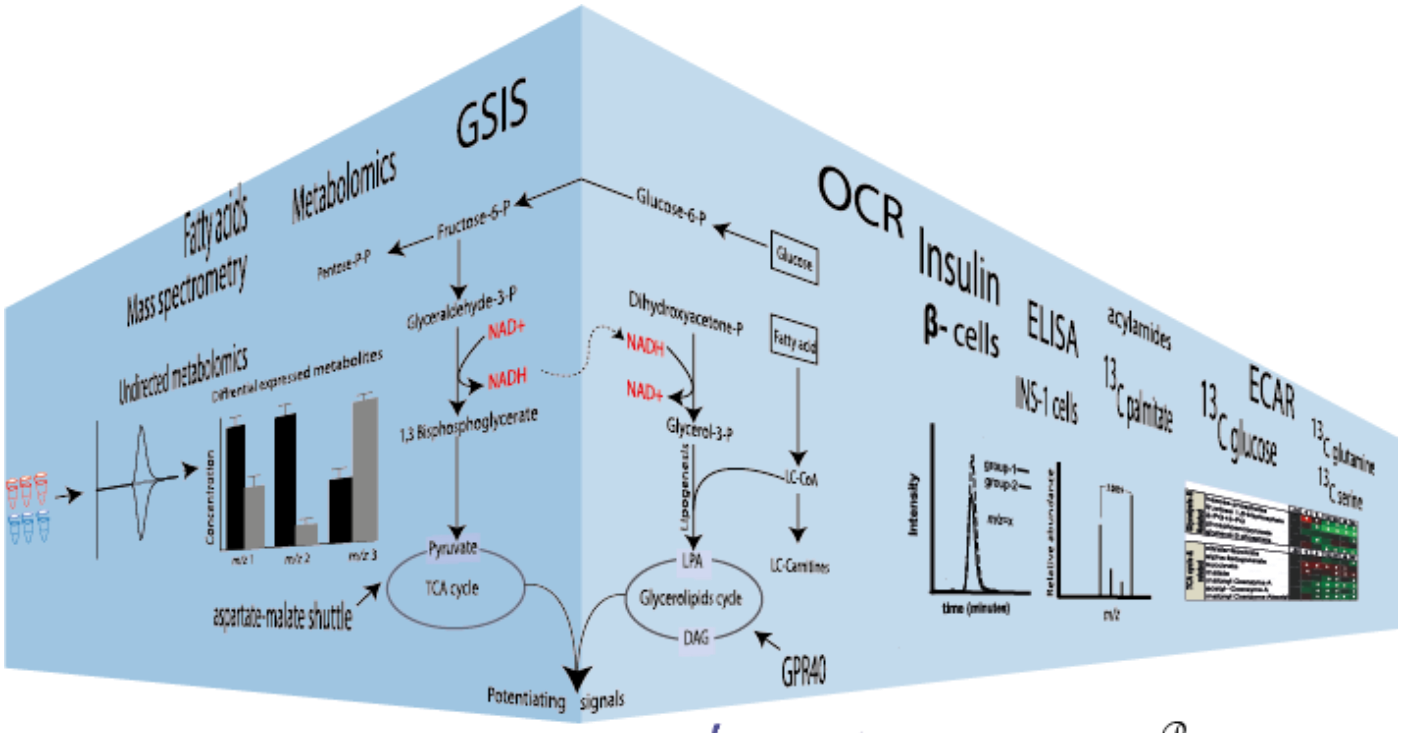

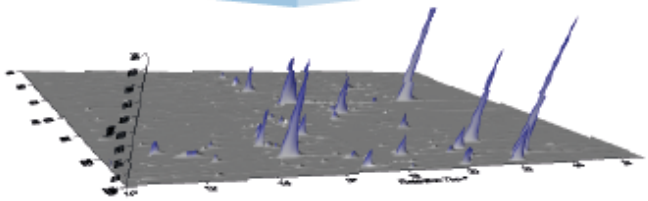

By:
Mahmoud Ahmed ElAzzouny

2014

DEDICATION

To my parents, my wife and my children

ACKNOWLEDGEMENTS

All gratitude goes to Allah for guiding me throughout my life; He is the best guardian, the Most Gracious and the Most Merciful.

Acknowledgments are cumulative, plenty of people helped me to reach the step of "writing my doctoral thesis". Their help was a must to reach this step and their help will never be forgotten.

Being raised and educated in Egypt, I did not have the chance to be involved in world class research or attend a highly ranked University. Netherlands was the first country who trusted my capabilities and offered me a complete scholarship to study in its best University (Utrecht University). Thus, I would like to thank the NUFFIC for their generous scholarship and Dr. Ed Moret for accepting me in Utrecht master's program and for writing me the support letter for the scholarship.

I would like to thank Dr. Reinout Raijmakers , Prof. Albert Heck, Prof. Ad deJong, Dr. Maarten Honing, and Dr. Martin Jaeger for joining their groups in Utrecht and Merck and for teaching me the state-of-the-art mass spectrometry approaches that changed my life. I was involved in world class research that motivated me to continue in this field and seek more knowledge. The experience I got from the Dutch groups and their letters of recommendation was a must to move one step higher and to be accepted in the PhD program in one of the best US universities (University of Michigan).

At the University of Michigan, I would like to deeply thank my PhD adviser, Prof. Robert Kennedy (Bob). I knew that he will be my adviser when I was still applying to the graduate school, I do not know how, but it happened! He accepted me in this famous lab and offered me a perfect project that was suitable to my background and my goals. He was very patient with my weird suggestions and my bad writing. He always spent time replying to our weekly progress reports. His comments and suggestions did shape my way of thinking and accelerated my progress.

Bob allowed me to work away from him, in the lab of his collaborator, Prof. Charles Burant. I would like to thank both of them for allowing me to act as a linkage between them and for allowing this collaboration to go smoothly.

I would like to thank Prof. Charles Burant (Chuck), for working in his lab and for his continuous encouragement and for his valuable time that he offered me during my stay in his

lab. Chuck being a physician, I was fascinated with the surplus of ideas that he was suggesting and the huge number of projects that he wanted to explore. I'm also indebted to the warm family environment that I felt and still feeling in his lab. Part of it was also because of Mary (Chuck's wife), who was helping us in our experiments and facilitating our research. I'm greatly thankful for this family.

A crucial advisor in my PhD work was Charles Evans, who was my continuous guide in mass spectrometry, biology, scientific writing and etiquette! He was kind enough to help me in many things without showing his discomfort. I highly appreciate his friendship and his help.

In both labs, there are many people whom I would like to thank, like Sydney Bridges, Angela Subauste, Kathrin Overmyer, Arun Das, Chunhai Ruan, Heidi Iglay-Reger, Stephen Brown, Eric Guetschow, Cynthia Cipolla, Shi Jin and Shusheng.

I would like to deeply thank Dr. Brandon Ruotolo and Prof. Kristina Hakansson for being on my committee, for their time listening to my presentations, and reading my research plans and dissertation. Their help, comments and suggestions were a must to finish my PhD. I would like to thank Dr. Ruotolo for also being my mentor during teaching CHEM 241. He was very accommodating to my special requests and vacations, especially during the delivery of my second son.

Those people helped me, but there is my family which was the continuous light for me throughout my PhD. I would like to thank my wife Somaia for creating and maintaining this warm family atmosphere. She took care of most things to keep me focused on my work. She took care of our children at home and carried the responsibility of their education. She sacrificed her ambitions to pursue further degree in order to raise her children in the appropriate way.

I would like to thank my children, Nour Eldin and Saif Eldin, whose smiles were enough to relieve any pain and acted as magic that encouraged me to work harder and harder.

Finally, I would like to thank my parents, my mother and father who sacrificed everything in their lives to help me, my brother and sister. Although they are old and need my help, they encouraged me to stay abroad and get higher degrees to have a better life than theirs. Their daily Skype call was of utmost importance for me, keeping me more focused and more determined.

Table of contents

LIST OF FIGURES

Chapter 1. GENERAL INTRODUCTION

SYSTEM'S BIOLOGY AND THE "OMICS"

The last two decades have witnessed a new era of research established after huge technological developments pertaining to the biological sciences. These technological developments include mass spectrometry, arrays technologies and high-throughput sequencing analysis. These advances in technology opened the way for improved understanding of complex diseases and development of new therapies and diagnostics. The outcome of the technological improvements was the capability to study large quantities of genes, RNA, proteins or metabolites simultaneously. The advent of these methods added new terminology to the field of science, including genomics (first described in 1986), proteomics (1995), metabolomics (1998) (1, 2) as well as other "omics" like transcriptomics. Genomics, transcriptomics, proteomics and metabolomics simply refer to the study of the complete set of cellular DNA, RNA, proteins and small molecules (metabolites) ,respectively. Judicious use of several or all of these techniques simultaneously enables improved understanding of the complete operation of any living system, which could be an organism, tissue, cell or even part of a cell. This broad-scope study of living entities is simply termed "systems biology" (3) (Figure 1-1).

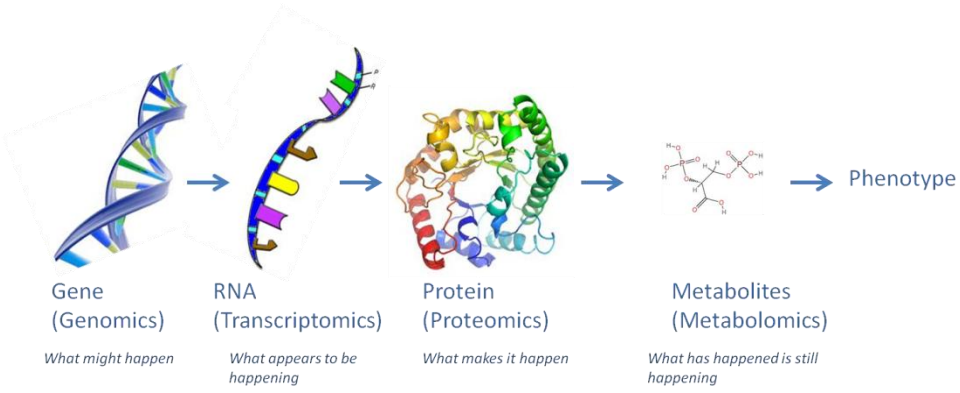

Figure 1-1: The "omics" cascade

METABOLOMICS

As shown in figure 1, metabolomics is the final step in the "omics" cascade, and the closest to the phenotype (4). Being the nearest to the phenotype, gives metabolomics the advantage of serving as a direct signature of biochemical activity and being described as "the apogee of omics" (5). Tools for comprehensive metabolomics analysis are still emerging and publications containing the word "metabolomics" have increased exponentially over the last 10 years (Figure 1-2), but still in its infancy compared to other "omics" such as "proteomics". The metabolome encompasses a large number of metabolites. The number of known metabolites in human serum is estimated to be approximately 4000 (6), which jump to approximately 40,000 metabolites when exogenous metabolites from food, drugs and the microbiome are included (7). The chemical diversity of the metabolome leads to the conclusion that, unlike genomics or proteomics, no single instrumental platform is able to analyze the entire metabolome (4).

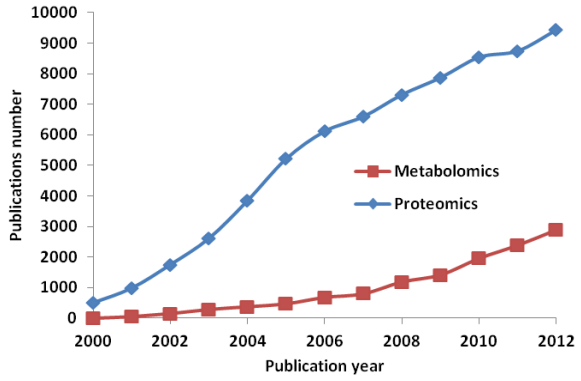

Figure 1-2: The frequency of metabolomics and proteomics term in literature. Bibliographic search using SciFinder using the term metabolomics or proteomics.

METABOLOMICS PLATFORMS

The challenge in profiling cellular metabolome is not limited to the large number of metabolites but also involves the great heterogeneity in chemical properties and abundance of those metabolites. The fact that these metabolites are only one part of a biological sample, which also contains other components such as DNA and protein, further increases the

complexity of the analysis. The most common platforms for metabolomic profiling and quantitation are nuclear magnetic resonance (NMR) and mass spectrometry (MS) instruments.

NMR-based metabolomics platform

Application of NMR in metabolomics is very useful as it can provide a "holistic view" for metabolites in a complex sample. It has many advantages, such as being non-destructive, so a sample can be re-used or re-measured several times. It provides detailed structural information that can help identifying unknown metabolites. It does not depend on analyte polarity and requires minimal sample preparation such as separation or derivatization (8, 9). NMR is good for metabolite quantitation, providing reproducible correspondence between signal intensity and metabolite concentration. Different nuclei can be used in NMR; the proton is the most widely used nucleus due to its high abundance and resulting in higher sensitivity. Other nuclei like ^{31}P and ^{13}C can be used for phosphorus-containing compounds and flux analysis, respectively (10). The main disadvantage of NMR in metabolomics is its relatively low sensitivity, rendering it non-suitable for low-abundance metabolites (9). Another drawback of NMR-based metabolomics is the challenge of identification of individual compounds in a complex mixture because of signal overlap (4). To reduce sample complexity, a prior sample separation can improve NMR identification but will further reduce the technique sensitivity as mentioned in the next sections.

MS based metabolomics:

MS is typically more sensitive than NMR, with the lower limit of detection in the femtomole range for most metabolites compared to the low nanomole range for NMR (11). However, unlike NMR, MS is a destructive technique, where the sample is usually lost after analysis and can't be reused. MS can measure several hundred of metabolites with various properties and concentrations simultaneously, as compared to NMR which typically detects high tens to just over 100 metabolites (9). MS can be used as a standalone platform by directly injecting the sample into the mass spectrometer or can be coupled to a separation technique. While direct sample analyses by mass spectrometer provides the shortest analysis time and a large range of metabolites can be covered (12), it has many disadvantages. Among these disadvantages is the competition of ionization between different molecules, which leads to an

ionization suppression of less efficiently ionized molecules by other highly ionized ones. Another disadvantage is the lack of a separation dimension, which often provides an additional confirmation of a metabolites' identity. Therefore, a typical MS-based metabolomics platform consists of a separation technique, a mass spectrometer and data analysis tools (Figure 1-3). Mass spectrometers vary in ionization and detection capability, which further affects metabolome analysis. These considerations are briefly discussed in the next section.

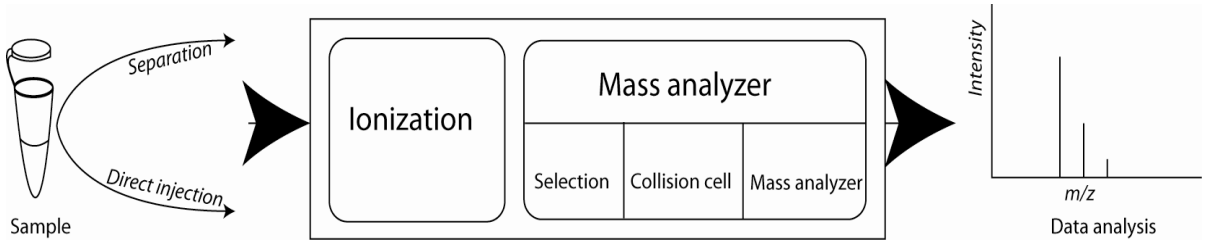

Figure 1-3: Work flow for a typical MS platform for metabolomics.

Ionization

In order for molecules to be analyzed by MS, they must be presented as ions in the gas phase. Several ionization techniques exist, however the most commonly used types in metabolomics are electropray ionization (ESI), atmospheric pressure chemical ionization (APCI), atmospheric pressure photoionization (APPI), electron impact ionization (EI) and matrix assisted laser desorption ionization (MALDI). These ionization techniques are complementary to each other, each having unique advantages and disadvantages which will be described briefly. Electron impact ionization (EI) is mainly suitable for volatile and thermally stable compounds, thus it is mostly used with gas chromatography (GC) separation methods. It has the advantage of providing a fingerprint-like fragmentation pattern for metabolites that can be searched against available spectral libraries (13). Recently the Fiehn lab has released a library of metabolites acquired by GC-EI-MS. The initial number of metabolites in the library was ~ 2000, but it is continually increasing (14). One of the disadvantage of EI is that fragmentation of the metabolite is often so extensive that the parent ion is entirely absent from the spectrum, which will increase the challenge of determining the precursor mass (13). Extensive fragmentation also complicates the interpretation of mass spectrum (13). MALDI is a widely used ionization technique for characterizing a variety of analytes. It has been used successfully in metabolomics

(15, 16) and provides quick analysis of metabolites in limited sample volume. However, MALDI has several disadvantages, mainly the difficulty of quantification and hyphenation to LC. The dried matrix-sample mixture is usually not homogenous, hindering quantification since the laser ionizes only a small portion of the sample in most cases. The hyphenation of a separation technique like LC is challenging, because it requires offline fractionation onto a MALDI plate.

Thus the three most common ionization techniques that are applied in metabolomics and can be hyphenated to liquid chromatography are ESI, APCI and APPI. These three modes of ionization have been compared before by several groups and their results confirm the complementarity of the three methods, although ESI offers the greatest extent of global metabolome coverage (17, 18). Because APPI or APCI involve application of high levels of heat, several metabolites including glycerophospholipids have been shown to fragment with those sources, unlike ESI (17). Neutral lipids have shown better linear response with APPI and APCI than ESI, however ESI offered improved limit of detection (via adduct formation) (19).

Mass analyzers

Choosing an appropriate mass analyzer is crucial in metabolomics studies, since different outputs are obtained from different types of instrumentation. If the goal is to analyze the concentration of a specific set of metabolites in a complex matrix, then a triple quadrupole mass analyzer is an ideal option. A quadrupole (Q) has limited resolution and mass accuracy which limits its application to identify metabolites. However, the low mass accuracy is compensated by the specificity of "multiple reaction monitoring" (MRM), a technique which can be performed using triple quadrupole MS instruments (QQQ). In MRM, a precursor ion is selected in Q1 and fragmented in Q2 by collision with gas molecules (collision induced dissociation) and fragments are then selected for quantification in Q3. This process excludes most ions except those that originate from the specific metabolite of interest, thus resulting in a high signal-to-noise ratio. However, the slow scanning speed of quadrupole limits the number of metabolites that can be analyzed simultaneously. If the primary goal is to identify and analyze as many metabolites as possible, then high scan speed and high resolution mass analyzers should be used. The highest resolution mass analyzer is the Fourier transform ion

cyclotron resonance instrument (FTICR), followed by the Orbitrap, followed by the time of flight mass analyzer (TOF) (Figure 1-4). Although the higher resolution of FTICR and Orbitrap instruments enables resolution of metabolites with similar masses and allows more definitive identification of unknown metabolites, they are not widely used in metabolomics (Figure 1-4). The less frequent application of these instruments in metabolomics is due to their substantially higher cost and the fact that their maximum scanning speed is several fold-lower than a TOF (20).

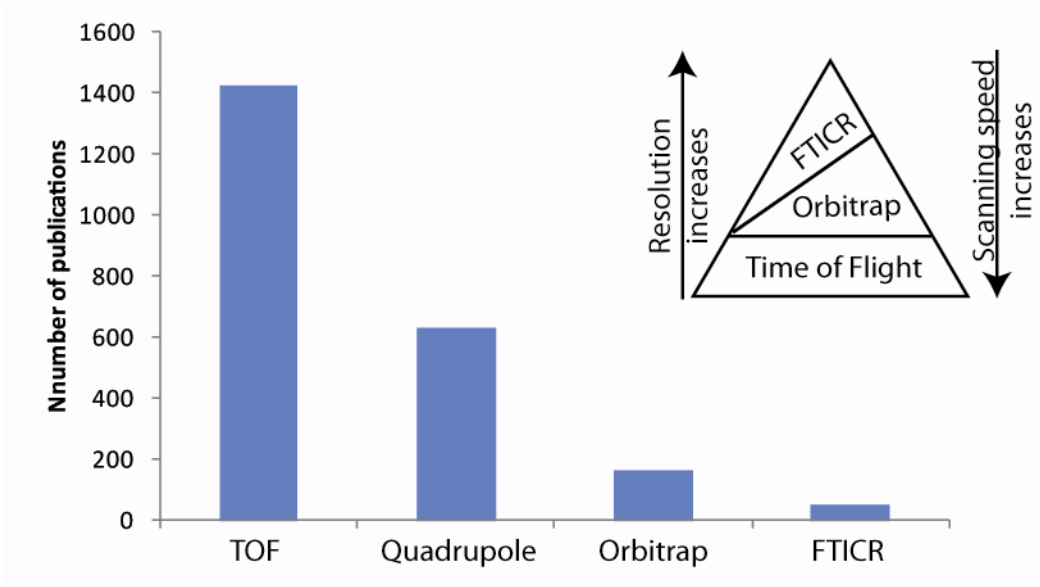

Figure 1-4: The frequency of the application of different mass spectrometers in metabolomics. Bibliographic search using Scifinder. The word metabolomics was searched followed by refining the results by the key words: "time of flight", "quadrupole", "Orbitrap" and "FTICR".

COMMON SEPARATION TECHNIQUES IN METABOLOMICS

As described above, separation is very important in metabolomics studies. Metabolite separation decreases sample complexity and provides further information about metabolites' chemical characteristics that aid in their identification (21). Separation can be utilized in both NMR and MS metabolomics platforms. Separation is crucial in mass spectrometry based metabolomics, since it allows the detection of low-abundant metabolites whose ionization could be suppressed by higher-abundant ones. Direct coupling of separation techniques such as liquid chromatography to NMR is complicated and suffers limitations that reduce the technique's sensitivity. Limitations include the post column peak broadening which occurs

during transport to the NMR flow cell; dilution of the chromatographic peak which occurs during filling of the flow cell, and challenges in chromatographic peak selection (22). Common separation techniques used in metabolomics include gas chromatography, liquid chromatography and capillary electrophoresis. These separation techniques are complementary to each other, each having pros and cons that are described briefly below.

Gas chromatography:

Gas chromatography has been regarded as the gold standard for metabolite analysis for several years (21). It is usually connected to a mass spectrometer equipped with an EI ionization source, which renders it less prone to ionization suppression from co-eluting compounds, unlike LC-MS (23). GC-MS requires that the metabolite be thermally stable and volatile, which are not common features for many polar metabolites. Thus, chemical derivatization to increase volatility is a requirement for many metabolites in order to widen the application range of this technique (24). Common drawbacks of derivatization include the loss of sample during derivatization, and the difficulty of identifying compounds because of the unknown or incomplete reaction of derivatization reagent molecules with unknown metabolites (25). Thus, identifying metabolites through an undirected analysis approach is often dependent on the availability of spectra of authentic standards in GC-MS libraries. However, GC-MS offers an excellent complementary technique to LC-MS, enabling detection of many metabolites that are not amenable to LC-MS analysis.

Liquid chromatography.

Liquid chromatography coupled to mass spectrometry (LC-MS) represents the technique of choice for global metabolite profiling (5). LC/MS allows the detection of thousands of peaks from biological samples. Peaks with unique mass and retention time are called “features”. The particle size of stationary phases ranges from 5 µm to 3 µm for conventional high pressure liquid chromatography “HPLC” or sub-2 µm for ultra pressure liquid chromatography “UPLC”. The advantage of UPLC is the reduction in total run time, improved separation efficiency by reduction in eddy diffusion and mass transfer kinetics. Elution of metabolites as sharper peaks results in increases in signal to noise ratio and consequently increases the number of detected

features (21, 25). As described above, metabolites vary in polarity, charge and stability. Thus, no single separation technique is able to resolve a complex sample, and orthogonal separation mechanisms should be used to ensure wider metabolome coverage (21). The combination of both reversed phase liquid chromatography (RPLC) and hydrophilic ion interaction chromatography (HILIC) methods provides a wide range of metabolome coverage (26). C18 is the most widely used RPLC stationary phase for the separation of non-polar metabolites. It provides a reproducible and predictable retention time, and effectively resolves a wide range of hydrophobic metabolites and lipids (21). However, hydrophilic metabolites are mainly eluted non-retained in the void volume.

HILIC separation is an orthogonal technique to RPLC. Several stationary phases have been developed for HILIC, each with different functional groups that provide different selectivity and separation mechanisms (27). Functional groups in HILIC stationary phase include the amino-propyl, amide and diol groups. The major drawback of HILIC is the increase in retention time drift relative to RPLC (21) as well as shorter column life. A new modification for HILIC was recently introduced, which is aqueous normal phase (ANP), based on a silica hydride stationary phase, that was shown to have more stable retention time (28). However for the coverage of metabolites associated with central carbon metabolism, our lab and others (26) have determined that the amino-propyl (29) HILIC column still offers the best coverage.

Capillary electrophoresis

Capillary electrophoresis (CE) separates metabolites based on their electrophoretic mobility, which is dependent on metabolite hydrodynamic radius (size)-to-charge ratio (30). Like LC, CE can be directly coupled to mass spectrometry by electrospray ionization. CE-MS has shown success in several metabolomics studies (31-37). Although it provides faster analysis and potentially higher resolution separations than LC, it is not as widely used in metabolomics (30) compared to chromatographic techniques described above (Figure 1-5). Among the limitations of CE are the low maximum injection volume (a few microliters for CE compared to hundreds microliters for LC or GC) (21). Also, since the capillary length and background electrolyte (BGE) ionic strength affect the migration time, there is usually day to day variation in the absolute

migration time of metabolites; however, relative migration time compared to a standard can be utilized (21, 30). Difficulties that are associated with the coupling of CE to MS are what really limit the widespread application of this technique in different labs (30). ESI-MS hyphenation to CE is not as straightforward as with LC, because a closed electrical circuit is required for both the CE separation and for ionization on the ESI-MS (38). Buffers normally used as a BGE for CE are not MS compatible, so these buffers need to be substituted with volatile MS-compatible buffers, which provide reduced quality of separation (39). Common CE-MS interfaces include both sheath and sheathless flow. Sheath flow involves using a co-axial liquid effluent to achieve electrical contact with the CE effluent; however, it causes post-capillary dilution (21, 39). Sheathless flow is still under development and few configurations have shown sufficient robustness for routine metabolomics analysis (21).

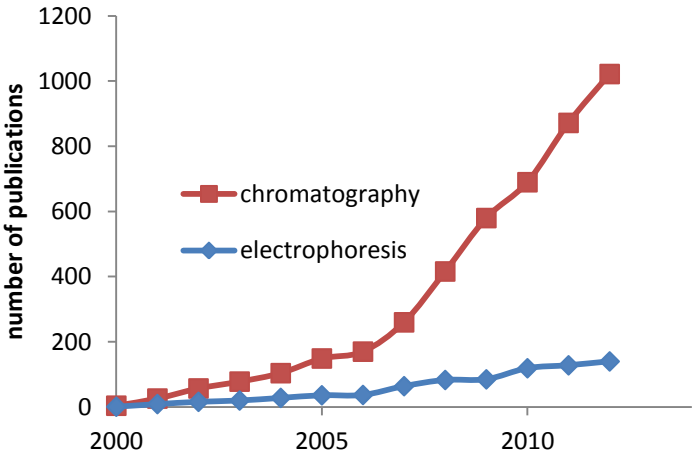

Figure 1-5:The frequency of the application of chromarography or electrophoresis in metabolomics. Bibliographic search using SciFinder using the word metabolomics and metabonomics, and further refined using either the term chromatography or electrophoresis.

As evidenced by the preceding discussion, multiple analytical strategies can be used to perform metabolomics research. While no method is comprehensive, careful selection of an appropriate analytical strategy is important to ensure all aims of a study can be met. In light of these considerations, the work described in this dissertation was performed by liquid chromatography-based separations, using HILIC for polar metabolites and RPLC for non-polar

metabolites. Both chromatographic methods were directly coupled via ESI ionization to a TOF high resolution mass analyzer.

DIRECTED AND UNDIRECTED METABOLOMICS

After the selection of an appropriate separation and detection method, experiment design is the next critical stage of metabolomics research. Two major approaches are available, which are targeted (directed) and untargeted (undirected) metabolomics. Directed analysis is the approach in which a specific set of metabolites are measured, usually focusing on one or more related pathway(s) of interest (40). In directed analysis, the analytical method (separation and detection) is optimized for the desired set of metabolites using authentic standards. This is followed by applying the method to biological samples, and reporting the results for this set of metabolites (Figure 1-6). On the other hand, undirected metabolomics is the approach which aims to analyze as many metabolites as possible (40). In undirected analysis (Figure 1-6), a global separation and detection method should be applied that can separate and detect a wide range of metabolites. It also requires a high resolution mass spectrometer (as described in the mass analyzers section) to accurately determine the mass and help to identify those metabolites. This global measurement is followed by extensive data analysis procedures described in the next section.

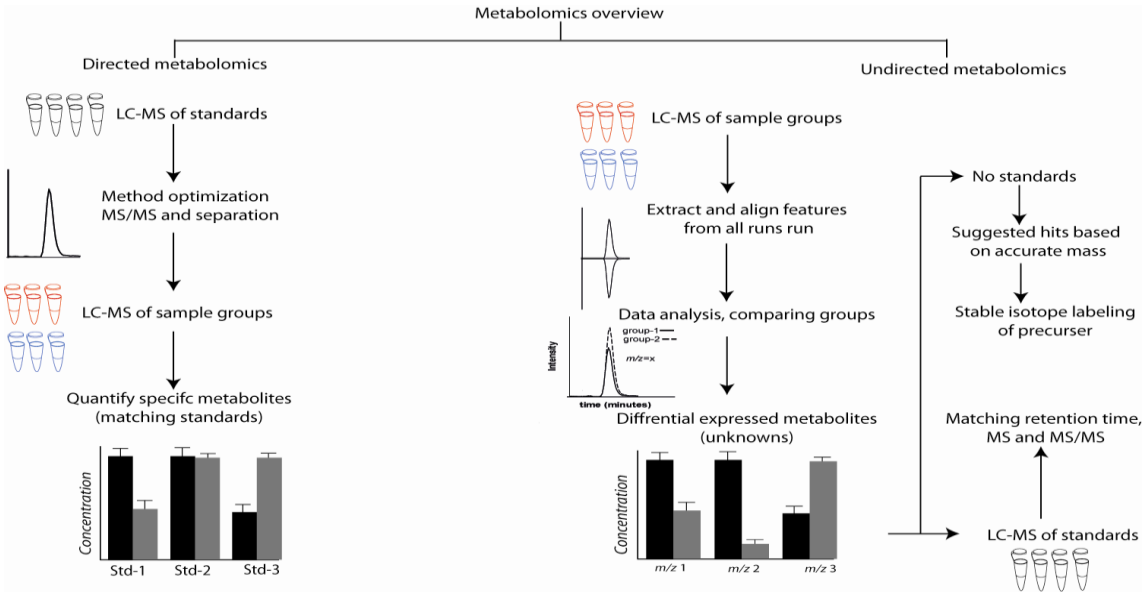

Figure 1-6: work flow for directed and undirected analysis.

DATA ANALYSIS

Data analysis techniques differ substantially between targeted and untargeted approaches. Data analysis for targeted metabolomics is relatively simple, where metabolites of interest are identified based on their mass and retention time matching with that of an authentic standard. Quantification can be performed by measuring metabolite peak area or peak height using the MS vendor software. Untargeted metabolomics involves several extra steps compared to targeted analysis. The first step is to identify features (peaks) with a specific mass and retention time. A normal LC-MS run contains, on average, a few thousand features, which necessitates automation of this step. Algorithms for feature selection software should be able to differentiate between a chromatographic peak and noise. Although seemingly simple, this task is usually performed imperfectly by all current software and thus requires manual inspection of the data. The second step is to align all features that are in common between different samples to allow for quantitative comparison in subsequent steps. The alignment step is a crucial issue, especially in HILIC-LC-MS, because of retention time shifts that occur through different samples. Shifts in retention time may arise from degradation of the column, change in mobile phase pH and sample carry over. The third step is to quantitate the data and measure the metabolites' relative abundances in different sample groups. Then, various methods of statistical analysis can be used to determine which metabolites differ significantly between sample groups.

The difference in features across groups can be visualized using different plots, including scatter plots, heat maps, volcano plots and cloud plots (Figure 1-7), with the later being the most comprehensive (41). Several software programs have been developed by many groups to facilitate and automate these steps, such as XCMS (42), MathDAMP, Metalign, and MZmine (5). Major mass spectrometer vendors have also developed software compatible with data from their systems to help in determination of differential abundance of metabolites and other biomarkers; some of these software packages include Mass Profiler by Agilent, SIEVE from Thermo Scientific, Marker View from Ab Sciex and MarkerLynx from Waters. The next step is to search the accurate mass of features of interest against different metabolite databases. Available metabolomics databases include: Metabolite link (METLIN), human metabolome data

base (HMDB), Kyoto encyclopedia of genes and genomes (KEGG), Mass bank, Madison metabolomics consortium database (MMCD) and lipid maps which is specialized in lipids (42). The final step is to confirm the identity of these database hits, when possible, by matching the retention time of the metabolite with that of a standard, and by using MS/MS. When a metabolite standard is not available, an alternative approach is to expose living cells to a labeled precursor of this metabolite, such that the cells will generate a new labeled standard that can confirm the identity of this metabolite (this process is described in detail later in the dissertation). The unique identification of metabolites remains a challenging step in some cases, although identification of lipids has recently been improved due to the availability of in-silco MS/MS fragmentation data contained within the "Lipid Blast" database (43).

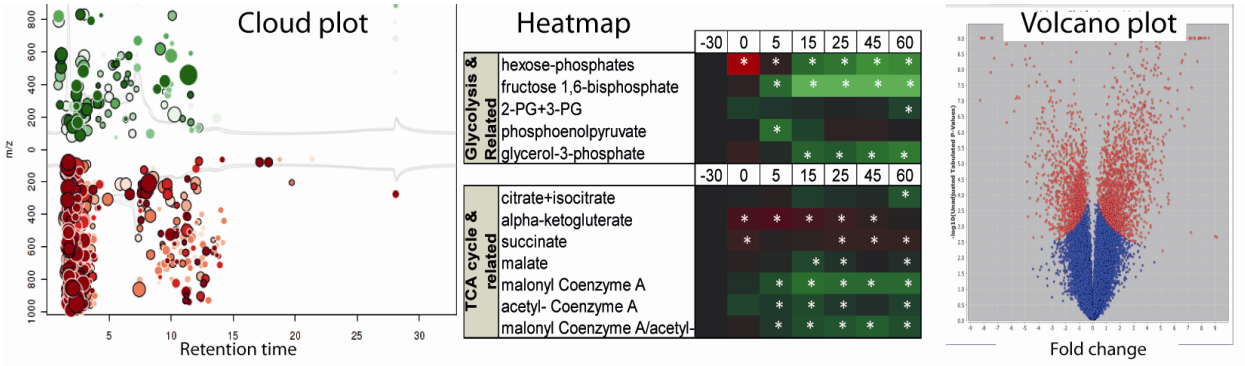

Figure 1-7: data visualization tools in metabolomics.

FLUX ANALYSIS

The previously-described directed and undirected metabolomics approaches enable quantitation of any increase or decrease in the abundance of specific metabolites within a biological system. These data clearly may provide useful information regarding the possible up-regulation or down-regulation of particular metabolic pathways. However, not every possible alteration in a metabolic pathway will necessarily be reflected as absolute changes in metabolite levels. It is possible for certain metabolic pathways to be differentially regulated between sample groups, but yet the absolute levels of metabolites remain constant because of different compensatory mechanisms. To reveal the true alteration in the metabolic pathways in such a scenario would require another level of metabolomics investigation. One excellent option would be to utilize metabolic tracers to investigate metabolic flux in those pathways.

The resulting technique, termed metabolic flux analysis, or MFA, is a key method to analyze and quantify in vivo rates of metabolic reactions (44). Different stable-isotope-labeled metabolic tracers can be used that include ^{13}C , ^{2}H, ^{15}N, and ^{18}O (45). In many cases ^{2}H readily exchanges with protons from water and other molecules; hence incorporation into the metabolome is not stable compared to ^{13}C. Both ^{13}C and ^{2}H can be used to assess flux in nearly all metabolites, while ^{15}N is mainly used for flux monitoring in nucleic acid and proteins, and ^{18}O is less commonly used. Because of the complexity of metabolic networks, mathematical modeling is needed to analyze flux in multiple metabolic pathways; the use of such techniques has been described in detail elsewhere (44). Mass isotopomer analysis is different from MFA, since the former does not measure metabolic flux or rate; it measures the distribution of carbons in specific metabolites. Using a metabolic tracer, mass isotopomer analysis enables the measurement of metabolites' isotopic enrichment. The isotope enrichment data provide useful information about pathways being utilized by metabolic tracers. Application of metabolic tracer to investigate metabolic pathways is described in chapter 2, 3, 4 and 5.

METABOLOMICS APPLICATIONS

By applying the analytical and data analysis tools just described, metabolomics has been successfully implemented in a wide range of challenges in various fields of biological research. Metabolomics has been applied to study metabolism in plants, animals and microorganisms. In plant science, metabolomics has been used to understand gene function and molecular breeding and to discover new phytochemicals that can be used for different purposes like pharmaceuticals (46). Metabolomics of biofluids and tissues from living animals has demonstrated successful identification of pathways involved in animal development and also in research involving disease and drug discovery (46). Microbial metabolomics is also currently of great interest, both because of potential industrial applications such as biofuel generation (47, 48), and due to the increasing interest in gut flora (termed the "microbiome") (49). A human being harbors ~ 100 trillion bacterial cells in his or her gut, a quantity 10 times greater than that of human cells in the same organism. This enormous amount of bacteria metabolizes food products and generates metabolites that participate in the development of several diseases and other phenotypes. Some cardiovascular diseases have recently been linked to

phosphatidylcholine (50, 51) and carnitine (52) metabolism by gut flora. Similar association of gut flora to diabetes and obesity has also been demonstrated (53-59), suggesting that flora modulation may provide an alternative approach for treatment of these complex diseases. Metabolomics has also been applied to the study of a variety of other diseases including cancer, psychological disorders, obesity and type 2 diabetes mellitus (T2DM) (46). The latter two conditions will be the primary focus of the metabolomics-based research presented in remainder of this dissertation.

APPLICATION OF METABOLOMICS TO THE STUDY OF TYPE 2 DIABETES

Background on diabetes:

Diabetes is a chronic disease that is characterized by high blood glucose levels (hyperglycemia), which is caused by relative deficiency of insulin hormone. Diabetes is classified as type 1 or type 2 based on the etiology of the insulin deficiency. In type 1 or juvenile diabetes, an autoimmune response destroys β-cells located in the pancreas, usually in childhood, which causes a complete loss of insulin secretion (Figure 1-8). In type 2, insulin resistance develops in the skeletal muscle and other organs, which leads to compensatory increase of insulin secretion into the blood by β- cells, resulting in hyperinsulinemia (Figure 1-8). Continuous increase of insulin secretion ultimately leads to the loss of β- cell function and the development of type 2 diabetes (60). The prevalence of diabetes in 2008 was estimated to be 347 million people worldwide (61, 62), which is ~ 5% of the estimated population of the earth. In the US alone, 25.8 million people were diagnosed with diabetes in 2011, representing 8.3 % of the US population (63). About 90 % of diabetic patients are diagnosed with type 2 diabetes (64).

The main complications of hyperglycermia are associated with its long term effects on other organs, which include micro and macro vascular complications that can be fatal (Figure 1-8). It is important to highlight that type 2 diabetes is a metabolic disorder, in which high glucose and high fatty acids, acting in concert with certain genetic factors, lead to β- cell toxicity and the development of the full range of medical complications associated with type 2 diabetes (60). Because of the high prevalence of type 2 diabetes, and the metabolic nature of the

disease, metabolomics provides a particularly useful strategy to gain insight into the molecular factors that contribute to this disease.

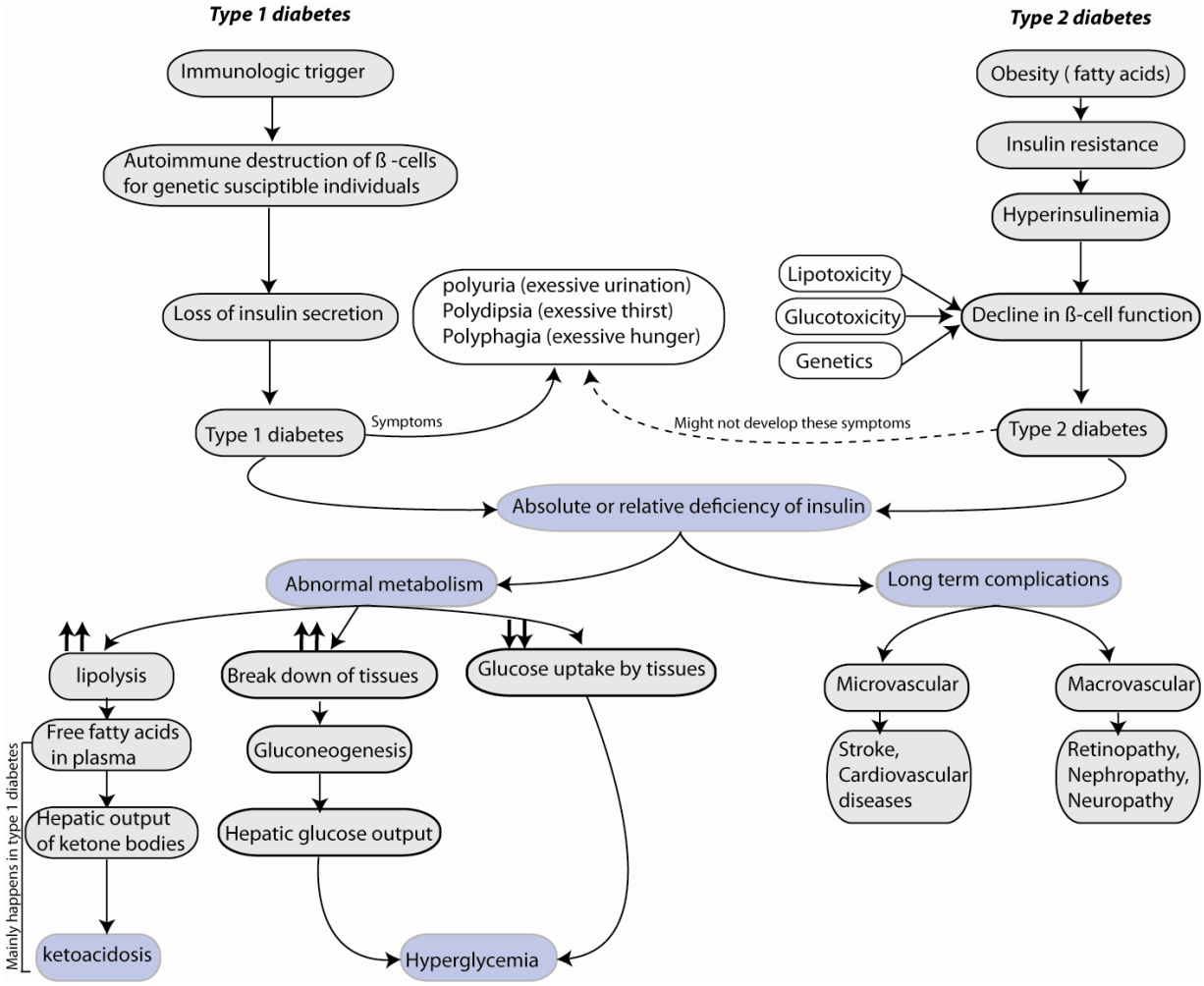

Figure 1-8: diagram for diabetes etiology and consequences, adapted from (60)

Metabolomics as a method to study type 2 diabetes

During the last decade, the growing field of metabolomics has offered new insights into the pathology of diabetes as well as biomarkers that can predict disease onset (64). Several biomarkers that are related to carbohydrate, lipid, amino acid, choline and bile acid metabolism have been shown to be up- or down-regulated in T2DM patients and have been thoroughly reviewed elsewhere (64, 65). Among the most common biomarkers are changes in amino acid profiles of diabatic patients. Branched chain amino acids (leucine, isoleucine and valine),

phenylalanine and tyrosine showed elevation in individuals susceptible to T2DM (66), and were detectable as elevated as early as 12 years before the onset of disease (67) . Lower levels of glycine (68), glutamate, and theronine were seen in T2D (66, 69). These data suggest the potential impact of amino acids on insulin action and glucose metabolism (64). Metabolites in lipid metabolism pathways also represent major biomarkers in diabetic patients. Acyl-carnitines have been shown to accumulate in the plasma of obese and diabetic patients, indicating a defect in fatty acid oxidation (70), together with accumulation of fatty acids and some forms of phosphatidylcholines (68).

Animal models and β- cell lines

Several animal models have been developed to study T2DM development and treatment. Understanding and treating the disease in human subjects is the ultimate goal, but the development of the disease and its complication in humans takes years. This long time and high cost for assessing intervention outcome in the disease progression, makes animal models of T2DM a very attractive option. Animal models develop the disease and its complications in shorter time spans and are more cost efficient (71). Rodent animal models, especially mice and rats, have been widely used because of the complete sequencing of their genome, the ease of genetic manipulation, their relatively short breeding spans, and the ability to perform physiological and invasive testing (71). Mouse models include the obese (ob/ob) mice and the diabetic (db/db) mice, which have a knockout of the gene responsible for production of leptin or leptin receptor, respectively (71, 72). The most known rat model of T2DM is the ZDF rat, which has a similar mutation to leptin receptor as the (db/db) mouse.

In addition to studies involving live animals, additional insight can be gained through studies of specific, isolated tissues involved in the development of T2DM. Of particular interest is the interaction of glucose and other nutrients on insulin secretion in pancreatic β- cells. Therefore, studies using islets obtained from human volunteers or animal models are of substantial interest. However, isolated islets have several issues. The first is that non-β-cells contribute to ~ 40% of the mass of islets, and these cells which have different signaling mechanisms which may complicate understanding of β- cells action. Also, the physical isolation

of islets may result in retention of some pancreatic exocrine tissue, which will be a variable in quantity from one sample group to another. Also, there is a risk of necrosis of inner cells in islets after isolation and culture because of the limited supply of O2 and nutrients to those cells (73). Beside those issues, since islets are very small microorgans and only limited quantities can be practically obtained for experimentation, performing metabolomics on islets is limited by low levels of metabolites and the need for relatively large number of islets per sample group to overcome the variation of sizes between islets.

These challenges led to the development of immortalized β- cell lines derived from rodent pancreatic tumors. Studies of these cell lines has been shown to be very effective in understanding fuel signaling in β-cells (73). The cell lines have the advantage of producing homogenous, pure β-cells. Limitations in quantities of cells are no longer a concern, as cells can be cultured in vitro until the needed amounts are obtained. For metabolomics, β-cell lines have the advantage that they can be cultured in a consistent manner, providing replicates with nearly equal cell numbers. The most widely used rat-derived β-cell lines are INS-1 cells, while the widely used mouse-derived β-cell lines are MIN-6 cells. Human β-cell lines have been recently described (74-76) but their availability are limited and their usefulness for metabolomics studies are yet to be investigated (73).

In spite of the utility of β-cell lines to gain understanding of the mechanism of insulin secretion, β-cell toxicity is still thought to be better studied using islets. Due to their derivation from cancerous tumors, β-cell lines may have a compensatory mechanism that can relieve lipotoxicity that might not be available in normal islets. Nevertheless, metabolomics has provided valuable information for understanding the mechanism of insulin secretion, which is described in the following sections.

Glucose stimulated insulin secretion

Glucose stimulates β- cells to secrete insulin in a biphasic manner. The first phase is called the K_{ATP} dependent pathway and it starts a few minutes after glucose stimulation and subsequently declines. It is considered ATP-dependent because the metabolism of increased concentrations of glucose generates more ATP, increasing the ATP/ADP ratio which leads to the

closure of K_{ATP} channels and cell depolarization. Voltage dependent calcium channels open subsequently and increase calcium influx into the cells, which causes insulin exocytosis (77, 78). Second-phase insulin secretion acts in synergy with the first phase, starting a few minutes after the first phase, and reaches its maximum at ~ 30-40 minutes after glucose stimulation (78). It is called the K_{ATP}-independent pathway, since glucose metabolism generates several other coupling signals that facilitate insulin exocytosis (77). Although not well understood, some coupling factors for this pathway are GTP, NADPH, LC-CoA, glycerolipids, glutamate, PEP, malonyl-CoA and others (73, 77, 78) (Figure 1-9).

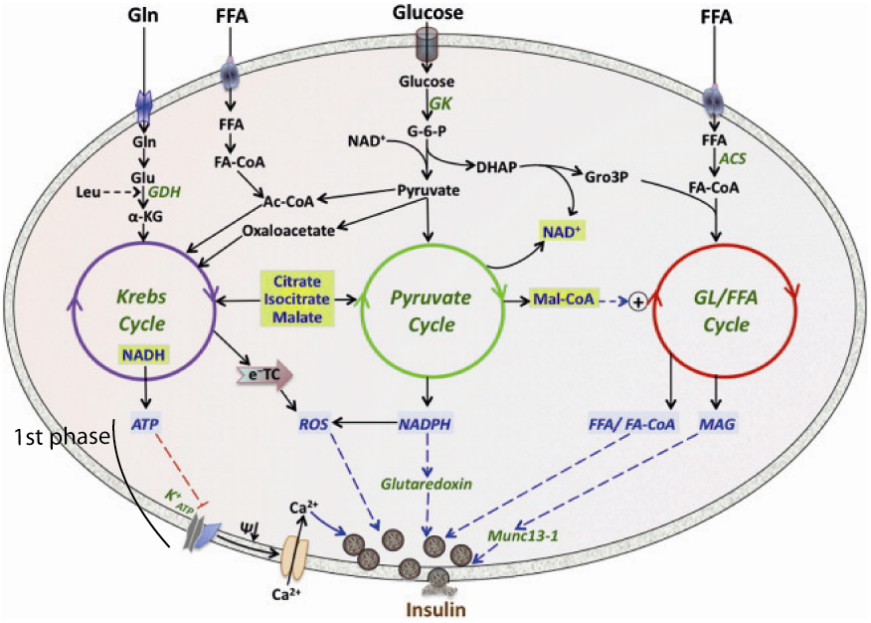

Figure 1-9: glucose stimulated insulin secretion proposed pathway, adapted from (73)

Although glucose is the most potent insulin secretagogue, some amino acids and other nutrients are also known to stimulate insulin secretion alone or in combination with each other, including leucine, glutamine, BCH, ketoisocaproate (KIC), methyl ester of succinate (MMS), acetoacetate, β-hydroxybutarate and fatty acids (79, 80). The main theory behind the activity of these different secretagogues is their ability to increase TCA cycle activity, which will increase ATP as well as different metabolic intermediates. The increase in both acetyl-CoA and oxaloacetate is required to ensure that the TCA cycle will be activated, and generates citric acid (Figure 1-10). Thus the function of those secretagogues (81) can be represented by the simplified diagram in (Figure 1-10).

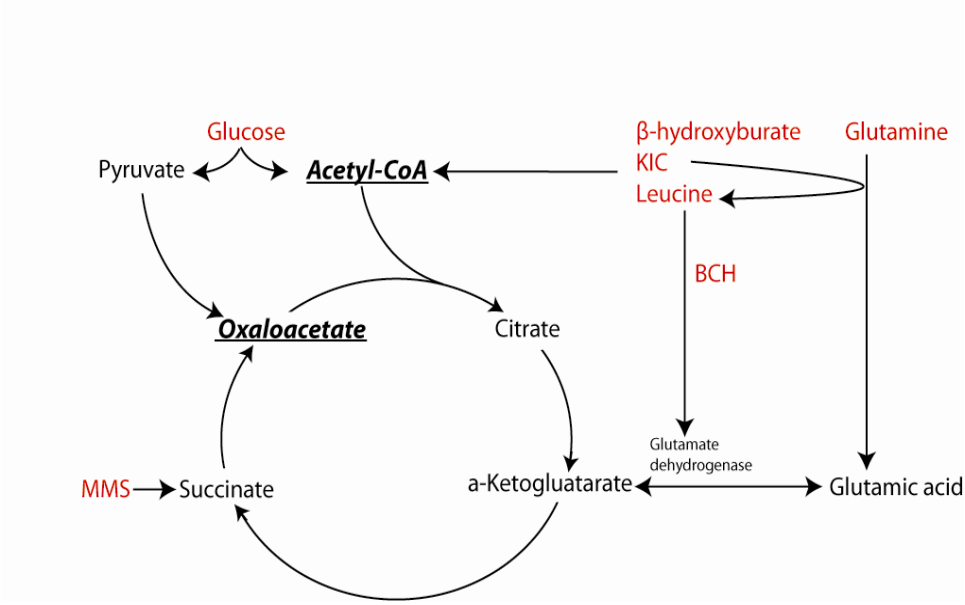

Figure 1-10: simplified pathway for secretagogues mechanism of insulin secretion.

Leucine activates glutamate dehydrogenase, increasing α-ketoglutarate and consequently oxaloacetate. At the same time it is metabolized into acetyl-CoA, therefore it can stimulate insulin secretion on its own. **KIC** is metabolized into leucine through a reaction that converts glutamine into glutamate, increasing α-ketoglutarate. It then acts as leucine, activating glutamate dehydrogenase and increasing acetyl-CoA. Therefore it can stimulate insulin secretion independently, and has been shown to be even more potent than leucine (81).

BCH is a non-metabolizable leucine analog, which only activates glutamate dehydrogenase, increasing α-ketoglutarate. Therefore, BHC is a weaker secretagogue than leucine (81). **Glutamine** can increase the level of α-ketoglutarate and hence oxaloacetate, but it cannot stimulate insulin secretion on its own. Addition of leucine to glutamine will provide the acetyl-CoA necessary for TCA cycle activation and the stimulation of insulin secretion (81). **B-hydroxybutare** is metabolized into acetyl-CoA, but cannot stimulate insulin secretion on its own. Addition of methyl ester succinate (MMS) will ensure the availability of oxaloacetate necessary for TCA cycle activation and the stimulation of insulin secretion (79).**Fatty acids** cannot stimulate insulin secretion on their own, but can augment GSIS by the activation of the glycerolipid cycle and by providing glycerolipid intermediates (73) (Figure 1-9)

DISSERTATION OVERVIEW

The goal of the research presented in this dissertation is to enhance understanding of the interaction of glucose and fatty acids to modulate insulin secretion. Understanding of glucose and fatty acid interaction requires an analytical method(s) that can probe glucose and fatty acid metabolism inside β- cell. Application of stable isotope labeling is important to monitor the extent of this interaction. Thus, chapter 2 describes method development for lipid analysis, while the appendix shows the application of different metabolic tracers to probe metabolic pathways involved in insulin secretion. We applied those methods in chapter 3 to understand how glucose stimulates insulin secretion and to probe important pathways that are involved in GSIS. Chapter 4 describes the mechanism of fatty acid can potentiate GSIS and explains how fatty acid is metabolized in β- cell and how this metabolism can affect glucose metabolism. Chapter 4 also describes the role of free fatty acid receptor (FFAR/GPR40) in controlling glucose and fatty acid metabolism. Chapter 5 describes the effect of starvation on β-cells using a starvation/exercise mimetic drug. Finally, Chapter 6 describes some future research plans, which involve studying the chronic toxicity of glucose and fatty acids, understanding how other secretagogues can stimulate insulin secretion and the application of metabolomics to human β- cell lines that were recently established.

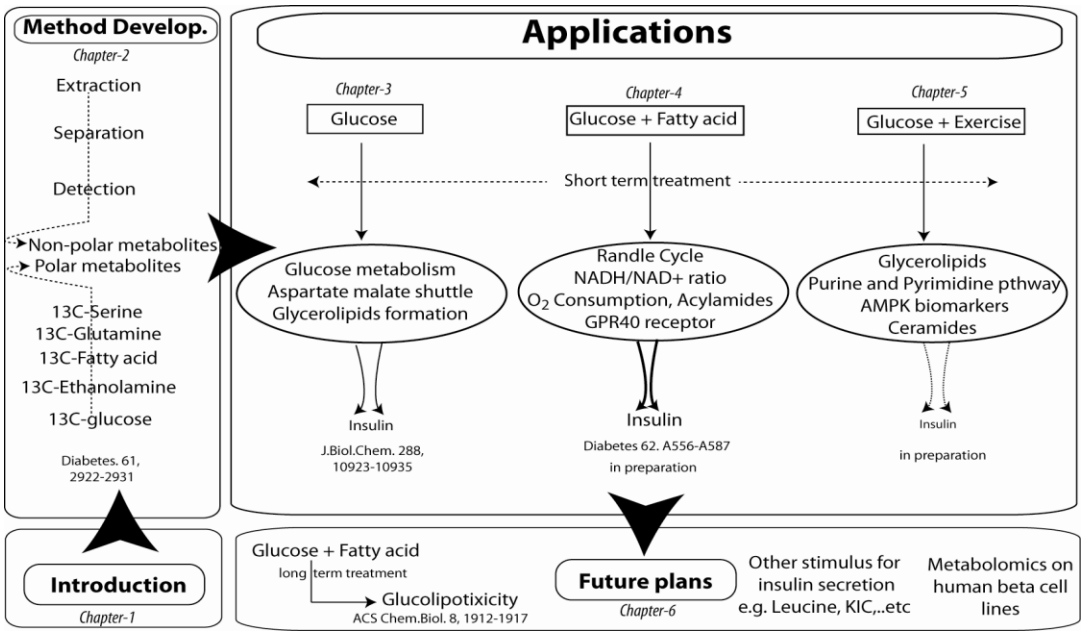

Figure 1-11: dissertation outline

REFERENCES

1. Oliver, S.G., Winson, M.K., Kell, D.B., and Baganz, F. (1998) Systematic functional analysis of the yeast genome. *Trends Biotechnol.* **16,** 373-378

2. Yadav, S.P. (2007) The wholeness in suffix -omics, -omes, and the word om. *J.Biomol.Tech.* **18,** 277

3. WANJEK, C. **Systems Biology as Defined by NIH**. *NIH catalyst.*

4. Dettmer, K., Aronov, P.A., and Hammock, B.D. (2007) Mass spectrometry-based metabolomics. *Mass Spectrom.Rev.* **26,** 51-78

5. Patti, G.J., Yanes, O., and Siuzdak, G. (2012) Innovation: Metabolomics: the apogee of the omics trilogy. *Nat.Rev.Mol.Cell Biol.* **13,** 263-269

6. Psychogios, N., Hau, D.D., Peng, J., Guo, A.C., Mandal, R., Bouatra, S., Sinelnikov, I., Krishnamurthy, R., Eisner, R., Gautam, B., Young, N., Xia, J., Knox, C., Dong, E., Huang, P., Hollander, Z., Pedersen, T.L., Smith, S.R., Bamforth, F., Greiner, R., McManus, B., Newman, J.W., Goodfriend, T., and Wishart, D.S. (2011) The human serum metabolome. *PLoS One.* **6,** e16957

7. Wishart, D.S., Jewison, T., Guo, A.C., Wilson, M., Knox, C., Liu, Y., Djoumbou, Y., Mandal, R., Aziat, F., Dong, E., Bouatra, S., Sinelnikov, I., Arndt, D., Xia, J., Liu, P., Yallou, F., Bjorndahl, T., Perez-Pineiro, R., Eisner, R., Allen, F., Neveu, V., Greiner, R., and Scalbert, A. (2013) HMDB 3.0--The Human Metabolome Database in 2013. *Nucleic Acids Res.* **41,** D801-7

8. Barding, G.A.,Jr, Salditos, R., and Larive, C.K. (2012) Quantitative NMR for bioanalysis and metabolomics. *Anal.Bioanal Chem.* **404,** 1165-1179

9. Zhang, A., Sun, H., Wang, P., Han, Y., and Wang, X. (2012) Modern analytical techniques in metabolomics analysis. *Analyst.* **137,** 293-300

10. Duarte, I.F., Lamego, I., Rocha, C., and Gil, A.M. (2009) NMR metabonomics for mammalian cell metabolism studies. *Bioanalysis.* **1,** 1597-1614

11. Pan, Z., and Raftery, D. (2007) Comparing and combining NMR spectroscopy and mass spectrometry in metabolomics. *Anal.Bioanal Chem.* **387,** 525-527

12. Fuhrer, T., Heer, D., Begemann, B., and Zamboni, N. (2011) High-Throughput, Accurate Mass Metabolome Profiling of Cellular Extracts by Flow Injection-Time-of-Flight Mass Spectrometry. *Anal.Chem.* **83,** 7074-7080

13. Dass, C. (2007) *Fundamentals of contemporary mass spectrometry,* , Wiley-Interscience, Hoboken, N.J.

14. Kind, T., Wohlgemuth, G., Lee do, Y., Lu, Y., Palazoglu, M., Shahbaz, S., and Fiehn, O. (2009) FiehnLib: mass spectral and retention index libraries for metabolomics based on quadrupole and time-of-flight gas chromatography/mass spectrometry. *Anal.Chem.* **81,** 10038-10048

15. Ibanez, A.J., Fagerer, S.R., Schmidt, A.M., Urban, P.L., Jefimovs, K., Geiger, P., Dechant, R., Heinemann, M., and Zenobi, R. (2013) Mass spectrometry-based metabolomics of single yeast cells. *Proc.Natl.Acad.Sci.U.S.A.* **110,** 8790-8794

16. Fagerer, S.R., Nielsen, S., Ibanez, A., and Zenobi, R. (2013) Matrix-assisted laser desorption/ionization matrices for negative mode metabolomics. *Eur.J.Mass.Spectrom.(Chichester, Eng).* **19,** 39-47

17. Tian, H., Bai, J., An, Z., Chen, Y., Zhang, R., He, J., Bi, X., Song, Y., and Abliz, Z. (2013) Plasma metabolome analysis by integrated ionization rapid-resolution liquid chromatography/tandem mass spectrometry. *Rapid Commun.Mass Spectrom.* **27,** 2071-2080

18. Nordstrom, A., Want, E., Northen, T., Lehtio, J., and Siuzdak, G. (2008) Multiple ionization mass spectrometry strategy used to reveal the complexity of metabolomics. *Anal.Chem.* **80,** 421-429

19. Cai, S.S., and Syage, J.A. (2006) Comparison of atmospheric pressure photoionization, atmospheric pressure chemical ionization, and electrospray ionization mass spectrometry for analysis of lipids. *Anal.Chem.* **78,** 1191-1199

20. Forcisi, S., Moritz, F., Kanawati, B., Tziotis, D., Lehmann, R., and Schmitt-Kopplin, P. (2013) Liquid chromatography-mass spectrometry in metabolomics research: mass analyzers in ultra high pressure liquid chromatography coupling. *J.Chromatogr.A.* **1292,** 51-65

21. Kuehnbaum, N.L., and Britz-McKibbin, P. (2013) New advances in separation science for metabolomics: resolving chemical diversity in a post-genomic era. *Chem.Rev.* **113,** 2437-2468

22. Schlotterbeck, G., and Ceccarelli, S.M. (2009) LC-SPE-NMR-MS: a total analysis system for bioanalysis. *Bioanalysis.* **1,** 549-559

23. Koek, M.M., Muilwijk, B., van der Werf, M.J., and Hankemeier, T. (2006) Microbial metabolomics with gas chromatography/mass spectrometry. *Anal.Chem.* **78,** 1272-1281

24. Koek, M.M., Jellema, R.H., van der Greef, J., Tas, A.C., and Hankemeier, T. (2011) Quantitative metabolomics based on gas chromatography mass spectrometry: status and perspectives. *Metabolomics.* **7,** 307-328

25. Milne, S.B., Mathews, T.P., Myers, D.S., Ivanova, P.T., and Brown, H.A. (2013) Sum of the parts: mass spectrometry-based metabolomics. *Biochemistry.* **52,** 3829-3840

26. Ivanisevic, J., Zhu, Z.J., Plate, L., Tautenhahn, R., Chen, S., O'Brien, P.J., Johnson, C.H., Marletta, M.A., Patti, G.J., and Siuzdak, G. (2013) Toward 'omic scale metabolite profiling: a dual separation-mass spectrometry approach for coverage of lipid and central carbon metabolism. *Anal.Chem.* **85,** 6876-6884

27. Buszewski, B., and Noga, S. (2012) Hydrophilic interaction liquid chromatography (HILIC)--a powerful separation technique. *Anal.Bioanal Chem.* **402,** 231-247

28. Chen, Q., Park, H.C., Goligorsky, M.S., Chander, P., Fischer, S.M., and Gross, S.S. (2012) Untargeted plasma metabolite profiling reveals the broad systemic consequences of xanthine oxidoreductase inactivation in mice. *PLoS One.* **7,** e37149

29. Bajad, S.U., Lu, W., Kimball, E.H., Yuan, J., Peterson, C., and Rabinowitz, J.D. (2006) Separation and quantitation of water soluble cellular metabolites by hydrophilic interaction chromatography-tandem mass spectrometry. *J.Chromatogr.A.* **1125,** 76-88

30. Issaq, H.J., Abbott, E., and Veenstra, T.D. (2008) Utility of separation science in metabolomic studies. *J.Sep.Sci.* **31,** 1936-1947

31. Sugimoto, M., Wong, D.T., Hirayama, A., Soga, T., and Tomita, M. (2010) Capillary electrophoresis mass spectrometry-based saliva metabolomics identified oral, breast and pancreatic cancer-specific profiles. *Metabolomics.* **6,** 78-95

32. Soga, T., Igarashi, K., Ito, C., Mizobuchi, K., Zimmermann, H.P., and Tomita, M. (2009) Metabolomic profiling of anionic metabolites by capillary electrophoresis mass spectrometry. *Anal.Chem.* **81,** 6165-6174

33. Monton, M.R.N., and Soga, T. (2007) Metabolome analysis by capillary electrophoresis-mass spectrometry. *Journal of Chromatography A.* **1168,** 237-246

34. Britz-McKibbin, P. (2012) New advances in amino acid profiling by capillary electrophoresis-electrospray ionization-mass spectrometry. *Methods Mol.Biol.* **828,** 83-99

35. Britz-McKibbin, P. (2011) Capillary electrophoresis-electrospray ionization-mass spectrometry (CE-ESI-MS)-based metabolomics. *Methods Mol.Biol.* **708,** 229-246

36. Kuehnbaum, N.L., and Britz-McKibbin, P. (2011) Comprehensive profiling of free and conjugated estrogens by capillary electrophoresis-time of flight/mass spectrometry. *Anal.Chem.* **83,** 8063-8068

37. Britz-McKibbin, P. (2011) Capillary electrophoresis-electrospray ionization-mass spectrometry (CE-ESI-MS)-based metabolomics. *Methods Mol.Biol.* **708,** 229-246

38. Janini, G.M., Conrads, T.P., Wilkens, K.L., Issaq, H.J., and Veenstra, T.D. (2003) A sheathless nanoflow electrospray interface for on-line capillary electrophoresis mass spectrometry. *Anal.Chem.* **75,** 1615-1619

39. Issaq, H.J., Janini, G.M., Chan, K.C., and Veenstra, T.D. (2004) Sheathless electrospray ionization interfaces for capillary electrophoresis-mass spectrometric detection advantages and limitations. *J.Chromatogr.A.* **1053,** 37-42

40. Patti, G.J., Yanes, O., and Siuzdak, G. (2012) Innovation: Metabolomics: the apogee of the omics trilogy. *Nat.Rev.Mol.Cell Biol.* **13,** 263-269

41. Patti, G.J., Tautenhahn, R., Rinehart, D., Cho, K., Shriver, L.P., Manchester, M., Nikolskiy, I., Johnson, C.H., Mahieu, N.G., and Siuzdak, G. (2013) A view from above: cloud plots to visualize global metabolomic data. *Anal.Chem.* **85,** 798-804

42. Tautenhahn, R., Cho, K., Uritboonthai, W., Zhu, Z., Patti, G.J., and Siuzdak, G. (2012) An accelerated workflow for untargeted metabolomics using the METLIN database. *Nat.Biotechnol.* **30,** 826-828

43. Kind, T., Liu, K.H., Lee do, Y., DeFelice, B., Meissen, J.K., and Fiehn, O. (2013) LipidBlast in silico tandem mass spectrometry database for lipid identification. *Nat.Methods.* **10,** 755-758

44. Mueller, D., and Heinzle, E. (2013) Stable isotope-assisted metabolomics to detect metabolic flux changes in mammalian cell cultures. *Curr.Opin.Biotechnol.* **24,** 54-59

45. Klein, S., and Heinzle, E. (2012) Isotope labeling experiments in metabolomics and fluxomics. *Wiley Interdiscip.Rev.Syst.Biol.Med.* **4,** 261-272

46. Putri, S.P., Nakayama, Y., Matsuda, F., Uchikata, T., Kobayashi, S., Matsubara, A., and Fukusaki, E. (2013) Current metabolomics: practical applications. *J.Biosci.Bioeng.* **115,** 579-589

47. Bergdahl, B., Heer, D., Sauer, U., Hahn-Hagerdal, B., and van Niel, E.W. (2012) Dynamic metabolomics differentiates between carbon and energy starvation in recombinant Saccharomyces cerevisiae fermenting xylose. *Biotechnol.Biofuels.* **5,** 34-6834-5-34

48. Amador-Noguez, D., Brasg, I.A., Feng, X.J., Roquet, N., and Rabinowitz, J.D. (2011) Metabolome remodeling during the acidogenic-solventogenic transition in Clostridium acetobutylicum. *Appl.Environ.Microbiol.* **77,** 7984-7997

49. Kim, B.S., Jeon, Y.S., and Chun, J. (2013) Current Status and Future Promise of the Human Microbiome. *Pediatr.Gastroenterol.Hepatol.Nutr.* **16,** 71-79

50. Wang, Z., Klipfell, E., Bennett, B.J., Koeth, R., Levison, B.S., Dugar, B., Feldstein, A.E., Britt, E.B., Fu, X., Chung, Y.M., Wu, Y., Schauer, P., Smith, J.D., Allayee, H., Tang, W.H., DiDonato, J.A., Lusis, A.J., and Hazen, S.L. (2011) Gut flora metabolism of phosphatidylcholine promotes cardiovascular disease. *Nature.* **472,** 57-63

51. Tang, W.H., Wang, Z., Levison, B.S., Koeth, R.A., Britt, E.B., Fu, X., Wu, Y., and Hazen, S.L. (2013) Intestinal microbial metabolism of phosphatidylcholine and cardiovascular risk. *N.Engl.J.Med.* **368,** 1575-1584

52. Koeth, R.A., Wang, Z., Levison, B.S., Buffa, J.A., Org, E., Sheehy, B.T., Britt, E.B., Fu, X., Wu, Y., Li, L., Smith, J.D., DiDonato, J.A., Chen, J., Li, H., Wu, G.D., Lewis, J.D., Warrier, M., Brown, J.M., Krauss, R.M., Tang, W.H., Bushman, F.D., Lusis, A.J., and Hazen, S.L. (2013) Intestinal microbiota metabolism of L-carnitine, a nutrient in red meat, promotes atherosclerosis. *Nat.Med.* **19,** 576-585

53. Gross, M. (2013) Does the gut microbiome hold clues to obesity and diabetes?. *Curr.Biol.* **23,** R359-62

54. Burcelin, R., Serino, M., Chabo, C., Garidou, L., Pomie, C., Courtney, M., Amar, J., and Bouloumie, A. (2013) Metagenome and metabolism: the tissue microbiota hypothesis. *Diabetes Obes.Metab.* **15 Suppl 3,** 61-70

55. Cotillard, A., Kennedy, S.P., Kong, L.C., Prifti, E., Pons, N., Le Chatelier, E., Almeida, M., Quinquis, B., Levenez, F., Galleron, N., Gougis, S., Rizkalla, S., Batto, J.M., Renault, P., ANR MicroObes consortium, Dore, J., Zucker, J.D., Clement, K., Ehrlich, S.D., Blottiere, H., Leclerc, M., Juste, C., de Wouters, T., Lepage, P., Fouqueray, C., Basdevant, A., Henegar, C., Godard, C., Fondacci, M., Rohia, A., Hajduch, F., Weissenbach, J., Pelletier, E., Le Paslier, D., Gauchi, J.P., Gibrat, J.F., Loux, V., Carre, W., Maguin, E., van de Guchte, M., Jamet, A., Boumezbeur, F., and Layec, S. (2013) Dietary intervention impact on gut microbial gene richness. *Nature.* **500,** 585-588

56. Everard, A., and Cani, P.D. (2013) Diabetes, obesity and gut microbiota. *Best Pract.Res.Clin.Gastroenterol.* **27,** 73-83

57. Zhao, L. (2013) The gut microbiota and obesity: from correlation to causality. *Nat.Rev.Microbiol.* **11,** 639-647

58. Kovatcheva-Datchary, P., and Arora, T. (2013) Nutrition, the gut microbiome and the metabolic syndrome. *Best Pract.Res.Clin.Gastroenterol.* **27,** 59-72

59. Le Chatelier, E., Nielsen, T., Qin, J., Prifti, E., Hildebrand, F., Falony, G., Almeida, M., Arumugam, M., Batto, J.M., Kennedy, S., Leonard, P., Li, J., Burgdorf, K., Grarup, N., Jorgensen, T., Brandslund, I., Nielsen, H.B., Juncker, A.S., Bertalan, M., Levenez, F., Pons, N., Rasmussen, S., Sunagawa, S., Tap, J., Tims, S., Zoetendal, E.G., Brunak, S., Clement, K., Dore, J., Kleerebezem, M., Kristiansen, K., Renault, P., Sicheritz-Ponten, T., de Vos, W.M., Zucker, J.D., Raes, J., Hansen, T., MetaHIT consortium, Bork, P., Wang, J., Ehrlich, S.D., Pedersen, O., Guedon, E., Delorme, C., Layec, S., Khaci, G., van de Guchte, M., Vandemeulebrouck, G., Jamet, A., Dervyn, R., Sanchez, N., Maguin, E., Haimet, F., Winogradski, Y., Cultrone, A., Leclerc, M., Juste, C., Blottiere, H., Pelletier, E., LePaslier, D., Artiguenave, F., Bruls, T., Weissenbach, J., Turner, K., Parkhill, J., Antolin, M., Manichanh, C., Casellas, F., Boruel, N., Varela, E.,

Torrejon, A., Guarner, F., Denariaz, G., Derrien, M., van Hylckama Vlieg, J.E., Veiga, P., Oozeer, R., Knol, J., Rescigno, M., Brechot, C., M'Rini, C., Merieux, A., and Yamada, T. (2013) Richness of human gut microbiome correlates with metabolic markers. *Nature.* **500,** 541-546

60. Champe, P.C., Harvey, R.A., and Ferrier, D.R. (2008) *Lippincott's illustrated reviews : biochemistry,* , Wolters Kluwer/Lippincott Williams & Wilkins, Philadelphia

61. Danaei, G., Finucane, M.M., Lu, Y., Singh, G.M., Cowan, M.J., Paciorek, C.J., Lin, J.K., Farzadfar, F., Khang, Y.H., Stevens, G.A., Rao, M., Ali, M.K., Riley, L.M., Robinson, C.A., Ezzati, M., and Global Burden of Metabolic Risk Factors of Chronic Diseases Collaborating Group (Blood Glucose) (2011) National, regional, and global trends in fasting plasma glucose and diabetes prevalence since 1980: systematic analysis of health examination surveys and epidemiological studies with 370 country-years and 2.7 million participants. *Lancet.* **378,** 31-40

62. World Health Organization (2013) Diabetes fact sheet N°312

63. Center of disease control and prevention 2011 National Diabetes Fact Sheet

64. Friedrich, N. (2012) Metabolomics in diabetes research. *J.Endocrinol.* **215,** 29-42

65. Lu, J., Xie, G., Jia, W., and Jia, W. (2013) Metabolomics in human type 2 diabetes research. *Front.Med.* **7,** 4-13

66. Newgard, C.B., An, J., Bain, J.R., Muehlbauer, M.J., Stevens, R.D., Lien, L.F., Haqq, A.M., Shah, S.H., Arlotto, M., Slentz, C.A., Rochon, J., Gallup, D., Ilkayeva, O., Wenner, B.R., Yancy, W.S.,Jr, Eisenson, H., Musante, G., Surwit, R.S., Millington, D.S., Butler, M.D., and Svetkey, L.P. (2009) A branched-chain amino acid-related metabolic signature that differentiates obese and lean humans and contributes to insulin resistance. *Cell.Metab.* **9,** 311-326

67. Wang, T.J., Larson, M.G., Vasan, R.S., Cheng, S., Rhee, E.P., McCabe, E., Lewis, G.D., Fox, C.S., Jacques, P.F., Fernandez, C., O'Donnell, C.J., Carr, S.A., Mootha, V.K., Florez, J.C., Souza, A., Melander, O., Clish, C.B., and Gerszten, R.E. (2011) Metabolite profiles and the risk of developing diabetes. *Nat.Med.* **17,** 448-453

68. Floegel, A., Stefan, N., Yu, Z., Muhlenbruch, K., Drogan, D., Joost, H.G., Fritsche, A., Haring, H.U., Hrabe de Angelis, M., Peters, A., Roden, M., Prehn, C., Wang-Sattler, R., Illig, T., Schulze, M.B., Adamski, J., Boeing, H., and Pischon, T. (2013) Identification of serum metabolites associated with risk of type 2 diabetes using a targeted metabolomic approach. *Diabetes.* **62,** 639-648

69. Lanza, I.R., Zhang, S., Ward, L.E., Karakelides, H., Raftery, D., and Nair, K.S. (2010) Quantitative metabolomics by H-NMR and LC-MS/MS confirms altered metabolic pathways in diabetes. *PLoS One.* **5,** e10538

70. Mihalik, S.J., Goodpaster, B.H., Kelley, D.E., Chace, D.H., Vockley, J., Toledo, F.G., and DeLany, J.P. (2010) Increased levels of plasma acylcarnitines in obesity and type 2 diabetes and identification of a marker of glucolipotoxicity. *Obesity (Silver Spring).* **18,** 1695-1700

71. Cefalu, W.T. (2006) Animal models of type 2 diabetes: clinical presentation and pathophysiological relevance to the human condition. *ILAR J.* **47,** 186-198

72. Rees, D.A., and Alcolado, J.C. (2005) Animal models of diabetes mellitus. *Diabet.Med.* **22,** 359-370

73. Prentki, M., Matschinsky, F.M., and Madiraju, S.R. (2013) Metabolic Signaling in Fuel-Induced Insulin Secretion. *Cell.Metab.*

74. Vasu, S., McClenaghan, N.H., McCluskey, J.T., and Flatt, P.R. (2013) Mechanisms of toxicity by proinflammatory cytokines in a novel human pancreatic beta cell line, 1.1B4. *Biochim.Biophys.Acta.*

75. Vasu, S., McClenaghan, N.H., McCluskey, J.T., and Flatt, P.R. (2013) Cellular responses of novel human pancreatic beta-cell line, 1.1B4 to hyperglycemia. *Islets.* **5,**

76. Ravassard, P., Hazhouz, Y., Pechberty, S., Bricout-Neveu, E., Armanet, M., Czernichow, P., and Scharfmann, R. (2011) A genetically engineered human pancreatic beta cell line exhibiting glucose-inducible insulin secretion. *J.Clin.Invest.* **121,** 3589-3597

77. Straub, S.G., and Sharp, G.W. (2002) Glucose-stimulated signaling pathways in biphasic insulin secretion. *Diabetes Metab.Res.Rev.* **18,** 451-463

78. Jitrapakdee, S., Wutthisathapornchai, A., Wallace, J.C., and MacDonald, M.J. (2010) Regulation of insulin secretion: role of mitochondrial signalling. *Diabetologia.* **53,** 1019-1032

79. MacDonald, M.J., Longacre, M.J., Stoker, S.W., Brown, L.J., Hasan, N.M., and Kendrick, M.A. (2008) Acetoacetate and beta-hydroxybutyrate in combination with other metabolites release insulin from INS-1 cells and provide clues about pathways in insulin secretion. *Am.J.Physiol.Cell.Physiol.* **294,** C442-50

80. MacDonald, M.J. (2007) Synergistic potent insulin release by combinations of weak secretagogues in pancreatic islets and INS-1 cells. *J.Biol.Chem.* **282,** 6043-6052

81. MacDonald, M.J., Fahien, L.A., Brown, L.J., Hasan, N.M., Buss, J.D., and Kendrick, M.A. (2005) Perspective: emerging evidence for signaling roles of mitochondrial anaplerotic products in insulin secretion. *Am.J.Physiol.Endocrinol.Metab.* **288,** E1-15

Chapter 2. METHOD DEVELOPMENT FOR LIPID ANALYSIS.

INTRODUCTION

The importance of lipids in insulin secretion. Lipids are a class of biomolecules that are diverse in structure and function. Eukaryotic cells can have over a dozen classes of lipids, where each class can have hundreds of individual molecular species (1). Lipids have multiple functions; they not only form the lipid bilayer and cellular matrix but also act as storage for energy sources and provide signaling molecules (1).

Lipid signals are of great important in insulin secretion and β- cell function. Glucose stimulated insulin secretion is known to be mediated through glucose metabolism which stimulates the generation of lipid signals that facilitate insulin exocytosis (2). Short term exposure of β- cells to fatty acid will generate lipid signals that contribute to the amplification of glucose stimulated insulin secretion (3, 4). On the other hand, long term exposure to fatty acid can contribute to β- cell dysfunction and impairment of insulin secretion (5-7).

Glycerolipids and glycerophospholipids are the most abundant lipid classes in cells. They can be thought of as the linkage between glucose and fatty acid. Their synthesis starts by the condensation between glycerol-3-phosphate and acyl-CoA to form lysophophatidic acid (LPA), which then forms other glycerolipids/glycerophospholipids (figure 1). Some glycerolipids have been suggested to act as a signal for insulin secretion (5). Ceramides, on the other hand, are part of the sphingolipid class, and are known to induce β- cell apoptosis (8). Fatty acid amides are a novel class of lipids that were recently discovered in neuronal cells and involve the linkage between a fatty acid and an amino acid like glycine and taurine (9). N-palmitoyl glycine and acyl-taurines were recently shown to increase calcium flux in neuronal cells (10) and β- cells (11) respectively. Acyl-carnitines are intermediates in the fatty acid oxidation pathway and are known to be a marker for insulin resistance and type 2 diabetes (12). The balance between fatty acid oxidation and esterification into lipids is crucial for insulin secretion (13) . The structure and the metabolic pathways for lipid classes of interest to β- cell signaling and GSIS are shown in figures 1 and 2.

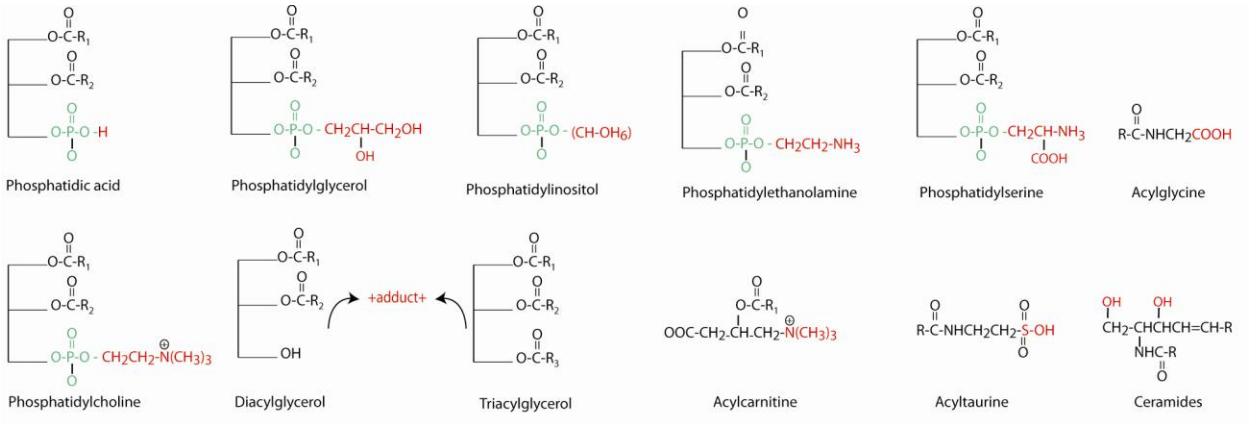

Figure 2-1: Chemical structure of different lipids classes

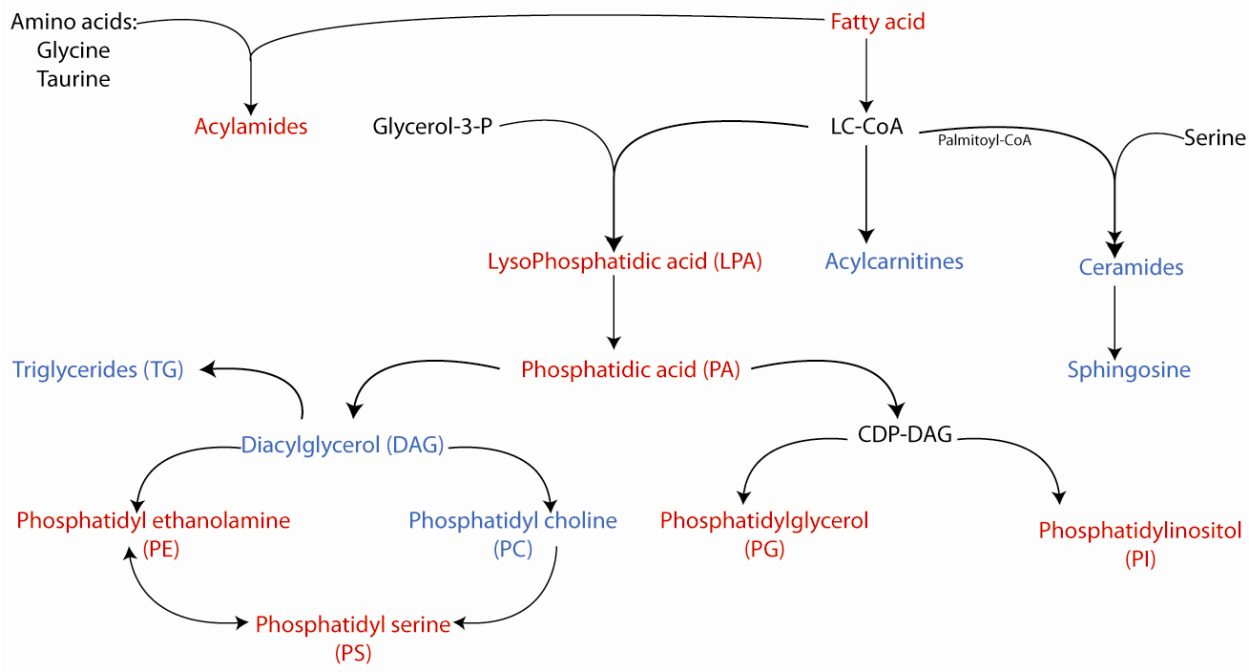

Figure 2-2: Metabolic pathways for different lipids classes. Red lipids can be detected in negative mode ionization mode; blue lipids can be detected in the positive mode ionization mode.

Separation and detection of non polar metabolites. The analysis and detection of lipids has improved dramatically in recent decades. In the 1980s, lipid classes were mainly separated by thin layer chromatography (TLC) followed by the determination of the whole total fatty acid composition using gas chromatography coupled to MS. This method was widely applied but it suffered from low throughput and the need of high sample quantity. It also does not differentiate phospholipid species within each spot (14). In the 2000s, global profiling of lipids using the total extract became feasible using high

resolution mass spectrometry (1). The application of mass spectrometry increased throughput of lipid analysis and provided a wealth of detailed information about different lipid species. Global profiling of lipids can be performed in both negative and positive mode ESI-MS, with different classes of lipids appearing in each ion mode depending on their ionizable head group (figure 2).

Although lipid extracts can be injected directly into the MS using the shotgun lipids approach (15), this technique suffers from high ion suppression of less abundant lipids and the difficulty of lipid identification. Performing flux experiments using labeled isotope nutrients further increases the sample complexity because it increases the number of lipids isotopes and requires a significant separation of lipid species to avoid overlap of masses. The two main methods for lipid separation are normal phase LC and reversed phase LC. Normal phase LC separates lipids classes based on their head group, while reversed phase LC separates based on the chain length of the fatty acid. Hydrophilic interaction liquid chromatography (HILIC) provides similar separation characteristics to normal phase chromatography, but with more convenient coupling to a mass spectrometer, especially when ESI is used (16) (figure 3). Different lipid classes were successfully separated using HILIC (17-19); however, it yields poor peak shape for many lipid classes and certain classes co-elute, which complicates identification. Reversed phase separation was successfully implemented for global lipid profiling (20, 21); however, long gradients (more than 60 minutes) were required to obtain good separation and peak shape. Two dimensional LC approach was used to separate lipids classes first using a normal phase column (22) or by solid phase extraction (21), followed by fractionation and injection into a RPC column. Although this approach allowed the identification of low abundant species, like phosphatidyl serine, it suffers from low throughput and complexity of data analysis.

Simultaneous extraction of polar and non polar metabolites. Polar and non polar metabolites are known to modulate insulin secretion (see chapter 1 for details), thus analyzing those diverse classes are equally important in understanding insulin secretion. Undirected metabolomics also requires an analysis of as many metabolites as possible, so it requires unbiased metabolite extraction and detection methods.

The traditional methods for lipid extraction from biological tissues use a two-layer solvent method that separates the lipid rich organic phase from the protein and salt rich aqueous phase. Methanol, chloroform and methyl tert- butyl ether (MTBE) are the most common organic solvents used in these two phase extraction methods (23). These extraction methods are not designed for the extraction of polar metabolites and have low throughput since they involve phase separation, drying and

reconstitution. Recent work tried to recover polar metabolites from the aqueous layer to allow for the simultaneous extraction of both polar metabolites and lipids (24). This method suffered from low throughput because of multistep extraction, phase separation and drying. Evaporation of the aqueous layer was not practical because of the high level of water and proteins in this layer. Relatively high temperature and long time used in the aqueous layer evaporation as well as the increased levels of proteins and enzyme activity, might lead to degradation of some metabolites. Probably these complications led to the reporting of acyl carnitines and fatty acids as a representative of the polar fraction, while nucleotides and metabolites in the central carbon metabolism pathway were ignored. A single-layer extraction using 100% methanol was reported to achieve similar lipid recovery to the two layer traditional methods (25), however the ability of this method to recover or analyze polar metabolites extraction was not addressed. Recent work described undirected metabolomics platform using single extraction solvent for polar and non polar metabolites (26). However, the lipids reported using the reversed phase analysis were mainly polar-lipids, such as acyl-amides and carnitines, and no attempt was made to analyze other moderately or highly non polar lipids such as most glycerolipids.

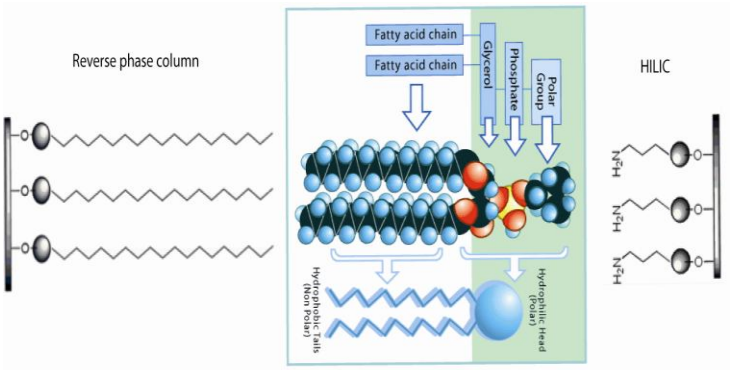

Figure 2-3: lipid separation mechanism using HILIC or RPC chromatography

To the best of our knowledge there is no comprehensive study that described simultaneous extraction of polar metabolites such as glycolysis and TCA cycle together with non polar metabolites such as glycerolipids, ceramides and acylamides. Also, there is no study that has evaluated different

chromatographic conditions such as column stationary phase, temperature and pH on lipid separation and detection. Most methods reported using C18 column, with acidic or uncontrolled mobile phase pH and a set temperature, without reporting the reason of those adjusted parameters.

Thus we decided to develop and optimize an LC-MS based platform that can be used for extracting and analyzing lipids and polar metabolites from adherent cell lines. Lipids of interest were those classes that are known to be involved in insulin secretion such as glycerolipids, acyl- carnitines, ceramides and acyl amides. We evaluated different methods for lipid separation, mainly using a HILIC column (amino propyl) that is used for polar metabolites analysis as well as several reversed phase columns (RPC) with different stationary phases (C18, C8 and C30). HILIC separation showed a superior performance compared to RPC in phosphatidyl serine class separation, while C18-RPC columns showed improved separation for most other lipids classes. C18 showed better separation efficiency than C8 for phosphatidic acid and tripalmitin. C30 showed higher resolution than C18 in separating positional isomer lipids, which could be useful if such resolution is important to biological interpretation, but it otherwise complicates metabolite profiling. Then we decided to further optimize a C18 separation method by evaluating different operating conditions including temperature and mobile phase pH and their effect on lipids separation and stability. Optimizing the separation method was followed by screening different extraction solvents for lipid extraction efficiency including MTBE or combinations of methanol and chloroform. Single layer extraction solvent was as efficient as the traditionally used 2 layer extraction solvents in extracting most lipids, with the exception of highly non-polar lipids.

MATERIALS AND METHODS:

Materials. INS-1 cells (832/3) were kindly provided by Dr. Christopher Newgard (Sarah W. Stedman Nutrition and Metabolism Center, Duke University, Durham, NC). All chemicals were purchased form Sigma-Aldrich (St. Louis, MO) unless otherwise noted. RPMI media, fetal bovine serum, 4-(2-hydroxyethyl)-1-piperazineethanesulfonic acid (HEPES), and penicillin-streptomycin were purchased from Invitrogen Corp, (Carlsbad, CA).

Cell culture. INS-1 832/13 cells were cultured in RPMI supplemented with 2 mM glutamine, 1 mM sodium pyruvate, 10% FBS, 10 mM HEPES, 100 U/mL penicillin, 100 µg/mL streptomycin, 250 ng/mL amphotericin B, and 50 µM β-mercaptoethanol. Cells were plated at a density of ~14 x 103 cells/cm2 and grown in 6 cm culture dishes at 37 °C and 5% CO2 in a humidified atmosphere to ~70% confluence. Krebs-Ringer-HEPES buffer (KRHB) was prepared containing 20 mM HEPES, 118 mM NaCl, 5.4 mM KCl, 2.4 mM CaCl2, 1.2 mM MgSO4, and 1.2 mM KH2PO4 and was adjusted to pH 7.4 with NaOH. Cells were incubated with 500 uM palmitic acid in KRHB for 45 minutes before being quenched. Each cell plate was extracted with 400 ul x two times of 8:1:1 methanol: chloroform: water. All extracts were pooled together to form a pooled sample for evaluation of different columns, temperatures and pH values. For comparing different extraction solvents, equal volumes of methanol were added to the cell plates and cells were transferred to a glass tube. Two parts of chloroform were added to the methanol extract for the Folch method, or two parts of MTBE were added for the MTBE method.

LC-MS. Reversed phase columns (RPC) were tested in pairs depending on their particle size: Capcell, C18 column vs. Thermo, C-30 column (both are 3 µm x 150 mm x 2 mm) and Waters C18 column vs Waters C-8 column (both are 2.5 µm x 150 mm x 2 mm). Luna NH2 (3 µm x 150 mm x 2 mm) was tested for the HILIC mode of separation. Solvents for reversed phase separation were as follows: A is (40% water, 40% Acetonitrile and 20 % methanol) and B is (80% isopropanol and 20% methanol). Both solvents are supplemented with 0.1 % formic acid and 0.028% ammonium hydroxide (MS grade) unless otherwise mentioned in the pH adjustment. The gradient for RPC started at 0% B and increased to 60% B in 10 minutes, then increased to 80% in 40 minutes, then increased to 100%B in 5 minutes, than held at 100% B for 10 minutes before going back to 0 % B in 0.1 minute and holding for 15 minutes. Temperature was kept at 35°C for the whole run unless otherwise mentioned. Detection was performed on an Agilent Technologies LC/MSD TOF using a dual electrospray ionization (ESI) source in both negative and positive ion modes.

RESULTS AND DISCUSSION:

Extract from β- cell line (INS-1) cells was pooled and analyzed using LC-MS. Different columns were tested including amino-propyl HILIC, C18, C8 and C30 reversed phase columns. Different chromatographic conditions such as temperature and pH were evaluated to identify the best operating condition for analyzing different lipid classes.

Method development for lipid analysis

HILIC separation of lipids

Lipids were separated using a Phenomenex luna NH2 HILIC column, which is the same column used for polar metabolite analysis (26-28). Phospholipid classes were separated based on the polar group as described in the introduction. Most lipid classes such as phosphatidylethanolamine (PE) or phosphatidylglycerol (PG) were unretained and eluted very early in the chromatogram with bad peak shape. An exception for this was the phosphatidylserine (PS) and phsophatidylinositol (PI) lipid classes which were more retained on the HILIC column than other lipids and yielded good peak shape (Figure 2-4).

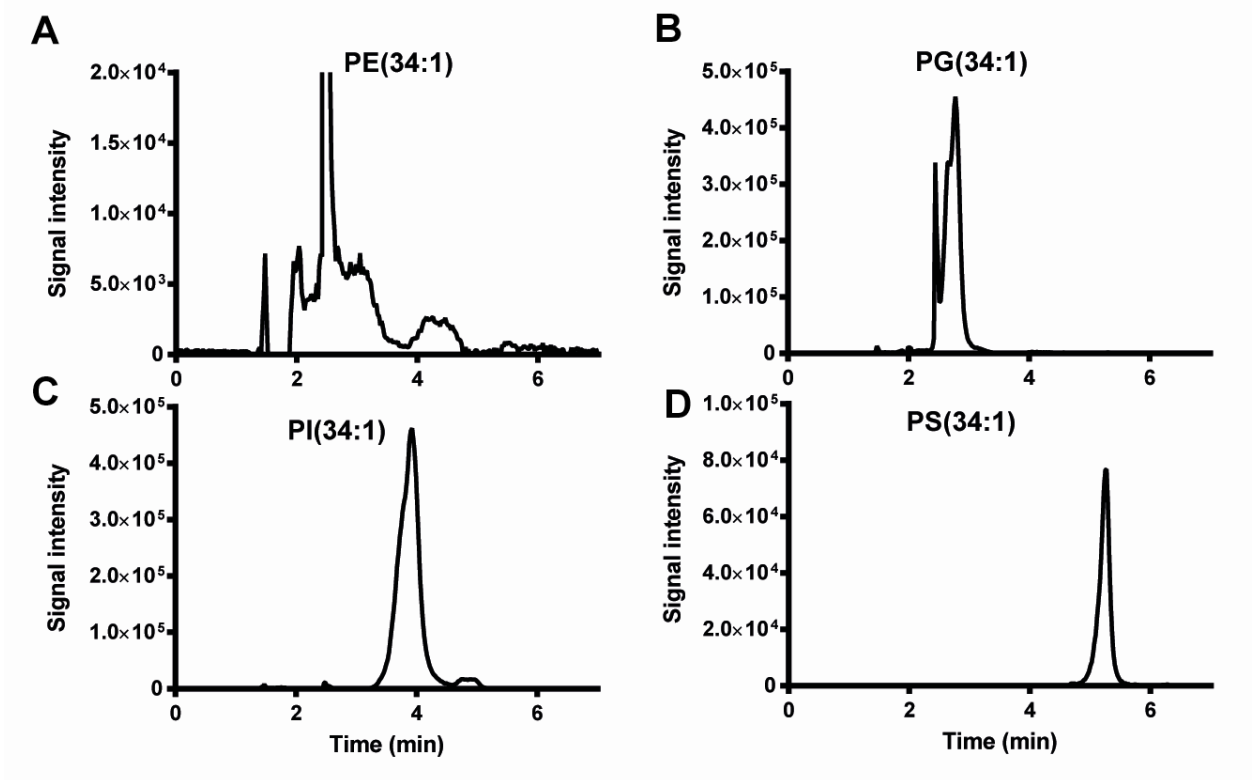

Figure 2-4: Chromatogram showing different lipid classes separation using HILIC column.

Lipid species plotted here are (34:1), which are usually the most abundant lipid species in all classes. These lipid species are representative for the other lipids in their class, which will elute at nearly the same retention time with very similar peak shape. The ability to separate PS lipids from other lipids using HILIC provides several advantages. First, it is a low abundant lipid that will strongly benefit from its separation away from highly abundant lipids like PE or PC. Second, PS can be only synthesized from PC and PE (Figure 2-2), which are very large pools. The type of PS species formed from PE and PC cannot be anticipated, unlike the rest of glycerolipids species, since fatty acids are not directly connected to PS. Third, it can be analyzed simultaneously with polar metabolites without the need for a separate separation method.

Reversed phase separation

To investigate a better separation technique for the rest of lipid classes, we tested several reversed phase columns including C8, C18 and C30. The same injection volume of pooled sample was injected on different columns using the same LC gradient. Peak shape for different lipid species was the main factor in giving cause to prefer one stationary phase than the other. The m/z values for representative moieties from each lipid class were used to generate extracted ion chromatograms and their peak shapes were investigated. INS-1 cells were incubated with palmitic acid, thus representative lipid species shown here mainly contain the palmitate moiety.

C18-vs C8 column

Xbridge BEH C18 and C8 columns (2.5 µm x 150 mm and 2 mm) were compared for their efficiency in lipid separation. Because the same LC gradient was applied for both columns, lipids eluted earlier on C8 compared to C18 (Figure 2-5A and B). Different lipid classes showed comparable peak shape between both columns (Figure 2-5C and D), however some lipids of interest like dipalmitoyl phosphatidic acid (Figure 2-5E and F), and tripalmitin (Figure 2-5G and H) showed poor peak shape on the C8 column that was consistent in several replicates. This might be attributable to the shorter chain length of C8 compared to C18, which might allow more direct (and undesirable) interaction of the lipid with the surface of with the silica particles.

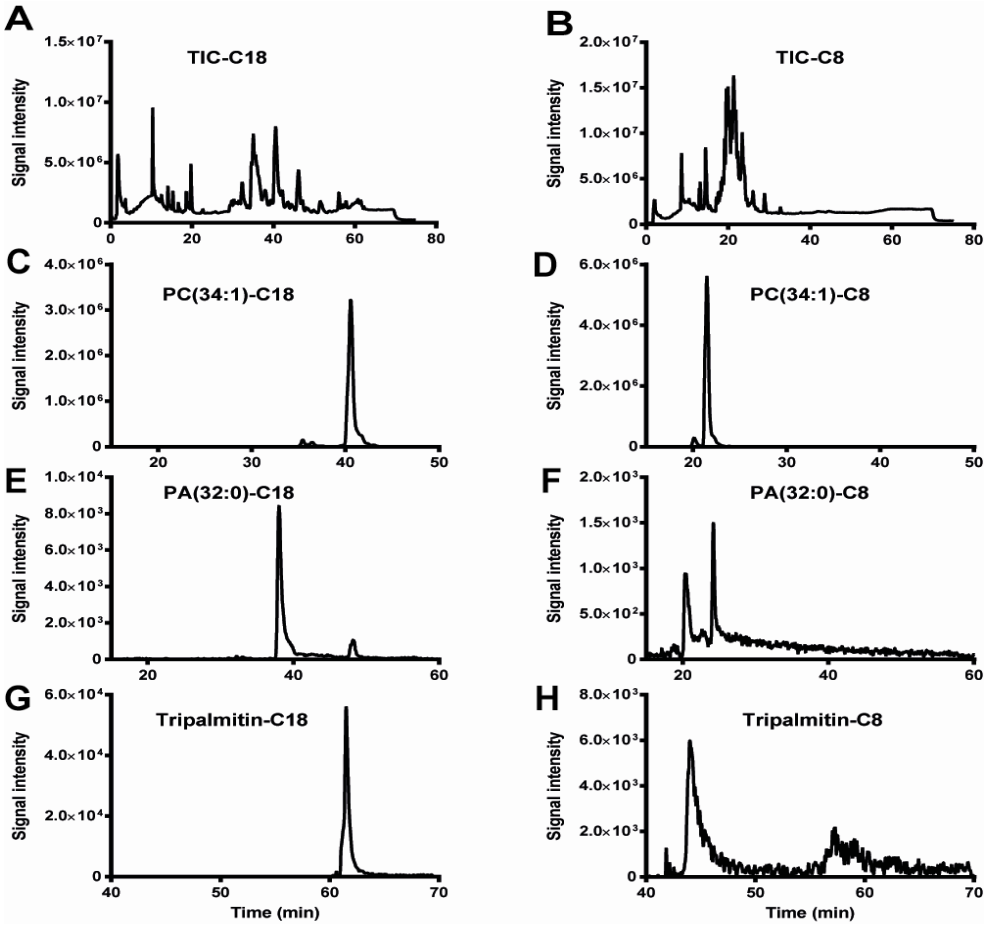

Figure 2-5: Chromatograms comparing C8 versus C18 column in separating different lipids species.

C18 and C30 columns

To further compare different reversed phase stationary phases, a C18 column was compared with a C30 column with the same dimension (3 µm x 150 mm and 2 mm). As expected, the longer hydrophobic chains of C30 column increased the retention time for most lipids (Figure 2-6). C30 offered better resolution than C18 for many lipid species and allowed the separation of lipids structural isomers (Figure 2-6C-E). This is in agreement with the manufacturer brochures and other data that support the superiority of this stationary phase in separating lipid isomers (29). Although isomer separation is very useful for lipid identification, it provides more complexity to a global metabolomics study. The goal of global lipid profiling is to separate all lipid classes that range from highly polar such as acyl amides to the most non polar such as triglycerides. The outcome of using the C30 column would be a distorted peak shape as shown in (Figure 2-6C-E), unless the LC method was optimized to resolve those structural isomers. A tailored method to separate one lipid isomer might not be suitable for another lipid, and

would result in a time consuming and impractical strategy for global lipid profiling. Bad peak shape will also complicate undirected analysis, where automated feature or peak selection is performed by software. Having shoulders in a peak will result in more errors in peak selection and improper quantitation.

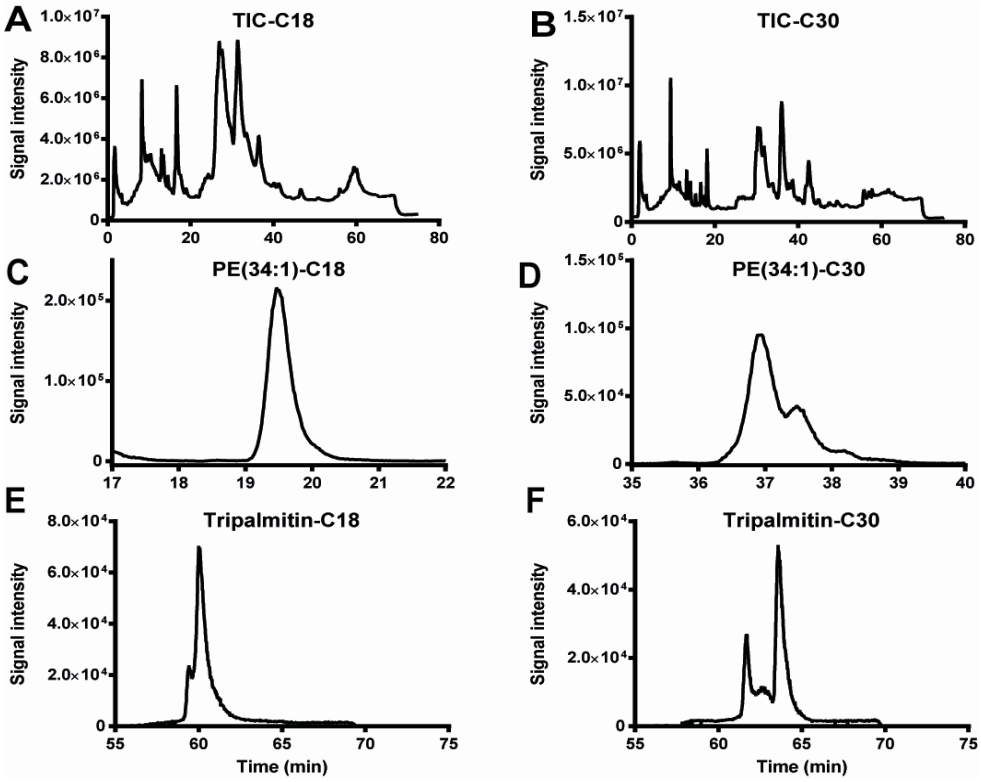

Figure 2-6: Chromatograms comparing C8 versus C18 columns in separating different lipid species

As a conclusion, we showed a brief comparison between different reversed phase stationary phases like C18, C8 and C30 and their capabilities for separating different classes of lipids. C18 reversed phase stationary phase represents a reasonable-compromise chain length that enabled good separation of lipid classes with varying polarities. Further optimization for the chromatography conditions like pH and temperature using a C18 column are described in the next sections.

Effect of temperature on lipid separation and detection using C18 column

To investigate the effect of temperature on lipids separation, we examined two factors which are peak shape and lipid stability. The peak shape factor was determined by the full width at half maximum (FWHM) value for different lipids, while the stability of lipids was represented by the peak area of lipids at different temperatures. Pooled samples were injected on a C18 column at different column temperatures (20, 35, 45 and 60 °C). The FWHM was plotted for each metabolite at those

temperatures (figure 7 for negative mode lipids and figure 8 for positive mode lipids). Lower temperature increased peak width for most investigated lipids (figures 7, 8, 9).

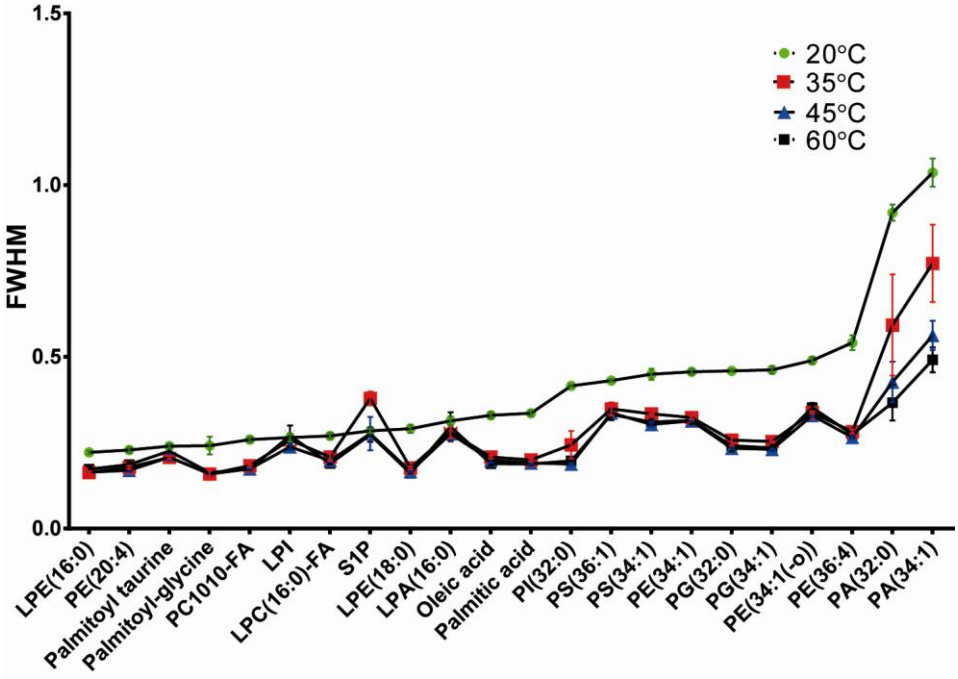

Figure 2-7: Effect of temperature on the peak width of lipids ionized on negative mode MS.

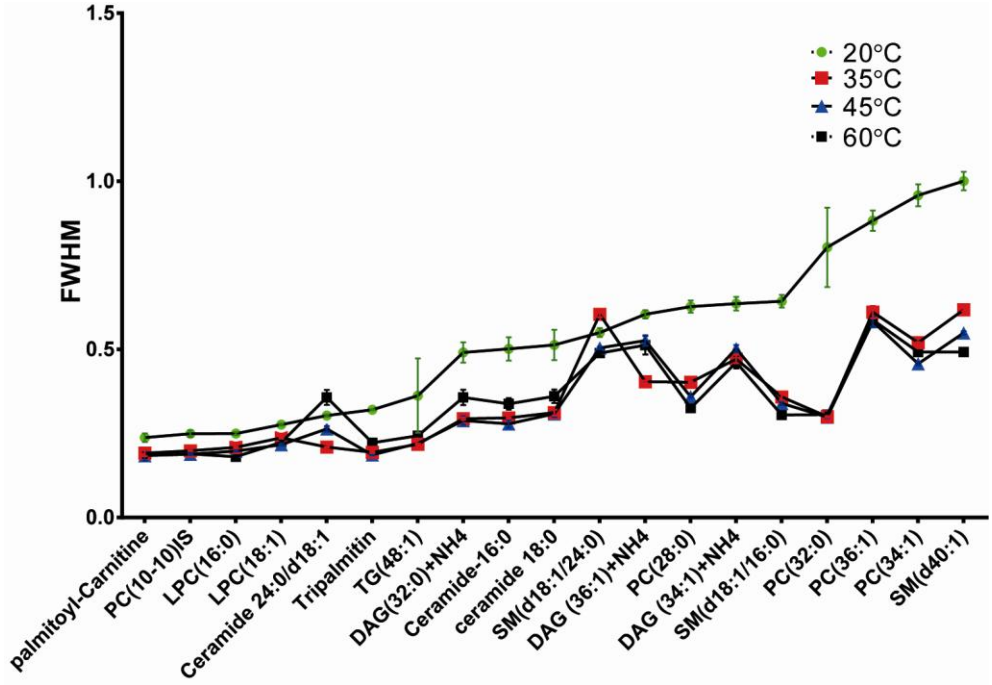

Figure 2-8: Effect of temperature on the peak width of lipids ionized on positive mode MS.

The decrease in peak width, which is also a measure of column efficiency, can be attributed to several factors based on the Van deemter equation :

$$H = A + \frac{B}{u} + C.u$$

$$H = 2\lambda\, d_p + 2\,\frac{\gamma D_m}{u} + \frac{\omega d_p^2}{D_m}\, u$$

Where H is plate height, λ is particle shape (with regard to the packing), dp is particle diameter, G, ω, and R are constants, Dm is the diffusion coefficient of the mobile phase. Based on this equation, increasing temperature will increase the diffusion coefficient of the mobile phase which will increase the B term. This is not very important in the case of high flow rate, but it will decrease the C term which will decrease the plate height, causing the observed improvement in peak shape and increase in column efficiency. Also, at high temperature, the kinetics of secondary interactions, which are often responsible for peak tailing are probably accelerated, thus reducing the tailing (30). Beside the improvement of peak shape, increasing temperature decreased the retention time of lipids (figure 9).

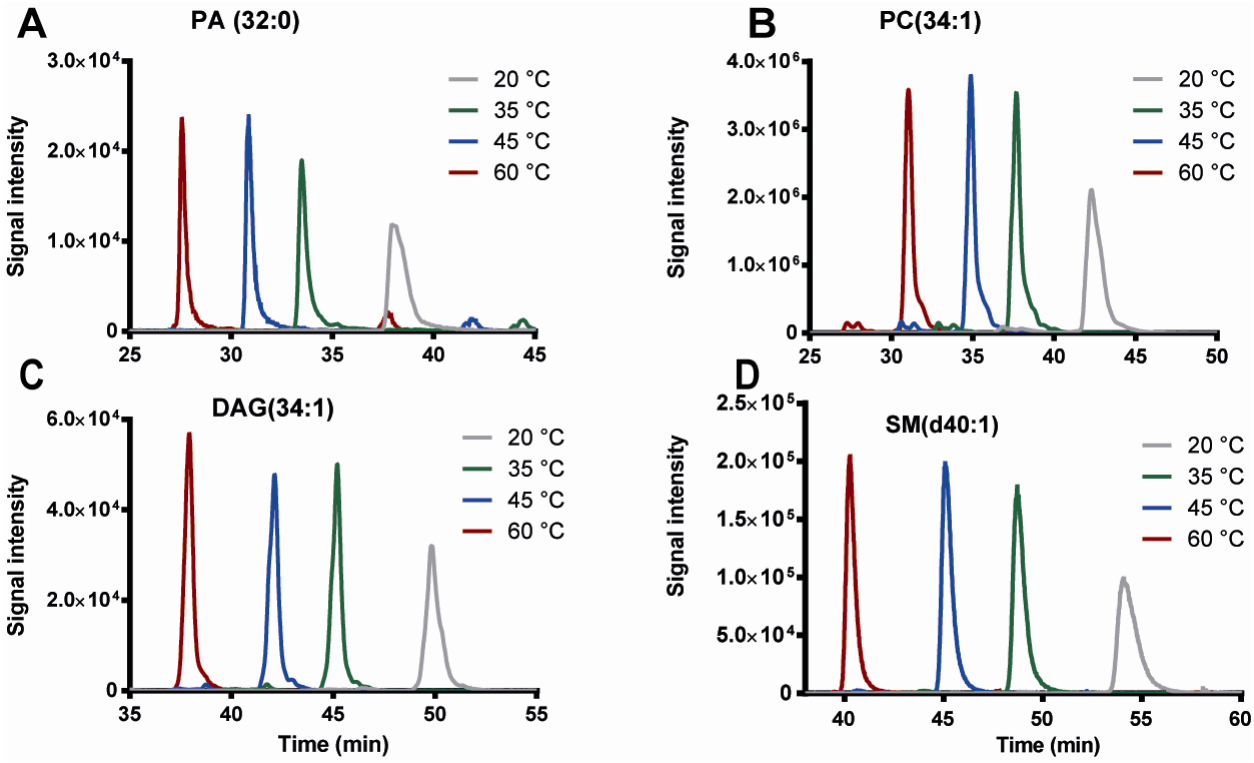

Figure 2-9: Chromatogram showing the effect of temperature on retention time and peak shape of several lipid classes.

This decrease in retention time can be explained by Van't Hoff equation (2):

$$\ln K = \frac{\Delta G}{RT} = \ln(k' + 1) \text{ (2)}$$

$$log\ k = -\frac{\Delta H}{2.3RT} + \frac{\Delta S}{2.3R} + log\ \Phi \text{ (2)}$$

Where K or k' are the retention factor or the capacity factor respectively, G is the Gibbs free energy, R is the universal gas constant, T is the absolute temperature, H and S are the enthalpy and the entropy respectively and Φ is the phase ratio of the system. This equation predicts that the retention factor is inversely proportional to temperature. This reduction in retention time is important since it improves the resolution, allows shortening the analytical run time and increasing the analysis throughput.

The previous results showed that higher temperature was useful to obtain a good peak shape and faster elution of lipids; however the effect of increasing temperature on lipids stability should be investigated. Several lipids were quantified and representative lipids were plotted (figure 10). Lower temperatures caused a great variation in hydrophobic lipids, like triglycerides and DAG. This can be attributed to the incomplete elution of those trigylcerides at low temperatures. On the other hand, high temperatures like 60°C decreased the signal for the polar lyso form of lipids like LPC and LPE. This reduction in signal is presumably because of increased degradation of those labile species, however further investigation is needed for ruling out any possible reason for this decreased signal. Therefore the optimum temperature is ~ 45° C, which will achieve good resolution and peak shape without reducing the signal of labile lipids.

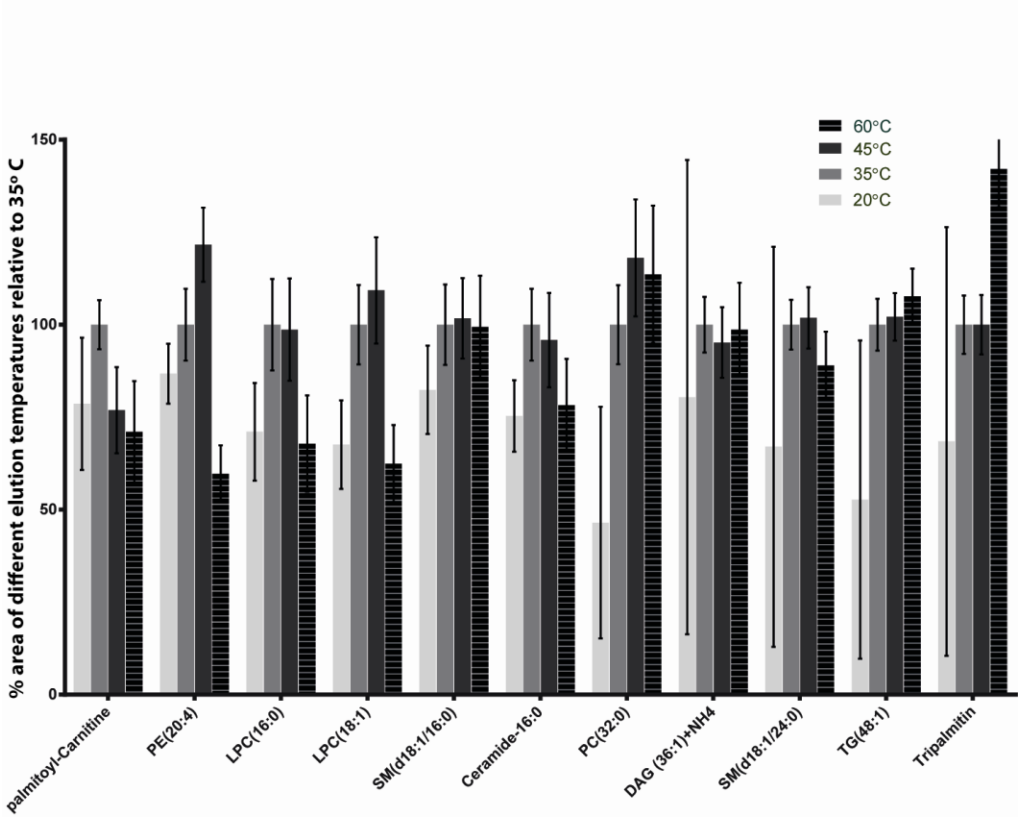

Figure 2-10: The effect of temperature on lipid quantification.

Effect of pH on lipid separation and detection using C18 column

To further optimize the LC-MS method for lipid separation and detection, the effect of changing mobile phase pH was investigated. Ammonium hydroxide percentage in the mobile phase (A and B) was increased from 0.028 % to 0.2 or 0.4 %, achieving approximate pH values of 2, 4 and 8 respectively (figure 11C). The pH was measured in the aqueous fraction of the mobile phase before the addition of any organic solvent.

Increasing the mobile phase pH reduced the signal for many lipids like sphingosine 1-phosphate and several lysophospholipids and distorted the peak shape of lipid species like LPA (figure 11).

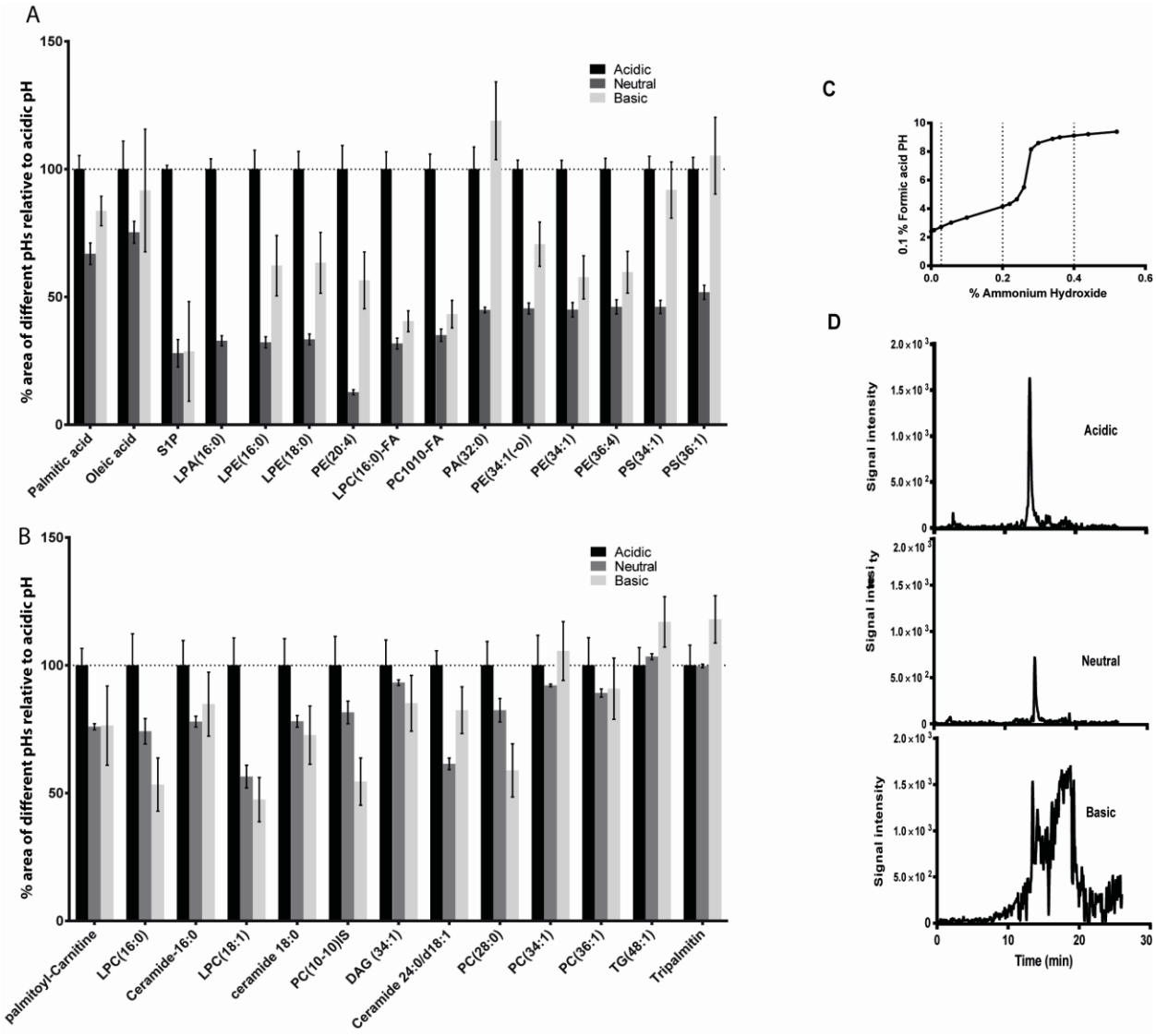

Figure 2-11: The effect of pH on lipids intensity. (A) Lipids ionized in negative mode. (B) Lipids ionized in positive mode. (C) pH titration curve (D) pH effect on LPA separation

On the other hand, some lipid classes, mainly those that contain several hydroxyl groups, did show enhanced ionization with basic pH (figure 13) in the negative ionization mode. This was true for acylamides, phosphatidylglycerol and phosphatidyl inositol.

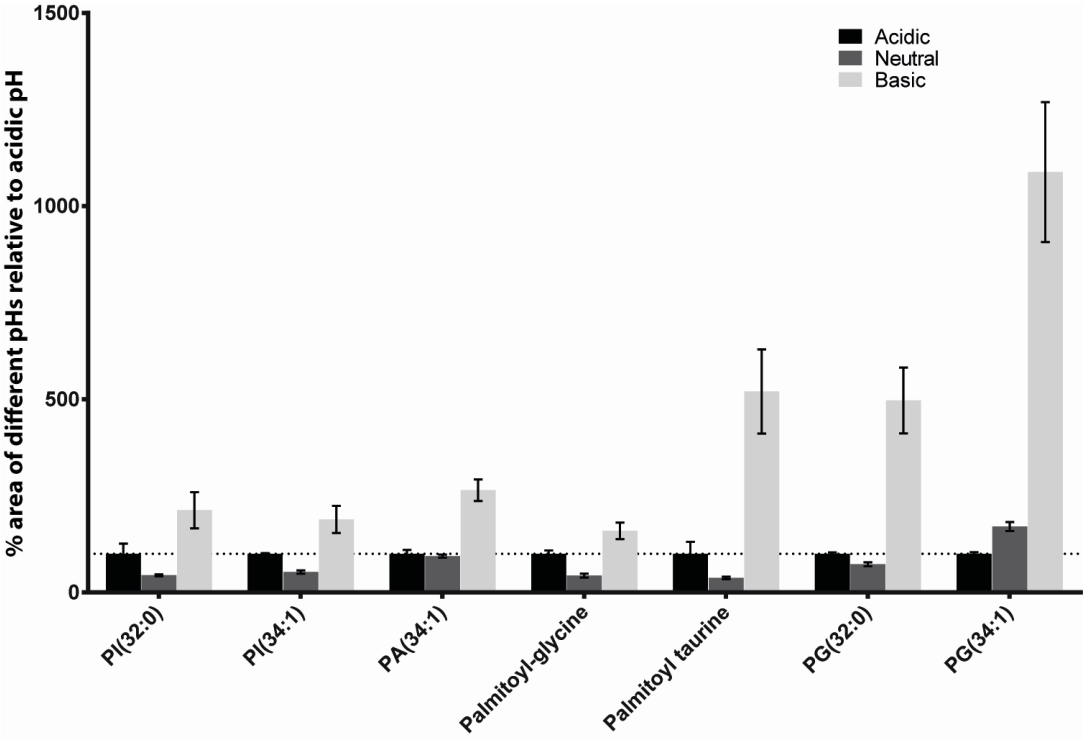

Figure 2-12: Showing the enhancement of ionization for some lipid classes under basic pH.

In conclusion, the choice of mobile phase temperature and pH should be carefully considered since both affect lipid separation and detection. A higher column temperature helped to improve the peak shape of lipids and shorten the LC run. However, high temperatures such as 60°C could lead to degradation of labile lipids such as the lyso-forms, and thus a moderate temperature should be used. Regarding the mobile phase pH, acidic pH provides good peak shape for all lipid classes and good signal intensity for the majority of lipids, thus acidic pH is the mainly used pH in most lipidomics analysis (21, 31, 32). However, the effect of this acidic pH in suppressing the ionization of some lipids classes such as PG and acylamides was not reported before. The later classes could benefit from increasing mobile phase pH, which will enhance their ionization but at the expense of losing some lipids like LPA. For global metabolomics purposes, acidic pH will be the pH of choice, unless a targeted analysis for some lipid classes was the goal, then the best pH that provides higher signal should be chosen.

Lipids extraction

Lipids have been mainly extracted from biological tissues with a two layer method that involves chloroform or MTBE; however, this extraction method is not designed for the extraction of polar metabolites and has low throughput because it involves phase separation, drying and reconstitution. The goal was to investigate if a single extraction solvent for both polar and lipids could achieve comparable results to the specialized lipid extraction methods. The Folch method that involves 2 parts of chloroform and 1 part of methanol was compared to the MTBE method that replaces chloroform with MTBE solvent. Both methods gave comparable results (figure 13) in agreement with other published data (23). This was followed by comparing the MTBE method to the 1 layer extraction solvent originally used for polar metabolites (8:1:1 methanol: chloroform: water) (33) . Lipids were plotted in order of elution time; the one layer extraction solvent provided comparable results to the MTBE method in most lipid classes. The one layer solvent showed better results in polar lipids like LPE and S1P; on the other hand, hydrophobic lipids like TG showed lower extraction efficiency with this one layer extraction solvent. These results demonstrate the efficiency of this one layer extraction solvent for global metabolites extraction for adherent cells. The results also highlight the limitation of this method for the extraction of highly non-polar lipids.

The ability of one layer extraction solvent to extract both polar and most non-polar metabolites is useful for undirected analysis and also for monitoring nutrients flux in different pathways. Undirected analysis requires unbiased extraction solvent that can extract most metabolites, ranging from highly polar to non polar metabolites. Any bias in extraction will lead to incomplete undirected metabolomics approach. This unbiased extraction approach was also adopted by other groups, though different extraction solvent was used for undirected metabolomics (26). Having one extraction solvent is important in during stable isotopic flux monitoring, because this will allow direct monitoring of the utilization of metabolites in several pathways and provide direct linkage between them. Performing the experiment twice for different extraction solvents might lead to incorrect replication of the same experiment besides being more time and money consuming.

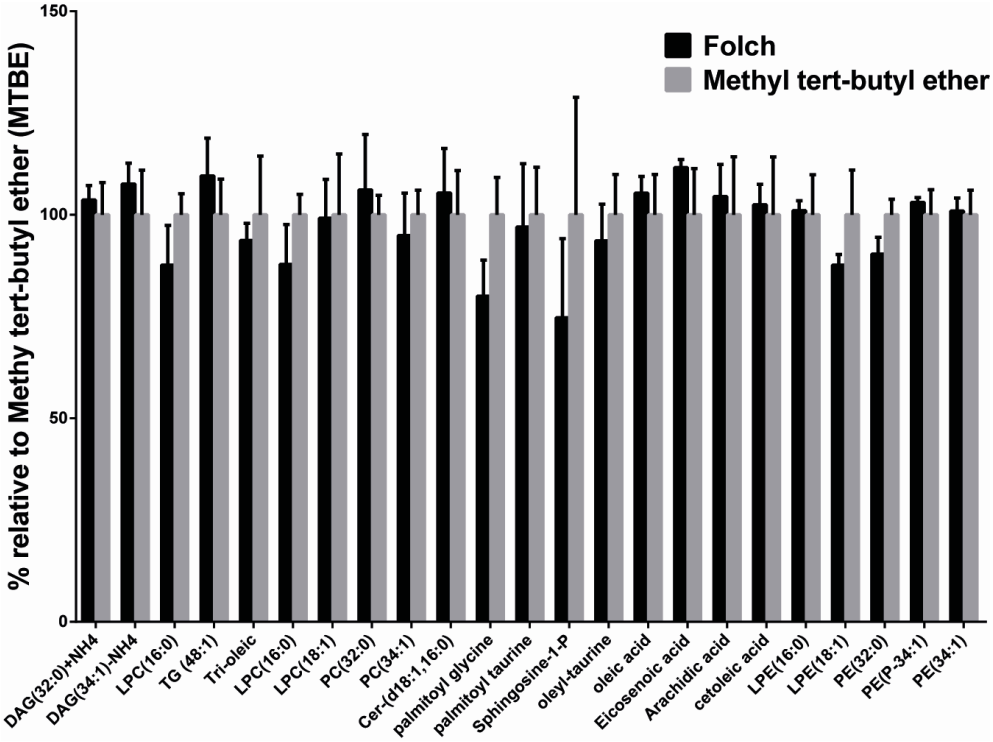

Figure 2-13: Comparing the MTBE with Folch method for lipid extraction

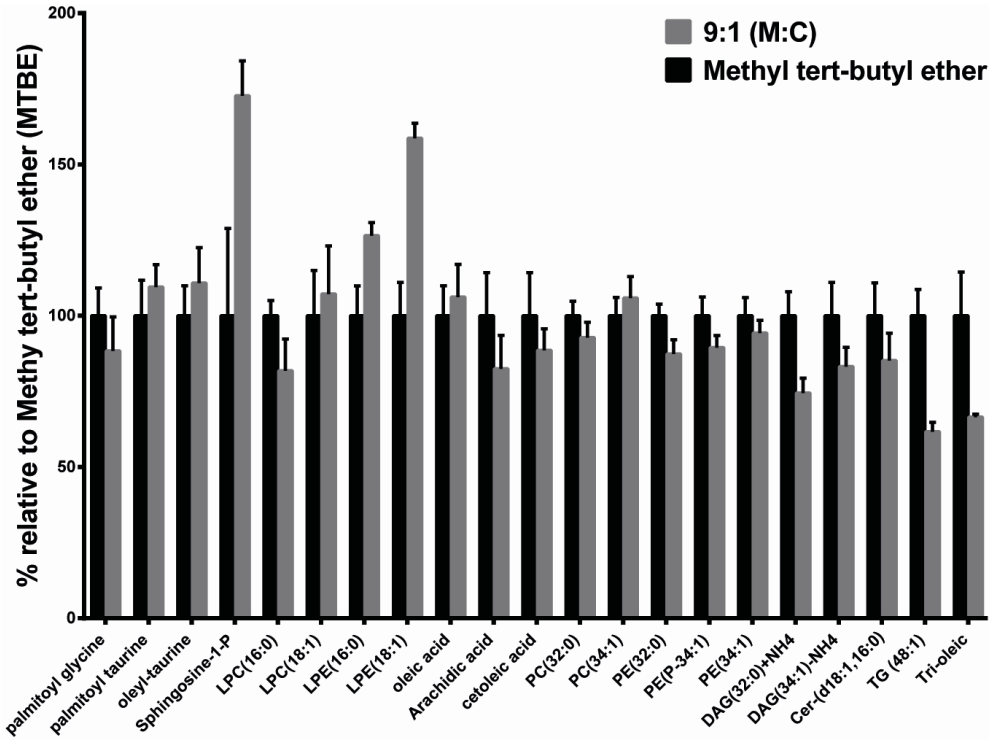

Figure 2-14: Comparing the MTBE with 8:1:1 method for lipid extraction

CONCLUSION

We developed a method for comprehensive polar and non polar metabolite analysis from adherent cell lines. One single extraction step provided good coverage of polar metabolites (33) as well as different lipid classes. Highly non-polar lipids such as triglycerides will need dedicated extraction methods for lipids that will not be suitable for polar metabolites. We described a method for separating low abundant lipids such as PS simultaneously with polar metabolites using a HILIC column. We also optimized a method for different lipid classes' separation using a C18 column, with a temperature of 45°C and acidic pH as general conditions. Basic pH could be selected for specific classes such as PG and acylamides because of the improvement in their ionization.

REFERENCES

1. Shevchenko, A., and Simons, K. (2010) Lipidomics: coming to grips with lipid diversity. *Nat.Rev.Mol.Cell Biol.* **11,** 593-598

2. Nolan, C.J., Madiraju, M.S., Delghingaro-Augusto, V., Peyot, M.L., and Prentki, M. (2006) Fatty acid signaling in the beta-cell and insulin secretion. *Diabetes.* **55 Suppl 2,** S16-23

3. El-Assaad, W., Buteau, J., Peyot, M.L., Nolan, C., Roduit, R., Hardy, S., Joly, E., Dbaibo, G., Rosenberg, L., and Prentki, M. (2003) Saturated fatty acids synergize with elevated glucose to cause pancreatic beta-cell death. *Endocrinology.* **144,** 4154-4163

4. Parker, S.M., Moore, P.C., Johnson, L.M., and Poitout, V. (2003) Palmitate potentiation of glucose-induced insulin release: a study using 2-bromopalmitate. *Metabolism.* **52,** 1367-1371

5. Prentki, M., and Madiraju, S.R. (2011) Glycerolipid/free fatty acid cycle and islet beta-cell function in health, obesity and diabetes. *Mol.Cell.Endocrinol.*

6. El-Assaad, W., Joly, E., Barbeau, A., Sladek, R., Buteau, J., Maestre, I., Pepin, E., Zhao, S., Iglesias, J., Roche, E., and Prentki, M. (2010) Glucolipotoxicity alters lipid partitioning and causes mitochondrial dysfunction, cholesterol, and ceramide deposition and reactive oxygen species production in INS832/13 ss-cells. *Endocrinology.* **151,** 3061-3073

7. Prentki, M., and Nolan, C.J. (2006) Islet beta cell failure in type 2 diabetes. *J.Clin.Invest.* **116,** 1802-1812

8. Lang, F., Ullrich, S., and Gulbins, E. (2011) Ceramide formation as a target in beta-cell survival and function. *Expert Opin.Ther.Targets.* **15,** 1061-1071

9. Tan, B., O'Dell, D.K., Yu, Y.W., Monn, M.F., Hughes, H.V., Burstein, S., and Walker, J.M. (2010) Identification of endogenous acyl amino acids based on a targeted lipidomics approach. *J.Lipid Res.* **51,** 112-119

10. Rimmerman, N., Bradshaw, H.B., Hughes, H.V., Chen, J.S., Hu, S.S., McHugh, D., Vefring, E., Jahnsen, J.A., Thompson, E.L., Masuda, K., Cravatt, B.F., Burstein, S., Vasko, M.R., Prieto, A.L., O'Dell, D.K., and Walker, J.M. (2008) N-palmitoyl glycine, a novel endogenous lipid that acts as a modulator of calcium influx and nitric oxide production in sensory neurons. *Mol.Pharmacol.* **74,** 213-224

11. Waluk, D.P., Vielfort, K., Derakhshan, S., Aro, H., and Hunt, M.C. (2013) N-Acyl taurines trigger insulin secretion by increasing calcium flux in pancreatic beta-cells. *Biochem.Biophys.Res.Commun.* **430,** 54-59

12. Schooneman, M.G., Vaz, F.M., Houten, S.M., and Soeters, M.R. (2013) Acylcarnitines: reflecting or inflicting insulin resistance?. *Diabetes.* **62,** 1-8

13. Herrero, L., Rubi, B., Sebastian, D., Serra, D., Asins, G., Maechler, P., Prentki, M., and Hegardt, F.G. (2005) Alteration of the malonyl-CoA/carnitine palmitoyltransferase I interaction in the beta-cell impairs glucose-induced insulin secretion. *Diabetes.* **54,** 462-471

14. Pulfer, M., and Murphy, R.C. (2003) Electrospray mass spectrometry of phospholipids. *Mass Spectrom.Rev.* **22,** 332-364

15. Han, X., Yang, K., and Gross, R.W. (2012) Multi-dimensional mass spectrometry-based shotgun lipidomics and novel strategies for lipidomic analyses. *Mass Spectrom.Rev.* **31,** 134-178

16. Buszewski, B., and Noga, S. (2012) Hydrophilic interaction liquid chromatography (HILIC)--a powerful separation technique. *Anal.Bioanal Chem.* **402,** 231-247

17. Zhu, C., Dane, A., Spijksma, G., Wang, M., van der Greef, J., Luo, G., Hankemeier, T., and Vreeken, R.J. (2012) An efficient hydrophilic interaction liquid chromatography separation of 7 phospholipid classes based on a diol column. *J.Chromatogr.A.* **1220,** 26-34

18. Zheng, L., T'Kind, R., Decuypere, S., von Freyend, S.J., Coombs, G.H., and Watson, D.G. (2010) Profiling of lipids in Leishmania donovani using hydrophilic interaction chromatography in combination with Fourier transform mass spectrometry. *Rapid Commun.Mass Spectrom.* **24,** 2074-2082

19. Schwalbe-Herrmann, M., Willmann, J., and Leibfritz, D. (2010) Separation of phospholipid classes by hydrophilic interaction chromatography detected by electrospray ionization mass spectrometry. *J.Chromatogr.A.* **1217,** 5179-5183

20. Gao, X., Zhang, Q., Meng, D., Isaac, G., Zhao, R., Fillmore, T.L., Chu, R.K., Zhou, J., Tang, K., Hu, Z., Moore, R.J., Smith, R.D., Katze, M.G., and Metz, T.O. (2012) A reversed-phase capillary ultra-performance liquid chromatography-mass spectrometry (UPLC-MS) method for comprehensive top-down/bottom-up lipid profiling. *Anal.Bioanal Chem.* **402,** 2923-2933

21. Sato, Y., Nakamura, T., Aoshima, K., and Oda, Y. (2010) Quantitative and wide-ranging profiling of phospholipids in human plasma by two-dimensional liquid chromatography/mass spectrometry. *Anal.Chem.* **82,** 9858-9864

22. Sommer, U., Herscovitz, H., Welty, F.K., and Costello, C.E. (2006) LC-MS-based method for the qualitative and quantitative analysis of complex lipid mixtures. *J.Lipid Res.* **47,** 804-814

23. Matyash, V., Liebisch, G., Kurzchalia, T.V., Shevchenko, A., and Schwudke, D. (2008) Lipid extraction by methyl-tert-butyl ether for high-throughput lipidomics. *J.Lipid Res.* **49,** 1137-1146

24. Chen, S., Hoene, M., Li, J., Li, Y., Zhao, X., Häring, H., Schleicher, E.D., Weigert, C., Xu, G., and Lehmann, R. (2013) Simultaneous extraction of metabolome and lipidome with methyl tert-butyl ether from a single small tissue sample for ultra-high performance liquid chromatography/mass spectrometry. *Journal of Chromatography A.* **1298,** 9-16

25. Zhao, Z., and Xu, Y. (2010) An extremely simple method for extraction of lysophospholipids and phospholipids from blood samples. *J.Lipid Res.* **51,** 652-659

26. Ivanisevic, J., Zhu, Z.J., Plate, L., Tautenhahn, R., Chen, S., O'Brien, P.J., Johnson, C.H., Marletta, M.A., Patti, G.J., and Siuzdak, G. (2013) Toward 'omic scale metabolite profiling: a dual separation-mass spectrometry approach for coverage of lipid and central carbon metabolism. *Anal.Chem.* **85,** 6876-6884

27. Bajad, S.U., Lu, W., Kimball, E.H., Yuan, J., Peterson, C., and Rabinowitz, J.D. (2006) Separation and quantitation of water soluble cellular metabolites by hydrophilic interaction chromatography-tandem mass spectrometry. *J.Chromatogr.A.* **1125,** 76-88

28. Lorenz, M.A., El Azzouny, M.A., Kennedy, R.T., and Burant, C.F. (2013) Metabolome Response to Glucose in the beta-Cell Line INS-1 832/13. *J.Biol.Chem.* **288,** 10923-10935

29. Emenhiser, C., Sander, L.C., and Schwartz, S.J. (1995) Capability of a polymeric C30 stationary phase to resolve cis-trans carotenoid isomers in reversed-phase liquid chromatography. *Journal of Chromatography A.* **707,** 205-216

30. Guillarme, D., Heinisch, S., and Rocca, J.L. (2004) Effect of temperature in reversed phase liquid chromatography. *Journal of Chromatography A.* **1052,** 39-51

31. Barroso, B., and Bischoff, R. (2005) LC–MS analysis of phospholipids and lysophospholipids in human bronchoalveolar lavage fluid. *Journal of Chromatography B.* **814,** 21-28

32. Ogiso, H., Suzuki, T., and Taguchi, R. (2008) Development of a reverse-phase liquid chromatography electrospray ionization mass spectrometry method for lipidomics, improving detection of phosphatidic acid and phosphatidylserine. *Anal.Biochem.* **375,** 124-131

33. Lorenz, M.A., Burant, C.F., and Kennedy, R.T. (2011) Reducing time and increasing sensitivity in sample preparation for adherent mammalian cell metabolomics. *Anal.Chem.* **83,** 3406-3414

Chapter 3. METABOLOME RESPONSE TO GLUCOSE IN INS-1 β-CELL LINE.

This project was performed in collaboration with Dr. Mathew Lorenz. I contributed to experiments and analysis related to figures (1, 2, 3, 4, 5, 7 and S1).The integrated project is presented to convey the complete project. A brief comparison with INS 832/3 is described in this study.

INTRODUCTION

β-cells in islets of Langerhans secrete insulin in response to increased blood glucose. An acute increase in glucose evokes a rapid release of insulin which is sustained for a short period, designated as 1^{st} phase, followed by an extended period of lower secretion (2^{nd} phase). The metabolic pathways that facilitate 1^{st} and 2^{nd} phase of glucose-stimulated insulin secretion (GSIS) by β-cells are not fully understood (1). GSIS is dependent upon glucose metabolism and is thought to be triggered by closure of K_{ATP} channels secondary to an increase in the ATP/ADP ratio. Closure of K_{ATP} channels causes membrane depolarization, opening of voltage sensitive Ca^{2+} channels, and subsequent exocytosis of a releasable pool of insulin vesicles (2). Evidence supports the concept that other metabolic processes also facilitate GSIS in K_{ATP}-independent or amplifying pathways (3-5). A variety of metabolic coupling factors (e.g., NADPH, long-chain acyl-CoAs, and glutamate) and pathways (e.g., pyruvate/citrate, pyruvate/isocitrate, pyruvate/malate, and glycerolipid/fatty acid cycling) have been implicated in both triggering and amplifying GSIS (3-5).

Measurement of metabolite changes in β-cells that correlate with GSIS has been limited to measuring a relatively small set of metabolites at extended time periods that cannot distinguish important alterations that occur in earliest phases of insulin secretion (6). In this work, we employed a recently developed liquid chromatography-time of flight-mass spectrometry (LC-TOF-MS) method to measure signal for hundreds of metabolites in INS-1 832/13 cells following exposure to glucose (7). We determined the identity and levels of 87 of these metabolites in response to different glucose concentrations and at short intervals after exposure to an increase in glucose. Specific compounds monitored included metabolites associated with glycolysis, the pentose phosphate shunt, and the tricarboxylic acid (TCA) cycle as well as an array of nucleotides and fatty acid species. We also utilized isotopologue analysis

of metabolites following U-[^{13}C]glucose stimulation to assess flux through specific pathways. The results allowed us to confirm or modify prevailing hypotheses regarding metabolism and its relationship to insulin secretion and identify new pathways that may play a role in the dynamics of insulin secretion following glucose exposure.

EXPERIMENTAL PROCEDURES

Materials. INS-1 832/13 (8) and INS-1 832/3 cells were kindly provided by Dr. Christopher Newgard (Sarah W. Stedman Nutrition and Metabolism Center, Duke University, Durham, NC). All chemicals were purchased form Sigma-Aldrich (St. Louis, MO) unless otherwise noted. HPLC grade acetonitrile was purchased from Burdick & Jackson (Muskegon, MI). RPMI media, fetal bovine serum, 4-(2-hydroxyethyl)-1-piperazineethanesulfonic acid (HEPES), and penicillin-streptomycin were purchased from Invitrogen Corp, (Carlsbad, CA).

Cell Culture. INS-1 832/13 cells cultured in RPMI supplemented with 2 mM glutamine, 1 mM sodium pyruvate, 10% FBS, 10 mM HEPES, 100 U/mL penicillin, 100 µg/mL streptomycin, 250 ng/mL amphotericin B, and 50 µM β-mercaptoethanol. Cells were plated at a density of ~14 x 10^3 cells/cm^2 and grown in either 6 cm or 10 cm culture dishes at 37 °C and 5% CO_2 in a humidified atmosphere to ~70% confluence over ~5 d prior to experimentation. Cells were preincubated in supplemented RPMI containing 3 mM glucose for ~20 h prior to experimentation. Krebs-Ringer-HEPES buffer (KRHB) was prepared containing 10 mM glucose, 20 mM HEPES, 118 mM NaCl, 5.4 mM KCl, 2.4 mM $CaCl_2$, 1.2 mM $MgSO_4$, and 1.2 mM KH_2PO_4 adjusted to pH 7.4 with HCl.

Glucose Stimulation Dose Response. Following preincubation, culture media was replaced with KRHB containing 0, 2, 5, 10, or 20 mM glucose + 0.2% BSA. Cells were incubated for 30 min after which an aliquot of buffer was removed for insulin measurement. Metabolism was immediately quenched and metabolites extracted as described previously (7).

Glucose Stimulation Time Course and Flux. Cells were transferred to KRHB containing 0.5 mM glucose and 0.2% BSA for 30 min prior to stimulation. Glucose was increased to 10 mM glucose by adding an aliquot of 1 M glucose stock. The media was sampled for insulin measurement 2-90 min after initial transfer to 0.5 mM KRHB (both pre and post stimulation).

For metabolite measurements, cells were treated as indicated above (without addition of BSA) and cell plates quenched from 25 to 75 min after transfer to KRHB (5 min before to 45 min after increasing glucose to 10 mM). Carbon flux through glucose was also assessed by stimulating cells with U-[^{13}C]glucose using the same protocol. In some studies, cells were pretreated with 10 mM phenylsuccinate (Sigma-Aldrich, St. Louis, MO) for 10 min to inhibit the mitochondrial oxoglutarate carrier (9).

For insulin and metabolite measurements with 5-amino-1-β-D-ribofuranosyl-imidazole-4-carboxamide riboside (AICAR) treatment, stimulation was conducted by conditioning cells in KRHB containing 0.5 mM glucose for 30 min and replacing the buffer with KRHB containing 10 mM glucose with or without 25 µM AICAR. Incubation buffer was sampled for insulin and plates quenched from 10 to 60 min following stimulation.

Insulin Measurement. Aliquots of KRHB were briefly stored on ice, centrifuged at 3000 rpm for 3 min to pellet any suspended cells, and an aliquot of supernatant was transferred to a fresh vial. Samples were stored at -20 °C and assayed using Rat/Mouse insulin ELISA Kit (Millipore, Billerica, MA). Insulin secretion rate was calculated by dividing the difference in insulin concentration of 2 consecutive time points by the time elapsed between sampling.

Metabolite Measurement. Cell plates were rinsed, metabolism quenched, and metabolites extracted using the procedure described previously (10). Briefly, cell plates were rapidly rinsed with water and quenched with liquid nitrogen. Metabolites were extracted with 75% 9:1 methanol:chloroform/25% water and assayed by high performance liquid chromatography with time-of-flight mass spectrometry (HPLC-TOF-MS). Chromatographic separations were performed with an Agilent Technologies (Santa Clara, CA) 1200 HPLC system equipped with a Phenomenex (Torrance, CA) Luna NH_2 2.0 x 150 mm, 3 µm HPLC column and a 2.0 x 4 mm guard column using the following conditions: mobile phase A was 100% acetonitrile (ACN); mobile phase B was 100% 5 mM ammonium acetate pH 9.9 with ammonium hydroxide; gradient program was (time, %B, flow rate) 0 min, 20%, 200 µL/min, 20 min, 100%, 200 µL/min, 20.1 min, 100%, 300 µL/min; column temperature was 35 °C; injection volume was 80 µL; autosampler temperature was 4 °C. Lipids were separated on a C18 Capcell column 2 x 150

mM, 3 um. Mobile phases and gradient were used as described (11). DAG and PA detection was performed in positive and negative mode respectively. Detection was performed on an Agilent Technologies LC/MSD TOF using a dual electrospray ionization (ESI) source in negative-ion mode as described previously (10).

Directed and undirected data processing was performed as described elsewhere (10). Combined peak areas are used for unresolved isomers (e.g., citrate + isocitrate and hexose phosphates). Several metabolites are not reported because of rapid degradation or interconversion. For example, pyruvate and oxaloacetate, are not reported because of rapid degradation of oxaloacetate to pyruvate (12). Similarly, glyceraldehyde-3-phosphate and dihydroxyacetone phosphate are unstable in solution (13).

Undirected analysis was performed by determining features (i.e., m/z signals at a given retention time) that changed in LC-MS peak area following a step change from 0.5 to 10 mM glucose for 25 min. Features were included in the analysis that were detected in every chromatogram and had <40% relative standard deviation (RSD) within each group as determined using Agilent Technologies MassHunter Quantitative software for peak picking and MassProfiler Professional for data alignment and statistical analysis. These metabolites were identified by searching the Human Metabolome Database to match mass, analyzing isotope ratios, and comparing to standards when available.

Calibration curves with standards that were available showed linear responses. To ensure that peak areas were linear with concentration even when analyzing a complex matrix of cell extract, standards for 24 analytes were spiked into an extract of INS-1 cells that had been incubated with 0.5 mM glucose for 2 h. Three to five concentration spikes were added to yield a concentration range that spanned that detected in cells and these standard addition experiments showed highly linear response for the majority of metabolited reported (Supplementary Figure S1). Residual protein was determined by Bradford Assay (14). Peak areas were measured from extracted ion chromatograms of $[M-H]^-$ metabolite ions with ± 70 ppm detection windows centered on the theoretical mass. $[M-2H]^{2-}$ ions were used for acetyl-CoA (aCoA) and other CoAs to improve sensitivity. Peak areas for internal standards were measured

using an identical procedure; however, values were only used to verify instrument stability and not used in endogenous metabolite quantification.

Western Blot. Glucose stimulated cells were placed on ice, washed once with ice cold PBS and solubilized in 75 µl Laemelli's/extraction buffer (20 mM HEPES pH 7.5, 1% Triton X-100, 20 mM □-glycerophosphate, 150 mM NaCl, 10 mM NaF, 1 mM sodium orthovanadate, and complete protease inhibitor cocktail) from Roche Diagnostics (Indianapolis, IN). Anti-ACC and anti-pACC were obtained from Cell Signaling and used at 1:1000. Anti-HMG-CoA-reductase was from US Biological and was used at 2 µg/ml. Blots were developed with ECL (Pierce, Rockford, IL) according to manufacturer's instructions.

Statistics. Data are expressed as mean ± 1 standard error of the mean (SEM). Statistical significance was determined using a non-corrected two-tailed Student's t test, unpaired assuming equal variance or ANOVA, as appropriate. A p-value of < 0.05 was considered significant.

RESULTS and DISCUSSION

Insulin Secretion and Static Metabolite Profiles. In these studies we employed LC-TOF-MS to identify and quantify the levels of specific metabolites in INS-1 832/13 cells (1) following glucose exposure and their relationship to insulin release. We used U-[^{13}C]glucose in secondary studies to more fully understand the dynamics of metabolite changes.

The EC_{50} value for insulin secretion from INS-1 832/13 cells in response to glucose was 6.2 mM with near maximal insulin secretion observed at ~10 mM glucose (Figure 1A), similar to previous reports (8). Insulin secretion rate following a step change from 0.5 to 10 mM glucose showed a relatively sharp peak at ~4 min (28 ng/mg protein/ min) and a smaller broad peak with maxima at ~25 min corresponding to 1st phase and 2nd phase of insulin secretion (Figure 1B, see also Figure S2 for calculation of secretion rate), consistent with previous reports of GSIS in islets (15) and INS-1 832/13 cells (16). Using LC-TOF-MS, a total of 1030 mass spectral features were detected in INS-1 832/13 cells at both 0.5 and 10 mM glucose. Following a step change from 0.5 to 10 mM glucose, 190 features showed statistically significant ($p < 0.05$) differences of at least 1.5-fold (Figure 1C). The identity of 87 metabolites was determined by

accurate mass search of the Human Metabolome Database, comparison of theoretical and observed isotopic distributions and, when available, coelution with authentic standards.

These metabolites were quantified relative to baseline at multiple times following a step increase in glucose from 0.5 to 10 mM glucose (Figure 1D). We also measured the effect of different glucose concentrations at a single time point (25 min). To determine if peak area changes were linearly related to concentration, we performed standard addition experiments for 24 metabolites (see Materials and Methods). As shown in Figure S1, responses were linear in the concentration range found suggesting that the peak area differences accurately reflect relative changes in concentration, thus matrix effects on ionization were low for these experiments. While we cannot rule out non-linear effects of matrix on some analytes, these results along with the observation that only a small fraction of the detected features actually changed with glucose, indicating a relative constant matrix, suggest that the peak areas a good measure of relative concentration change. Metabolome of INS-1 832/3 was also profiled following a step increase in glucose from 0 till 16.6 mM (Figure 1E). Due to difference in cell lines some metabolites were of low levels and were not detected. However most detected metabolites showed similar response to glucose in both cell lines, confirming the importance of these pathways in glucose stimulated insulin secretion.

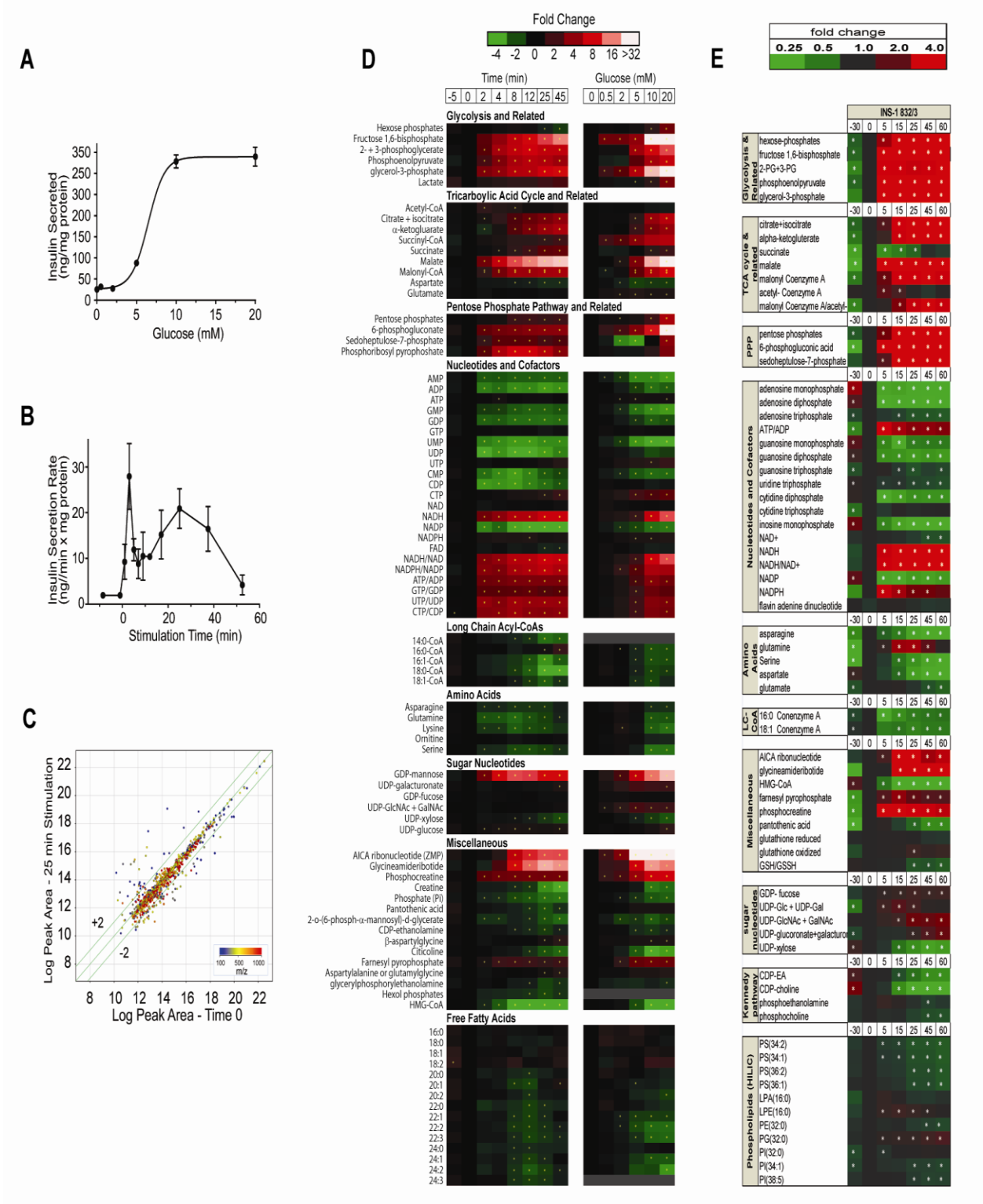

Figure 3-1.Temporal and dose-response metabolite profiles and insulin release with glucose stimulation in INS-1 832/13 cells and 832/3. (A) Insulin secreted by INS-1 832/13 cells versus glucose concentration. Cells incubated in KRBH +0.2% BSA and 0 to 20 mM glucose for 30 min. Error bars are SEM, n = 3. (B) Insulin secretion rate versus stimulation time. INS-1 cells incubated in KRHB + 0.2% BSA + 0.5 mM glucose for 30 min and stimulated with 10 mM glucose for 50 min. (C) Effect of 10 mM glucose treatment on LC-MS "feature" peak area. The log-log plot is for all features detected at time 0 (0.5 mM glucose) versus 25 min of 10 mM glucose stimulation. Features are color coded by m/z. The 1030 features plotted were

detected in all replicates with RSD < 40% for either Time 0 or 25 min groups. 130 feature peak areas change >1.5 fold (shown outside the lines parallel to the correlation line) and are statistically different with p < 0.05. (D) Heat maps showing temporal (left) and dose response (right) changes to glucose in INS-1 (832/13) metabolite levels. Levels expressed as fold change versus time 0. For temporal response, cells were incubated in KRHB with 0.5 mM glucose for 30 min then stimulated to 10 mM glucose and sampled over 45 min. For dose response (right) INS-1 cells were incubated in KRHB + 0.2% BSA and treated with a step change from 0.5 to the new glucose concentration for 30 min. (E) Heat map showing temporal changes to glucose in INS-1 (832/3) metabolite levels. For both heat maps, asterisk indicates significant difference in peak area versus time 0 with p < 0.05.

Metabolites associated with modulation of K_{ATP} Channels. K_{ATP} channel closure through rise in the ATP/ADP ratio is an established trigger for GSIS. In agreement with this concept, we detected a rapid increase in ATP/ADP ratio (Figure 1D and 2C) that coincided with 1^{st} phase insulin release. This observation matches previous reports of a several-fold increase in ATP/ADP in mouse β-cells that reached a maximum 1 to 3 min following glucose stimulation (17) and an ~2-fold increase in mouse islets within 5 min of glucose stimulation (18).

The absolute increases in ATP concentration were <15% while both ADP and AMP fell markedly (Figure 1D and 2A) supporting the observations that K_{ATP} channel may be more influenced by reductions in ADP concentration (19) than increases in ATP. These measurements do not take into account the apparent rapid ATP turnover indicated by rapid rise in the level of phosphocreatine (Figure 1D and 2B). Phosphocreatine has been suggested to serve as a shuttle for energy rich phosphate from mitochondria to plasma membrane with metabolism by K_{ATP} channel-associated creatine kinase to phosphorylate ADP to ATP, increasing the local ATP concentration (20). INS-1 832/3 cell line showed similar behavior in the increase in ATP/ADP ratio and phosphocreatine (Figure 2E and 2F). Although ATP level showed slight stability in INS-1 832/13, it slightly decreased in INS-1 832/3 cell line. The marked decrease in ADP in INS-1 832/3 cell (figure 2D) allowed the significant rise of ATP/ADP ratio, and confirming the importance of the decrease in ADP in K_{ATP} channel modulation.

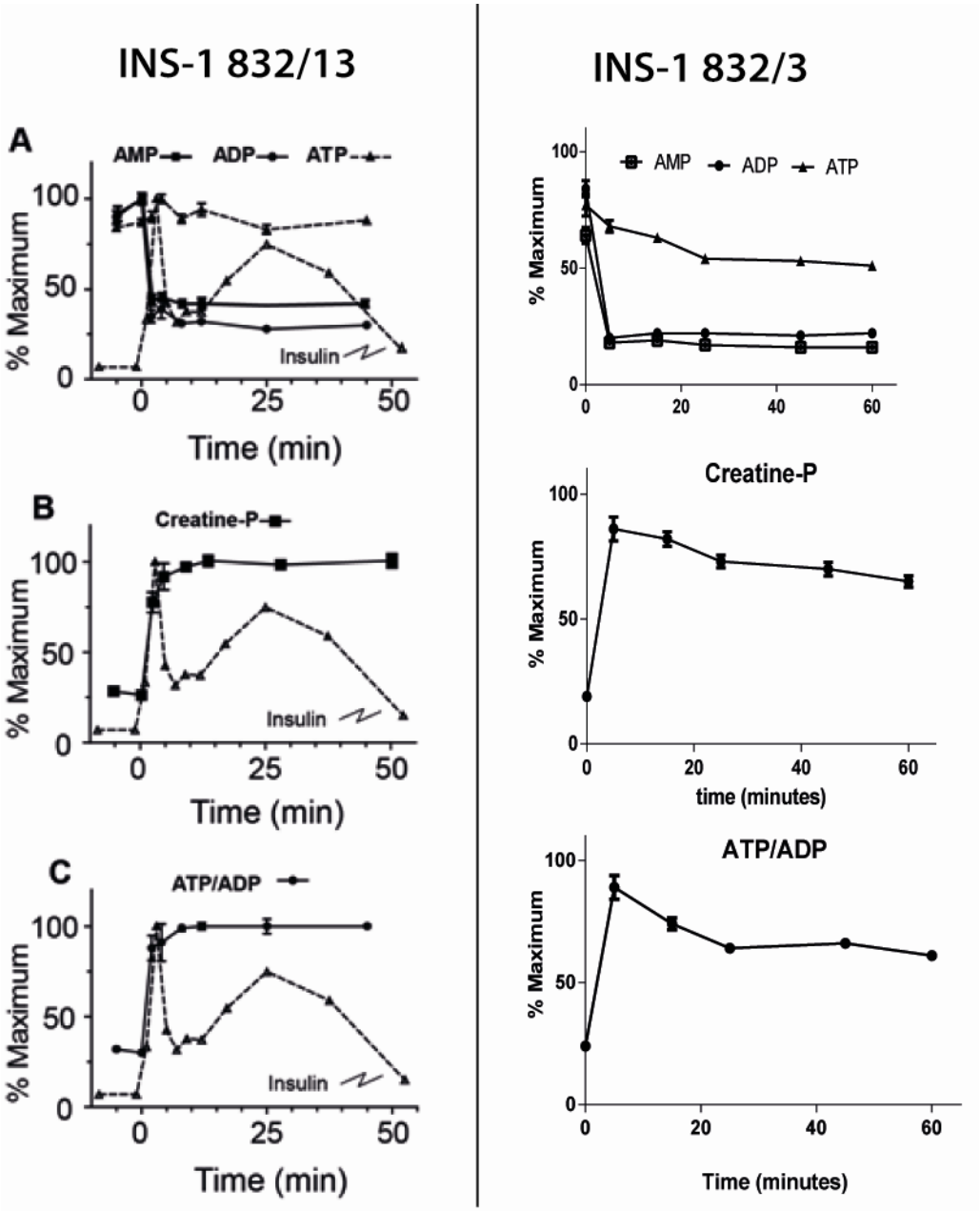

Figure 3-2. Glucose stimulated time course of adenine nucleotides. INS-1 cells were treated with 10 mM glucose and sampled at the indicated time points from -5 to45 min. (A) ATP, ADP and AMP. (B) Phosphocreatine, (C) ATP/ADP ratios. Insulin secretion rate is overlaid for comparison. Error bars represent 1 SEM, n = 3 for each time point. INS-1 (832/3) cell line was treated with 16.6 mM glucose and sampled at indicated time points (D): ATP, ADP and AMP. (E) phosphocreatine. (F) ATP/ADP ratio.

In addition to adenine nucleotides and phosphocreatine, long-chain acyl-CoAs have been proposed to modulate K_{ATP} activity such that decreases in concentration aid closure of K_{ATP} channels (21,22). Previous studies have been discordant on the actual concentration changes of long-chain acyl-CoAs associated with glucose stimulation (23,24). We found an inverse dose-response relationship of long-chain acyl-CoAs to glucose (Figure 1D). The decrease in long-chain acyl-CoAs was rapid and concurrent with Phase 1 GSIS, e.g. 16:0-CoA decreased ~50% within 2 min of glucose stimulation to ~0.46 □mole/mg protein (Figure 3A). Similar changes were observed in 14:0, 16:1, and 18:1 CoA upon glucose stimulation with time and in glucose dose-response profiles (Figure 1D). This rapid decrease in long chain acyl-CoA was true also in INS-1 832/3 cell line (Figure 1E).

To understand the fall in LC-CoA levels, we measured diacylglycerol and phosphatidic acid and found both species increase following glucose stimulation (not shown). When INS-1 cells were stimulated with U-[^{13}C]glucose, there was a non-significant trend for increases in phosphatidic acid and diacylglycerol species (Figure 3B). However, we did observe a significant and rapid rise in a M+3 phosphatidic acid (34:1) 5 and 10 minutes after glucose addition ($p=9.4*10^{-4}$ and $2.3*10^{-3}$, respectively) and similar rises in diacylglycerol (34:1) M+3 isotopologues ($p=5.2*10^{-4}$ and $2.9*10^{-3}$, at 5 and 10 min, respectively) (Figure 3B) suggesting addition of 3 carbons from ^{13}C-glycerol-3-phosphate, which is rapidly generated by glycolysis (Figure 3C and 3D, see below).

These results indicate that esterification, utilizing de novo generated glycerol-3-phosphate, facilitates removal of long chain acyl-CoAs from cytosol during the initial phase of glucose stimulated insulin release. Such a decrease may be expected to aid closure of K_{ATP} channels, especially during first phase secretion (21,22). In addition to modulating K_{ATP} channel activity, long chain acyl-CoAs may also participate in additional downstream signaling events. One potential route is via the malonyl-CoA/long-chain acyl-CoA pathway in which glucose derived acetyl-CoA is carboxylated by acetyl-CoA-carboxylase (ACC) to form malonyl-CoA. Malonyl-CoA inhibits carnitine palmitoyl transferase 1 (CPT1) reducing fatty acid uptake and causing cytosolic accumulation of long-chain acyl-CoAs (or downstream metabolites). It has been proposed that the resulting long chain acyl-CoAs, or downstream metabolites, are

important signaling molecules or coupling factors in secretory processes such as vesicular trafficking (25,26). The metabolomic data provide a means to assess the changes expected from this pathway.

After stimulation with 10 mM glucose, acetyl-CoA doubles at 2 min followed by a gradual decrease to levels near baseline by 5 minutes (Figure 1D and Figure 3E). Similar 2 fold increase in acetyl-CoA levels was seen in INS-1 832/3 cells after 5 minutes of glucose stimulation that decreased to baseline by 15 minutes (figure 1E). This decrease is likely due to rapid turnover of acetyl-CoA as evidenced by the decrease in ^{12}C-labled and a significant increase ($p=3.4*10^{-6}$ and $3.5*10^{-7}$ at 5 and 10 min, respectively) in M+2 ^{13}C-labeled species following stimulation with U-[^{13}C]glucose (Figure 3F). Similarly, there is an increase in total (Figure 3G) and ^{13}C-labled malonyl-CoA ($p=2.3*10^{-5}$ and $5.5*10^{-9}$ at 5 and 10 min, respectively) (Figure 3H) with only +2 m/z increasing, suggesting a rapid carboxylation of newly formed acetyl-CoA, likely derived via citrate and ATP-citrate lyase (see below) (27,28).

We also found near complete dephosphorylation/activation of ACC, after only 2 min of glucose exposure (Figure 3I). The inhibition of CPT1 by malonyl-CoA may redirect acyl-CoAs to autonomous signaling events or condensation with de novo generated glycerol-3-phosphate, described above, to generate phosphatidic acid and diacylglycerols to participate in amplification of insulin secretion (29). This rapid increase in phosphatidic acid and diacylglycerol suggests that the generation of diacylglycerol for amplification not only comes from the activation of phospholipase (see (30) for discussion), but also from rapid generation via esterification of fatty acids. Thus, our results support a model in which glucose derived G3P rapidly reacts with long-chain acyl-CoAs resulting in the removal of long chain acyl-CoAs, which, as pointed out above, could enhance closure of the K_{ATP} channel (21,22) while simultaneously generate coupling factors for GSIS. Further, the malonyl CoA production supports the supply of long-chain CoA for this pathway, likely in addition to that derived from phospholipase activity of membrane phospholipids (31).

Glycolysis. Glycolysis, which comprises the first steps in glucose metabolism, supports the change in ATP/ADP ratio and closure of the K_{ATP} channel (32) and provides carbon for the pentose phosphate pathway (PPP) and tricarboxylic acid (TCA) cycle.

Hexose phosphates, comprised primarily of glucose-6-P and fructose-6-P (which are not resolved chromatographically) changed little over 45 min following stimulation with 10 mM glucose, increasing 1.2 fold over 8 min, then decreasing by 50% to ~58 µmole/mg protein (Figure 1D). Dose-response studies show a 3-fold increase at 20 mM glucose (Figure 1D). Rapid increase in concentrations of fructose bisphosphate, 2-phosphoglycerate with 3-phosphoglycerate and phosphoenolpyruvate (32-, 6.7- and 5.5-fold, respectively) was observed following glucose stimulation (Figure 1D), suggesting that phosphofructokinase is not rate limiting to glycolysis in these cells. The increase in glycolytic intermediates with glucose stimulation was further confirmed using the INS-1 832/3 cell line. Using 16.6 mM glucose, glycolytic intermediates increased by at least 4 fold, confirming the previous data obtained from INS-832/13 cell line.

Reoxidation of NADH to NAD+ is critical to maintaining glycolytic flux. The formation of glycerol-3-phosphate from dihydroxyacetone phosphate (DHAP) by cytosolic glycerol-3-phosphate dehydrogenase utilizes NADH to regenerate NAD^+, allowing continuing flux through glycolysis. The proposed glycerol-3-phosphate shuttle posits a subsequent reoxidation of glycerol-3-phosphate to DHAP by mitochondrial glycerol-3-phosphate dehydrogenase, delivering NADH to the mitochondria (33). As indicated above, glycerol-3-phosphate increased 3.4-fold within 2 min of glucose stimulation (Figure 3C). Stimulating cells with 10 mM U-[^{13}C]glucose showed that the increase in glycerol-3-phosphate is due exclusively to de novo synthesis over the first 10 min of stimulation, demonstrated by the significant rise in an M+3 glycerol isotopologue ($p=1.1*10^{-5}$ and $2.2*10^{-6}$ at 5 and 10 min, respectively) (Figure 3D). While the high levels of the glycerol phosphate shuttle in islets has been proposed to be important in GSIS (34), disruption of the mitochondrial glycerol-3-phosphate dehydrogenase does not affect GSIS (35). Our finding that there is a rapid esterification of fatty acids with de novo generated glycerol-3-phosphate (Figure 3B), suggests that in addition to generating

signaling intermediates, the esterification may also play a role in regeneration of cytosolic NAD^+, enhancing glycolytic flux, thus maintaining a high ATP/ADP ratio.

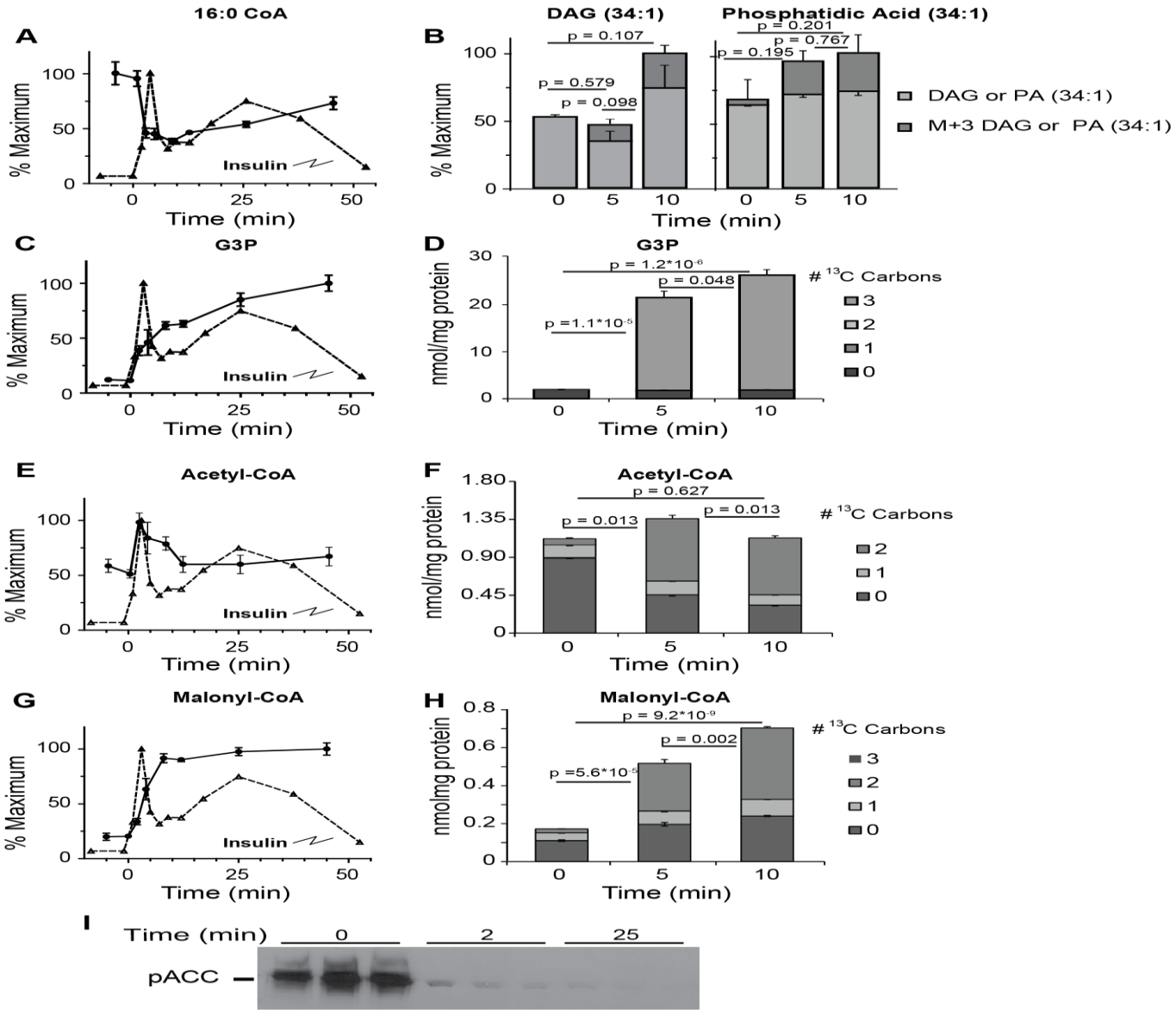

Figure 3-3.Changes in metabolites associated with the malonyl-CoA mechanism of insulin secretion. Time dependent changes in the relative concentration of 16:0 acyl-CoA (A), glycerol-3-phosphate (C), acetyl-CoA (E) and malonyl-CoA (G) levels following stimulation with 10 mM glucose in INS-1 cells. Changes in total mass and 13C-labeled isotopologues of phosphatidic acid (B), glycerol-3-phosphate (D), acetyl-CoA (F) and malonyl-CoA (H) following stimulation with 10 mM U-[13C]glucose. Error bars represent 1 SEM, n = 3. (I) Levels of pACC at baseline and following stimulation of INS1 cells with 10 mM glucose for 2 or 25 min. p-values are given for total pool size on the graph. p-values for isotopologue analysis are indicated in the text

TCA cycle and anaplerotic shuttles. Metabolites in the TCA cycle participate in pathways that generate metabolites and cofactors which play a role in augmenting GSIS (3-5). The β-cell can increase TCA intermediates from pyruvate through pyruvate dehydrogenase and pyruvate carboxylase (36) and through additional anaplerotic reactions (37). As shown above, acetyl-CoA increased 1.5-fold within 2 min of stimulation and returned to prestimulation concentration within 12 min of glucose addition. Span 1 intermediates citrate + isocitrate (Figures 1D, 4A) and α-ketoglutarate (Figure 1D) increased 3- to 4-fold while, succinyl-CoA, and succinate showed much smaller absolute changes (Figure 1D). The Span 2 metabolite malate, increased ~30-fold after glucose stimulation (Figures 1D and 4B).

To assess the mechanisms of change in TCA cycle metabolites, we measured their isotopic enrichment over the initial 10 min of exposure to 10 mM U-[^{13}C]glucose. Acetyl-CoA is generated primarily from glucose as the M+2 isotopologue contributes to the majority of the de novo accumulated acetyl-CoA ($p=3.4*10^{-6}$ and $3.5*10^{-6}$, at 5 and 10 min, respectively) (Figures 3E and 3F) and is accompanied by a ~40% rise in citrate/isocitrate, from 20 nmol/mg protein to 28 nmol/mg protein at 5 and 10 min (Figure 4D). Approximately 90% of the increase in citrate mass was contributed by the M+2 isotopologue of citrate/isocitrate ($p=3.0*10^{-6}$) (Figure 4D). The labeled pool continued to increase and after 10 min, the majority of the label as M+2 and less than 3% as M+3 or M+4 citrate/isocitrate. Thus, while total citrate/isocitrate levels rise slowly during the initial phases of insulin secretion, there is rapid turnover, with new citrate/isocitrate derived largely from pyruvate dehydrogenase (PDH) generated M+2 [^{13}C]acetyl-CoA. The minimal increase in M+3 and M+4 isotopologues of citrate/isocitrate suggest that the majority of citrate/isocitrate exits the TCA cycle with minimal 'turns', at least in the early stages of GSIS.

Only a small percentage of glutamate is labeled with ^{13}C in the first 10 min following glucose exposure (Figure 4F). Importantly, there is a significant ($p < 0.04$) decrease in ^{12}C-glutamate, about ~20% of the pool, suggesting minimal anaplerotic flux into glutamate. Mitochondrial-derived glutamate has been proposed to participate in GSIS, in part through rapid accumulation of glutamate within the insulin secretory granules (38). While our data agree with previous studies (39), they do not support the hypothesis of rapid increases in

intracellular glutamate during GSIS (40). We cannot rule out that the reduction in glutamate is due to uptake and subsequent release to the medium via secretory granules. And as a confirmation for the previous data, INS-1 832/3 showed also a reduction in glutamate with glucose stimulation (Figure 1E).

Although oxaloacetate could not be accurately measured because of its instability, we found a ~3-fold increase in malate after 5 min and 4.8-fold after 10 min (Figure 1D and 4B). A novel finding is that in cells exposed to 16.7 mM U-[^{13}C]glucose, the observed increase in malate was largely accounted for by accumulation of ^{12}C-malate, increasing the estimated concentration from 12 nmol/mg protein to 70 nmol/mg at 10 min, with only about 15% of the increase in mass due to de novo entry of ^{13}C-label into malate (Figure 4E). About 60% of this de novo derived ^{13}C-malate is the M+3 isotopologue and ~40% M+2 (Figure 4E), suggesting near-equal generation from pyruvate carboxylase (M+3) and TCA cycle (M+2). The source of the 'unlabeled' malate is likely the relatively large pool of aspartate (via oxaloacetate). At 10 min, malate levels continue to rise and aspartate levels are restored to near baseline levels, with the increase due to accumulation of M+2 and M+3 isotopologues of aspartate in a similar proportion to that found in malate (Figure 4G). This finding is consistent with a partial operation of the 'malate-aspartate shuttle', though we propose that the influx of aspartate is operating to provide anaplerotic oxaloacetate/malate to the TCA cycle and the transfer of NADH to the interior of the mitochondria. A previous study (41) provided evidence that a decrease in aspartate was correlated with GSIS, and provided anaplerotic substrates to the TCA cycle. However, based on the isotopic labeling observed, our findings do not support the contention that the aspartate is derived from glucose or is in a separate metabolic pool from malate, as suggested elsewhere (41).

These results also do not support a robust activity of the pyruvate shuttle (1,42,43) to generate oxaloacetate/malate, at least in the earliest time points of insulin secretion. If the pyruvate shuttle were responsible for the rise in malate, then decarboxylation of citrate would be expected to give rise to equal amounts of M+2 and 'unlabled' malate and, with the contribution of TCA cycle derived M+2 malate, even a relatively greater amount of M+2 malate.

The observed transient decrease in α-ketoglutarate concentrations in early time points following the addition of glucose (Figure 1D) may be due to the transamination of α-ketoglutarate from aspartate to generate glutamate and oxaloacetate, with the latter subsequently reduced to malate, allowing the transfer of the glycolytically derived NADH to the mitochondria (see Figure 7 for schematic). The glutamate can be converted back to α-ketoglutarate through glutamate dehydrogenase, with the generation of NAD(P)H and $NH4^{+}$.

To further support the role of the malate-aspartate shuttle in the rise in malate we pretreated INS-1 cells with phenylsuccinate, which inhibits the oxoglutarate carrier, to reduce efflux of α-ketoglutarate and entry of malate into the mitochondria (9). Pretreatment with phenylsuccinate did not impair reduction in AMP levels (Figure 4H) or reduction in NAD^{+}/NADH ratio (Figure 4H and 4I) following glucose stimulation. The rise in citrate (Figure 4J) was blunted and glutamate levels fell (Figure 4K) following phenylsuccinate treatment and this was largely due to changes in the levels of ^{12}C-labeled isotopologues. There was a marked and significant reduction in the rise in malate following phenylsuccinate treatment (Figure 4L), primarily in the ^{12}C-label isotopologue. We suggest that the fall in malate is due to consumption of mitochondrial malate without replenishment by cytosolic malate. Aspartate levels are likewise reduced by phenylsuccinate treatment and, as with malate, the ^{13}C-isotopologue distribution is not changed (Figure 4M).

As inhibition of the oxoglutarate carrier inhibits glucose-induced insulin release (44), these data further confirm that malate-supported anaplerosis and/or shuttling of reducing equivalents by malate into the mitochondria are critical to sustaining insulin secretion. The observed rapid increase in malate can also clarify data by Lu et al. (39) who, through modeling of NMR-derived spectra of INS-1 cells extracts, proposed the presence of two distinct pools of pyruvate that enter into the Krebs cycle following glucose stimulation of β-cells, one derived from glycolysis and the other from a non-glycolytically derived pool. We believe our finding of a rapid rise in malate derived from a non-glucose source could, via cytosolic malic enzyme, generate pyruvate, giving rise to the 'second' pool of pyruvate. Alternatively, the labeling pattern of highly glucose-responsive INS-1 cells lines presented by Lu et al, may be explained by rapid increase in mitochondrial malate, via import into the mitochondria which would also

result in a relative 'dilution' of the glutamate pool. We favor the latter explanation as phenylsuccinate treatment results in a significant reduction in the ^{12}C-isotopologue concentration of glutamate with minimal change in the M+2 ^{13}C-isotopologue levels, presumably derived from PDH derived M+2 ^{13}C-acetylCoA (Figure 4K).

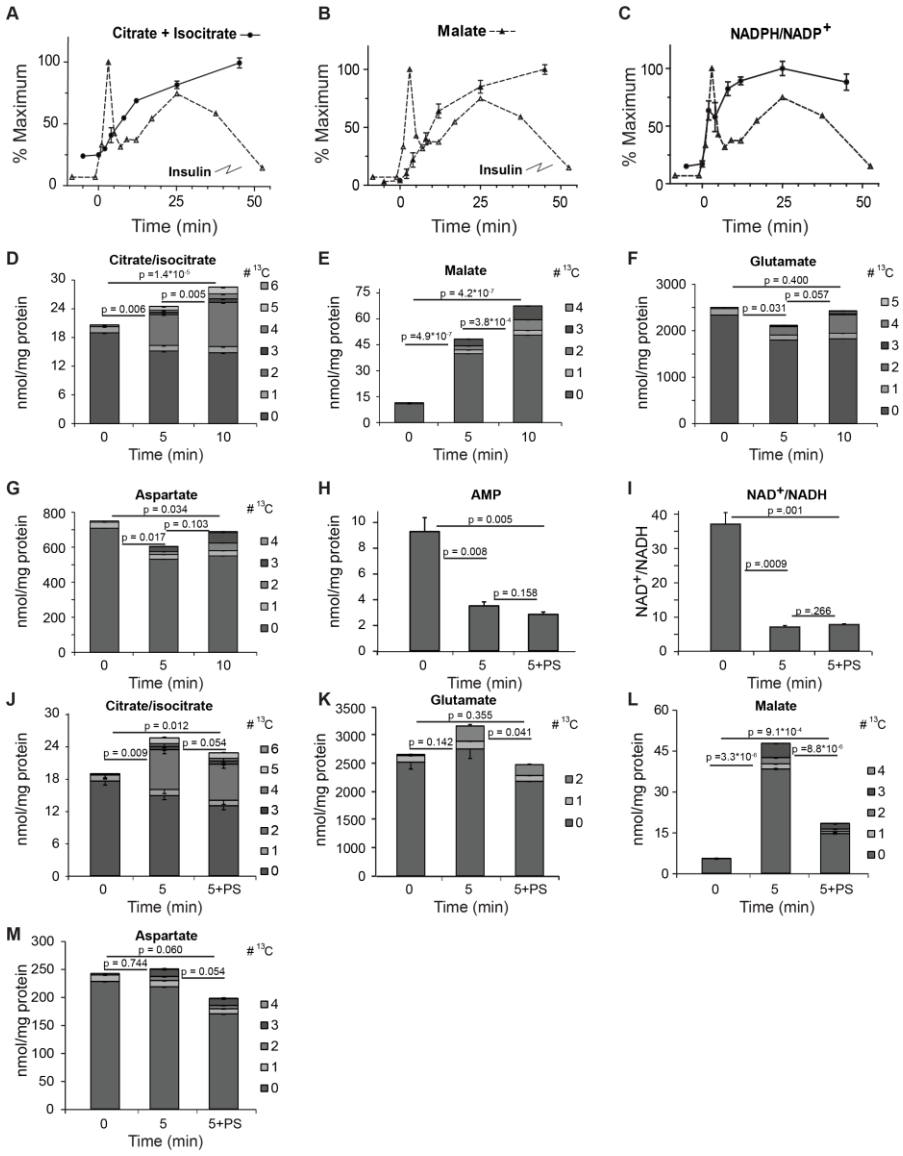

Figure 3-4.Temporal changes of TCA cycle and related metabolites following addition of 10 mM glucose to INS-1 cells. A-D. Changes in the relative concentration of citrate/isocitrate (A), malate (B) and NADPH/NADP+ ratio (C). D-E. Changes in total mass and 13C-labeled isotopologues of Citrate/isocitrate (D), Malate (E), Glutamate (F) and Aspartate (G) following stimulation with 10 mM U-[13C]glucose. H-N. Effect of phenylsuccinate on metabolite levels. Cells were preincubated without or with 10 mM phenylsuccinate for10 min prior to addition of 10 mM glucose. Total metabolite concentration of AMP (H) and NAD/NADH ratio (I) and changes in relative concentration of 13C-labeled isotopologues of citrate/isocitrate (D), malate (K), glutamate (L) and aspartate (M) Error bars represent 1 SD, n = 3. Note 3, 4 and 5 13C-containing isotopologues of glutamate were obscured by presumptive breakdown products of phenylsuccinate. p-values for isotopologue analysis are indicated in the text

NADPH. NADPH has been cited as a critical metabolite for GSIS. NADPH increased slightly (1.3-fold) but insignificantly over ~12 min of glucose stimulation which is similar in magnitude to changes reported in islets (45) (Figure 1D). The NADPH/$NADP^+$ ratio increased abruptly after addition of glucose and increased 5.8 fold over 25 min, correlating well with 1^{st} and 2^{nd} phase insulin secretion (Figure 1D and 4C). It has been proposed that cycling of metabolites from mitochondria to the cytosol, via citrate, isocitrate or malate to pyruvate results in generation of cytosolic metabolites and/or NADPH which participate in GSIS (1,42). The relatively rapid rise in M+2 malonyl-CoA isotopologue (Figure 3H), suggests a significant flux of citrate from the mitochondria which generates M+2 acetyl-CoA (Figure 3F) serving as a substrate for ACC via ATP-citrate lyase (46). This efflux of citrate/isocitrate, can generate NADPH by the conversion of isocitrate to α-ketoglutarate in the cytosol. In addition to the proposed generation of NADPH from α-ketoglutarate in the cytosol due to the malate-aspartate shuttle-mediated influx of aspartate (see above), could be primary sources of NADPH, augmenting GSIS. In INS-1 832/3, NADPH increased significantly upon glucose stimulation, on the other hand, NADP+ decreased significantly. The higher changes in those metabolites compared to INS-1 832/13 cell line might explain the improved glucose responsiveness of INS-1 832/3 cell line (62).

Succinate and short chain fatty acids. Succinate has been proposed as a key metabolite that participates in the generation of molecules that can act as second messengers for potentiation of insulin secretion (43) including short chain fatty acids, acetoacetate, malonyl-CoA and 3-hydroxy-3-methyl-glutaryl-CoA (HMG-CoA) (43,47). Following glucose exposure, we found a rapid increase in succinate levels (Figure 1D and 5A) and malonyl-CoA (Figure 1D and 3H) in the INS-1 832/13 cells. In contrast we found a significant reduction in HMG-CoA (Figure 1D and 5B), similar to previous reports (48). The reduction in HMG-CoA levels appears to be due to rapid consumption as cells incubated for 5 or 10 min with U-[^{13}C]glucose showed a rapid decrease in fully ^{12}C-labeled HMG-CoA isotopologue and an increase in various ^{13}C-labeled isotopologues suggesting de novo synthesis that cannot keep up with consumption (Figure 5D). The reduction in HMG-CoA is apparently not due to changes in HMG-CoA reductase activity as

we do not observe a change in the phosphorylation state of HMG-CoA reductase following glucose stimulation of INS-1 832/13 cells (Figure 5E).

Farnesyl pyrophosphate, a downstream product of the HMG-CoA pathway involved in isoprenylation of proteins (49), was found to increase rapidly following glucose stimulation (Figure 5C) in a time course that mirrors that of the fall in HMG-CoA and 1st phase insulin secretion. Recent studies have suggested that specific small G-proteins (Cdc42 and Rac1) play an important role in GSIS (50,51). These signaling proteins undergo prenylation at their C-terminal cysteine residues which is essential for the transport and fusion of insulin-containing secretory granules with the plasma membrane and the exocytosis of insulin which has been implicated in GSIS (50). The rapid increase in substrate for isoprenylation, farnesyl pyrophosphate, suggests that such modifications can occur in a time frame to be relevant for 1st phase insulin secretion. Further, the dramatic reduction in HMG-CoA suggests that it may become limiting to flux through this pathway and therefore limiting GSIS.

INS-1 (832/3) cell line showed similar decrease in HMG-CoA and increase in FPP upon glucose stimulation (figure 1E) confirming the higher glucose flux through the mevalonate pathway during GSIS. However, succinate showed different response compared to INS-1 (832/13), where it decreased after glucose stimulation. This decrease can be attributed to the higher flux in TCA cycle and its rapid consumption.

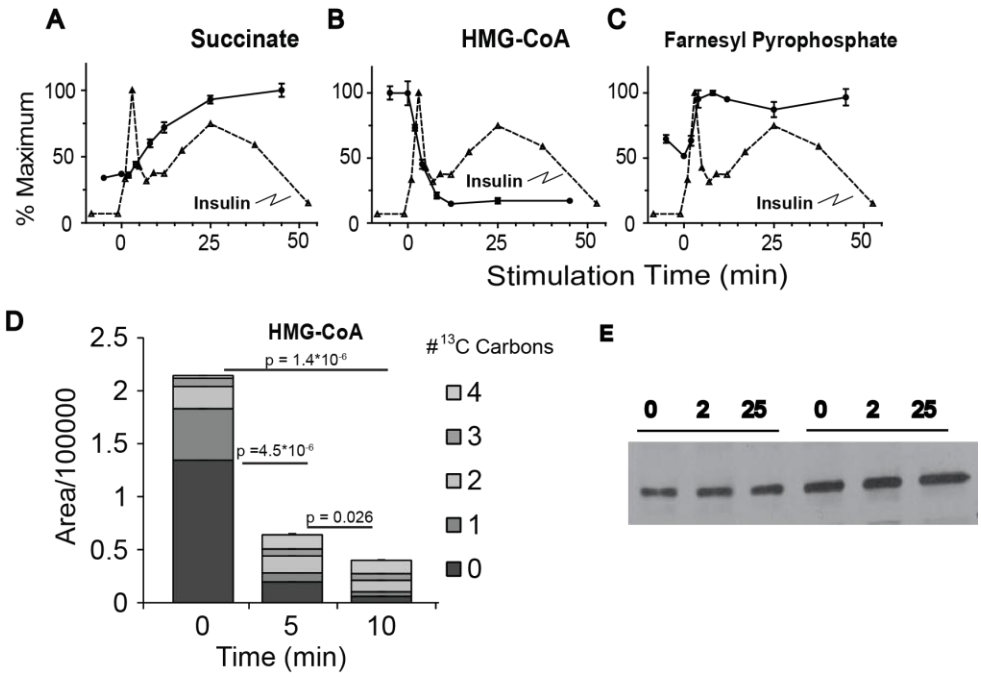

Figure 3-5.Metabolites participating in the succinate mechanism of glucose stimulated insulin secretion. A-C. Time-dependent changes in Succinate (A), HMG-CoA (B) and farnesyl pyrophosphate (C). D. Changes in total mass and 13C-labeled isotopologues of HMG-CoA following stimulation with 10 mM U-[13C]glucose. Error bars represent 1 SEM, n = 3. E. Phosphorylated HMG-CoA reductase at baseline and following stimulation with glucose for 2 or 25 min. p-values for isotopologue analysis are indicated in the text

Pentose Phosphate Pathway (PPP) derived metabolites. Metabolites in the PPP are not often measured in investigations of GSIS but play a key part in cellular metabolism by supplying 5-carbon substrates for purine, pyrimidine, and histidine synthesis and generating NADPH for lipid biosynthetic pathways. However, the PPP is not highly active in β-cells and likely contributes little to the generation of NADPH (42). We observed that most PPP metabolites increased in parallel to increasing glucose concentration (Figure 1A and B). Rapid and substantial relative increases in the pentose phosphate pathway metabolites pentose phosphates, 6-phosphogluconate, sedoheptulose phosphates and phosphoribosyl pyrophosphate (1.8-, 3.2-, 2.4-, and 7.4- fold increases, respectively) were observed. Significant labeling of 6-phosphogluconate following stimulation of cells with U–[^{13}C]glucose was observed (not shown), indicating direct flux into the PPP. Although large relative increases in PPP metabolite levels with glucose stimulation are detected, the pool size of these metabolites is substantially smaller than for those of the TCA cycle supporting previous findings that the bulk

of glucose carbon enters the TCA cycle and does not enter the PPP (52) and a relative unimportance for this pathway in the generation of NADPH in supporting GSIS.

ZMP is an endogenous metabolite in the purine synthesis pathway and a precursor to IMP. Although measurements of endogenous ZMP levels have not been reported in β-cells, we detected a 9-fold increase to ~4.0 μmole/mg protein that reached a maximum ~25 min after glucose stimulation (Figure 1D and 6A). Supporting an increase by de novo biogenesis as opposed to stabilization of ZMP, we found that both phosphoribosyl pyrophosphate which links the PPP to the nucleotide synthesis pathway and glycinamide ribotide, a ZMP precursor, were also detected and increased both temporally and in a dose-response manner after addition of glucose (Figure 1D and 6A, B). This was true also in INS-1 832/3 cell line, where all pentose phosphate pathway metabolites as well as ZMP increased significantly after glucose stimulation (figure 1E).

ZMP can substitute for AMP in enhancing phosphorylation and activation of AMP-activated protein kinase (AMPK), an important regulator of cellular energy balance (53). Indeed, AICA riboside (AICAR), which is phosphorylated in cells to generate ZMP, is widely used to activate AMPK. Acute exposure to AICAR has been found to both decrease (54,55) and potentiate insulin release (56). Based on the timing of the increase in endogenous ZMP found in our studies, we hypothesized that it may serve as a negative regulator of GSIS during the second phase of insulin release. To test this idea, we treated INS-1 832/13 cells with 10 mM glucose and 25 μM AICAR and achieved ~4x higher intracellular ZMP levels at 40 min relative to control cells stimulated with 10 mM glucose only (Figure 6C). This increase in ZMP was accompanied by 20% reduction in rate of insulin release 40 to 60 min post glucose stimulation (Figure 6D). Although ZMP increases, there was no evidence of activation of AMPK as no change was seen in the phosphorylation of HMG-CoA reductase and a decrease in ACC-1 phosphorylation was observed following glucose addition (Figure 3I). Therefore, while ZMP may restrain GSIS, at endogenous levels this effect does not seem to be through AMPK; perhaps through an alternate route such as altering lipid metabolism independent of AMPK activation (57).

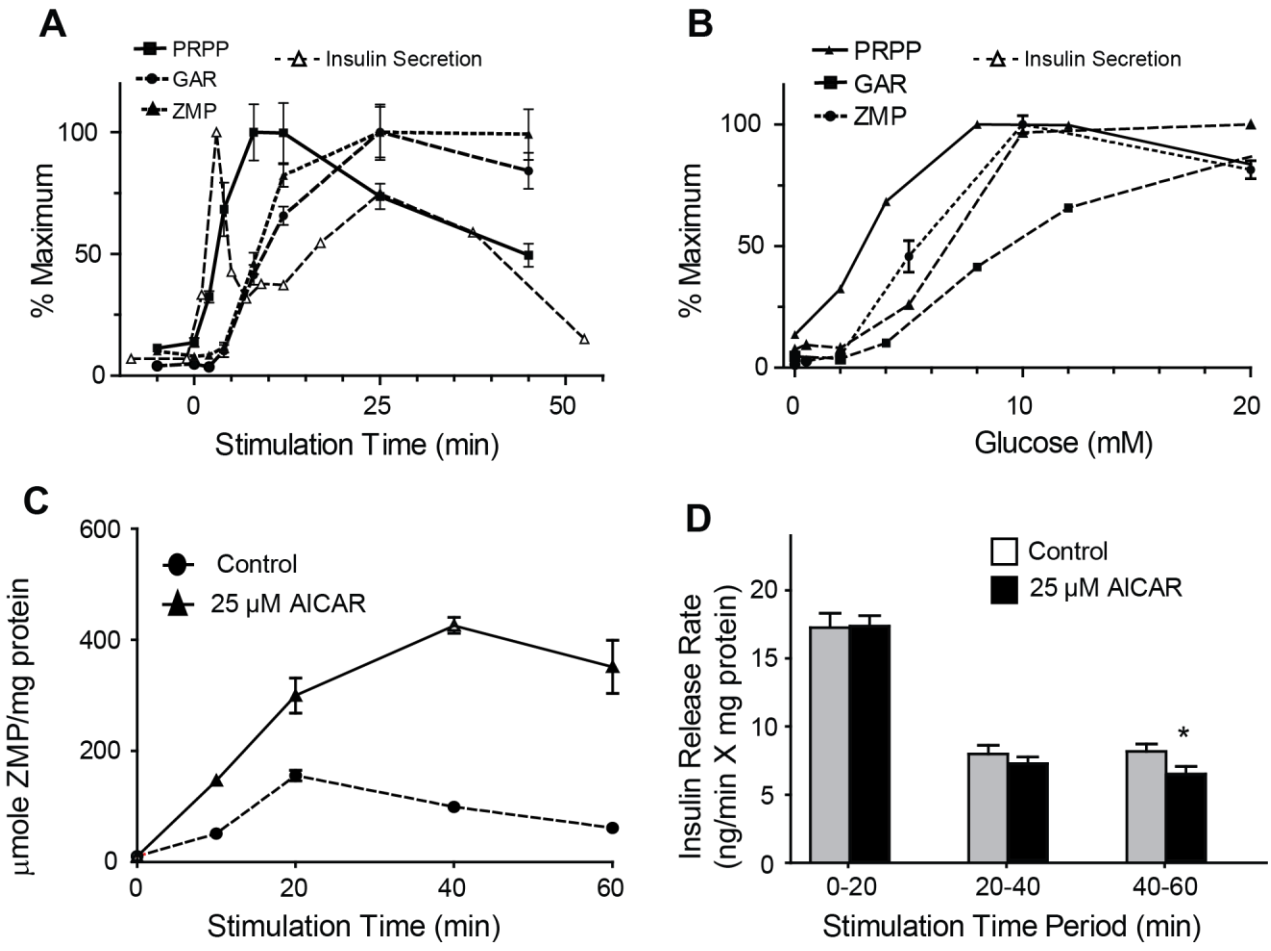

Figure 3-6. Formation and effect of ZMP in INS-1 cells. A and B. Time (A) and concentration-dependent (B) changes in purine metabolic pathway in INS-1 cells stimulated with glucose. PRPP = Phosphoribosylpyrophosphate, GAR = glycinamide ribotide, ZMP = 5-amino-4-imidazolecarboxamide ribotide. (C) Time-dependent formation of ZMP in INS-1 cells stimulated with 10 mM glucose with or without 25 µM AICAR. Error bars represent 1 SEM, n = 3. (D) insulin secretion rate measured by change in incubation buffer insulin concentration over indicated time period. Error bars represent 1 SEM, n = 8. Asterisk indicates significant difference in insulin release rate with $p < 0.05$.

Sugar Nucleotide Donors. We detected 8 common sugar nucleotide donors with GDP-mannose changing the most substantially (Figure 1D). GDP-mannose forms from conversion of glycolytic intermediate fructose-6-phosphate to mannose-6-phosphate and mannose-1-phosphate before condensing with GTP (58). This metabolite has not previously been quantified in β-cells; but, we observe a rapid increase that peaked at 14-fold over basal (~4.2 µmole/mg protein) within 8 min of glucose followed by a gradual decrease. GDP-fucose, a product of GDP-mannose metabolism (59), was unchanged. While determination of these metabolites in β-cells have not been previously explored, we have previously described that activation of the insulin-like growth factor II (IGF-II)/mannose-6-phosphate (M-6-P) receptor by

IGF-II results in augmentation of insulin secretion, even at low concentrations of glucose (60). The binding of mannose-6-phosphate-tagged proteins may play a regulatory role in insulin secretion by interaction with insulin secretory vesicles.

Additional metabolites. In these studies, we identified additional metabolites that showed dynamic changes following glucose exposure in INS-1 (832/13). In addition to adenosine, other mono- and diphosphonucleotides decreased by 1.7-4.3 fold within 2 min of glucose stimulation. GTP increased only slightly (< 5%) whereas UTP and CTP increased 40% and 80%, respectively with reciprocal falls in their mono and dinucleotides (Figure 1D). These results were different in Ins-1 832/3 cells, were GTP and UTP slightly decreased with glucose stimulation, while CTP did not change. Recent studies have provided evidence for a significant role for mitochondrial GTP in GSIS (61). While GTP levels do not change significantly, the pool of mitochondrial GTP is small compared to the cytosolic pool, thus changes in the mitochondrial pool may not be detectable.

We also observed decreases in pantothenic acid with glucose in both cell lines. As this metabolite is important for CoA synthesis, its decrease may reflect consumption in *de novo* production of CoAs. Besides long-chain acyl-CoAs and farnesyl pyrophosphate discussed above, we also found changes in other compounds involved in lipid metabolism including decreases in free fatty acids and citicolline, an intermediate in production of phosphatidylcholine. Citicolline or CDP-choline and CDP-ethanolamine decreased upon glucose stimulation in INS-1 832/3 cell as well. This decrease seen in both cell lines is presumably due to the denovo-lipogenesis that consume those intermediates to form PC and PE respectively. While investigation of all these pathways is beyond the scope of this paper, these results indicate that this analytical method may be used for studying a wide range of metabolites and pathways connected to insulin secretion.

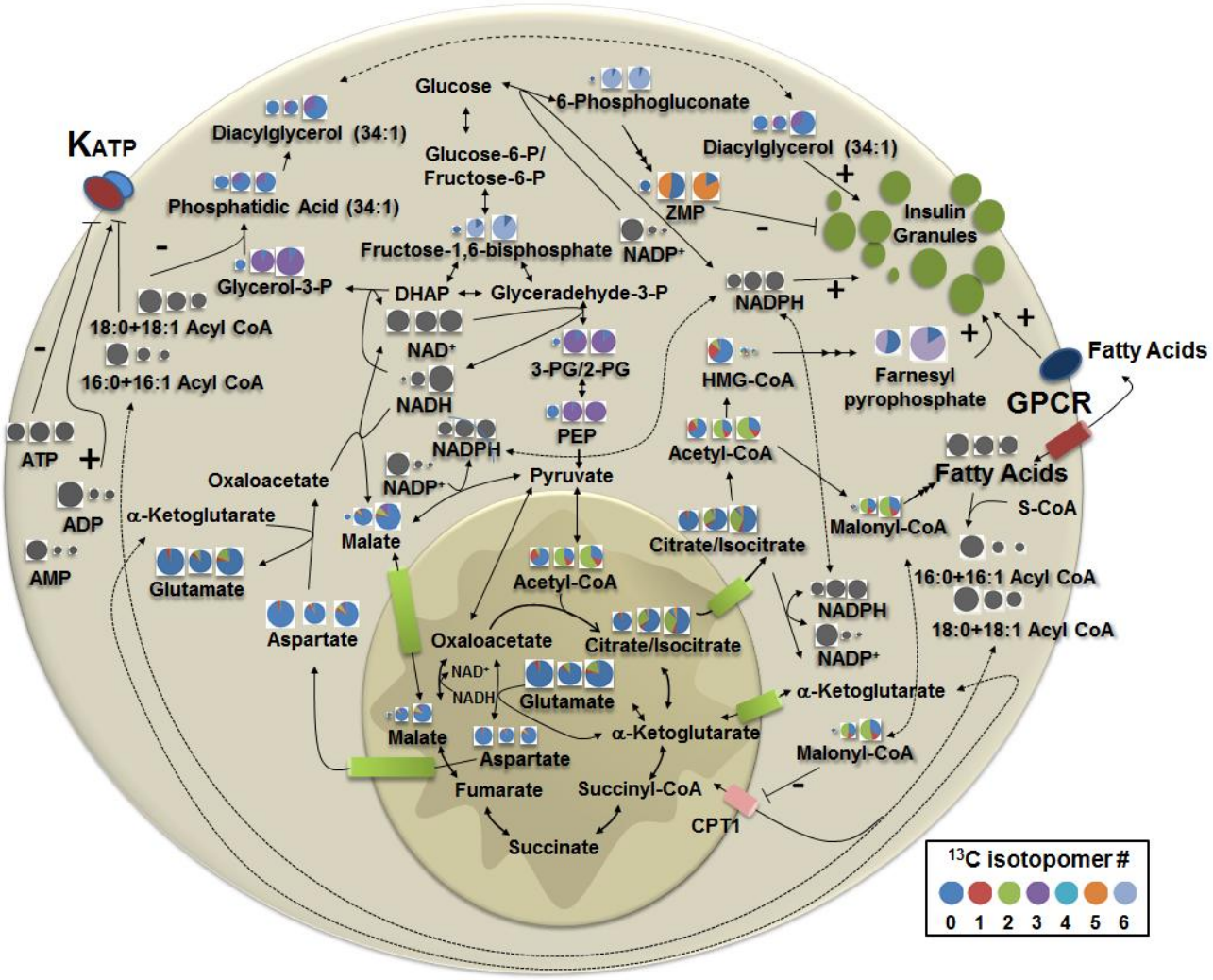

Figure 3-7. Schematic of metabolite levels and 13C enrichment of indicated metabolites at baseline and after 5 and 10 min exposure to 10 mM glucose. The size of each circle denotes the relative concentration of that metabolite, but does not reflect the relative concentration among the metabolites. 13C isotopologue percentage is indicated by the gradation of the pie and includes the baseline natural enrichment of 13C of ~1%. Grey circles indicate that the isotopic enrichment was not determined for those metabolites.

Conclusions. The use of LC-TOF-MS has allowed us to measure the temporal and dose response to increasing glucose concentration for a wide range of metabolites in INS-1 832/13 cells. By combining static (Figure 1) measurements and flux analysis (Figures 3-5) we have confirmed, extended or proposed modifications to several prevailing hypotheses regarding the metabolic pathways associated with GSIS (Figure 7). The simultaneous measurement of glycolytic and TCA cycle intermediates, nucleotides, long- and short-chain

acyl-CoAs and other intermediates show a novel interaction of metabolites. Novel findings include: 1. rapid esterification of long chain acyl-CoA with de novo synthesized glycerol-3-phosphate which explains the rapid fall in acyl-CoAs, allowing enhanced closure of the K_{ATP} channel and generation of phosphatidic acid and diacylglycerols to act as possible second messengers. 2. Rapid turnover of Span 1 TCA metabolites and rapid increases in the Span 2 metabolite, malate, which increases primarily by influx of malate into the mitochondria. 3. Rapid generation of malonyl-CoA from citrate coincident with a glucose-induced dephosphorylation of ACC1. 4. Significant flux of glucose-derived carbon into HMG-CoA and a rapid depletion of this metabolite with a parallel, rapid rise in farnesyl pyrophosphate, providing substrate for isoprenylation of proteins. 5. De novo synthesis of ZMP from glucose entering the pentose phosphate pathway which may modulate insulin release. 6. Increases in sugar nucelotides, including GDP-mannose, which may provide substrate for modification of proteins important for secretion.

These studies are limited to the glucose-responsive INS1 (832/13) cells but most findings were also reproduced in another glucose responsive cell line INS-1 (832/3). The studies presented here provide several hypotheses for metabolic pathways that may play varying roles in the augmentation of GSIS which can be tested in additional experiments in both INS-1 cells and in isolated isles. Assessing the alterations of specific metabolites in response to high glucose or fatty acid exposure may also provide information as to how chronic insulin resistance associated with obesity may result in altered β-cell metabolism which may lead to altered insulin secretory dynamics and diabetes mellitus.

REFERENCES

1. Jensen, M. V., Joseph, J. W., Ronnebaum, S. M., Burgess, S. C., Sherry, A. D., and Newgard, C. B. (2008) *Am J Physiol Endocrinol Metab* **295**, E1287-1297

2. Kwan, E. P., and Gaisano, H. Y. (2007) *Diabetes Obes Metab* **9 Suppl 2**, 99-108

3. Henquin, J. C., Nenquin, M., Ravier, M. A., and Szollosi, A. (2009) *Diabetes Obes Metab* **11 Suppl 4**, 168-179

4. Jitrapakdee, S., Wutthisathapornchai, A., Wallace, J. C., and MacDonald, M. J. (2010) *Diabetologia* **53**, 1019-1032

5. Muoio, D. M., and Newgard, C. B. (2008) *Nature Reviews Molecular Cell Biology* **9**, 193-205

6. Spegel, P., Malmgren, S., Sharoyko, V. V., Newsholme, P., Koeck, T., and Mulder, H. (2011) *Biochemical Journal* **435**, 277-284

7. Lorenz, M. A., Burant, C. F., and Kennedy, R. T. (2011) *Anal Chem* **83**, 3406-3414

8. Hohmeier, H. E., Mulder, H., Chen, G., Henkel-Rieger, R., Prentki, M., and Newgard, C. B. (2000) *Diabetes* **49**, 424-430

9. McKenna, M. C., Waagepetersen, H. S., Schousboe, A., and Sonnewald, U. (2006) *Biochem Pharmacol* **71**, 399-407

10. Matthew A. Lorenz, C. F. B., Robert T. Kennedy. (2011) *Analytical Chemistry* **TDB**, TBD

11. Sato, Y., Nakamura, T., Aoshima, K., and Oda, Y. (2010) *Anal Chem* **82**, 9858-9864

12. Wilcock, A. R., and Goldberg, D. M. (1972) *Biochemical Medicine* **6**, 116-126

13. Hall, L. M. (1960) *Biochemical and Biophysical Research Communications* **3**, 239-243

14. Bradford, M. M. (1976) *Analytical Biochemistry* **72**, 248-254

15. Straub, S. G., and Sharp, G. W. (2004) *Am J Physiol Cell Physiol* **287**, C565-571

16. Straub, S. G., and Sharp, G. W. G. (2002) *Diabetes/Metabolism Research and Reviews* **18**, 451-463

17. Nilsson, T., Schultz, V., Berggren, P. O., Corkey, B. E., and Tornheim, K. (1996) *Biochemical Journal* **314 (Pt 1)**, 91-94

18. Detimary, P., Van den Berghe, G., and Henquin, J.-C. (1996) *Journal of Biological Chemistry* **271**, 20559-20565

19. Fridlyand, L. E., Ma, L., and Philipson, L. H. (2005) *American Journal of Physiology - Endocrinology And Metabolism* **289**, E839-E848

20. Krippeit-Drews, P., Bäcker, M., Düfer, M., and Drews, G. (2003) *Pflügers Archiv European Journal of Physiology* **445**, 556-562

21. Tarasov, A., Dusonchet, J., and Ashcroft, F. (2004) *Diabetes* **53 Suppl 3**, S113-122

22. Bränström, R., Aspinwall, C. A., Välimäki, S., Östensson, C. G., Tibell, A., Eckhard, M., Brandhorst, H., Corkey, B. E., Berggren, P. O., and Larsson, O. (2004) *Diabetologia* **47**, 277-283

23. Liang, Y., and Matschinsky, F. M. (1991) *Diabetes* **40**, 327-333

24. Prentki, M., Vischer, S., Glennon, M. C., Regazzi, R., Deeney, J. T., and Corkey, B. E. (1992) *Journal of Biological Chemistry* **267**, 5802-5810

25. Corkey, B. E., Deeney, J. T., Yaney, G. C., Tornheim, K., and Prentki, M. (2000) *J Nutr* **130**, 299S-304S

26. Roduit, R., Nolan, C., Alarcon, C., Moore, P., Barbeau, A., Delghingaro-Augusto, V., Przybykowski, E., Morin, J., Masse, F., Massie, B., Ruderman, N., Rhodes, C., Poitout, V., and Prentki, M. (2004) *Diabetes* **53**, 1007-1019

27. Faergeman, N. J., and Knudsen, J. (1997) *Biochem J* **323 (Pt 1)**, 1-12

28. Hashimoto, T., Isano, H., Iritani, N., and Numa, S. (1971) *Eur J Biochem* **24**, 128-139

29. Nolan, C. J., Madiraju, M. S., Delghingaro-Augusto, V., Peyot, M. L., and Prentki, M. (2006) *Diabetes* **55 Suppl 2**, S16-23

30. Prentki, M., and Madiraju, S. R. (2012) *Mol Cell Endocrinol* **353**, 88-100

31. Poitout, V. (2008) *Am J Physiol Endocrinol Metab* **294**, E214-216

32. Henquin, J. C. (2000) *Diabetes* **49**, 1751-1760

33. Bender, K., Newsholme, P., Brennan, L., and Maechler, P. (2006) *Biochem Soc Trans* **34**, 811-814

34. Eto, K., Tsubamoto, Y., Terauchi, Y., Sugiyama, T., Kishimoto, T., Takahashi, N., Yamauchi, N., Kubota, N., Murayama, S., Aizawa, T., Akanuma, Y., Aizawa, S., Kasai, H., Yazaki, Y., and Kadowaki, T. (1999) *Science* **283**, 981-985

35. Brown, L. J., Koza, R. A., Everett, C., Reitman, M. L., Marshall, L., Fahien, L. A., Kozak, L. P., and MacDonald, M. J. (2002) *J Biol Chem* **277**, 32892-32898

36. Wollheim, C. B., and Maechler, P. (2002) *Diabetes* **51 Suppl 1**, S37-42

37. Jensen, M. V., Joseph, J. W., Ronnebaum, S. M., Burgess, S. C., Sherry, A. D., and Newgard, C. B. (2008) *Am J Physiol Endocrinol Metab* **295**, E1287-1297

38. Maechler, P., and Wollheim, C. B. (2001) *Nature* **414**, 807-812

39. Lu, D., Mulder, H., Zhao, P., Burgess, S. C., Jensen, M. V., Kamzolova, S., Newgard, C. B., and Sherry, A. D. (2002) *Proc Natl Acad Sci U S A* **99**, 2708-2713

40. Hoy, M., Maechler, P., Efanov, A. M., Wollheim, C. B., Berggren, P. O., and Gromada, J. (2002) *FEBS Lett* **531**, 199-203

41. Simpson, N. E., Khokhlova, N., Oca-Cossio, J. A., and Constantinidis, I. (2006) *Diabetologia* **49**, 1338-1348

42. MacDonald, M. J. (1995) *Journal of Biological Chemistry* **270**, 20051-20058

43. MacDonald, M. J., Fahien, L. A., Brown, L. J., Hasan, N. M., Buss, J. D., and Kendrick, M. A. (2005) *Am J Physiol Endocrinol Metab* **288**, E1-15

44. Odegaard, M. L., Joseph, J. W., Jensen, M. V., Lu, D., Ilkayeva, O., Ronnebaum, S. M., Becker, T. C., and Newgard, C. B. (2010) *J Biol Chem* **285**, 16530-16537

45. Luciani, D. S., Misler, S., and Polonsky, K. S. (2006) *The Journal of Physiology* **572**, 379-392

46. Guay, C., Madiraju, S. R., Aumais, A., Joly, E., and Prentki, M. (2007) *J Biol Chem* **282**, 35657-35665

47. Hasan, N. M., Longacre, M. J., Seed Ahmed, M., Kendrick, M. A., Gu, H., Ostenson, C. G., Fukao, T., and MacDonald, M. J. (2010) *Arch Biochem Biophys* **499**, 62-68

48. Corkey, B. E., Glennon, M. C., Chen, K. S., Deeney, J. T., Matschinsky, F. M., and Prentki, M. (1989) *Journal of Biological Chemistry* **264**, 21608-21612

49. McTaggart, S. J. (2006) *Cell Mol Life Sci* **63**, 255-267

50. Kowluru, A., Veluthakal, R., Rhodes, C. J., Kamath, V., Syed, I., and Koch, B. J. (2010) *Diabetes* **59**, 967-977

51. Kowluru, A. (2008) *J Cell Mol Med* **12**, 164-173

52. Schuit, F., De Vos, A., Farfari, S., Moens, K., Pipeleers, D., Brun, T., and Prentki, M. (1997) *Journal of Biological Chemistry* **272**, 18572-18579

53. Hardie, D. G. (2008) *Int J Obes* **32**, S7-S12

54. da Silva Xavier, G., Leclerc, I., Varadi, A., Tsuboi, T., Moule, S. K., and Rutter, G. A. (2003) *Biochemical Journal* **371**, 761-774

55. Zhang, S., and Kim, K. H. (1995) *Journal of Endocrinology* **147**, 33-41

56. Akkan, A. G., and Malaisse, W. J. (1994) *Diabetes Res* **25**, 13-23

57. Jacobs, R. L., Lingrell, S., Dyck, J. R. B., and Vance, D. E. (2007) *Journal of Biological Chemistry* **282**, 4516-4523

58. Sullivan, F. X., Kumar, R., Kriz, R., Stahl, M., Xu, G. Y., Rouse, J., Chang, X. J., Boodhoo, A., Potvin, B., and Cumming, D. A. (1998) *J Biol Chem* **273**, 8193-8202

59. Becker, D. J., and Lowe, J. B. (2003) *Glycobiology* **13**, 41R-53R

60. Zhang, Q., Tally, M., Larsson, O., Kennedy, R. T., Huang, L., Hall, K., and Berggren, P. O. (1997) *Proc Natl Acad Sci U S A* **94**, 6232-6237

61. Kibbey, R. G., Pongratz, R. L., Romanelli, A. J., Wollheim, C. B., Cline, G. W., and Shulman, G. I. (2007) *Cell Metab* **5**, 253-264

62 Ronnebaum, S.M., Jensen, M.V., Hohmeier, H.E., Burgess, S.C., Zhou, Y.P., Qian, S., MacNeil, D., Howard, A., Thornberry, N., Ilkayeva, O., Lu, D., Sherry, A.D., and Newgard, C.B. (2008)

Supplmentary information

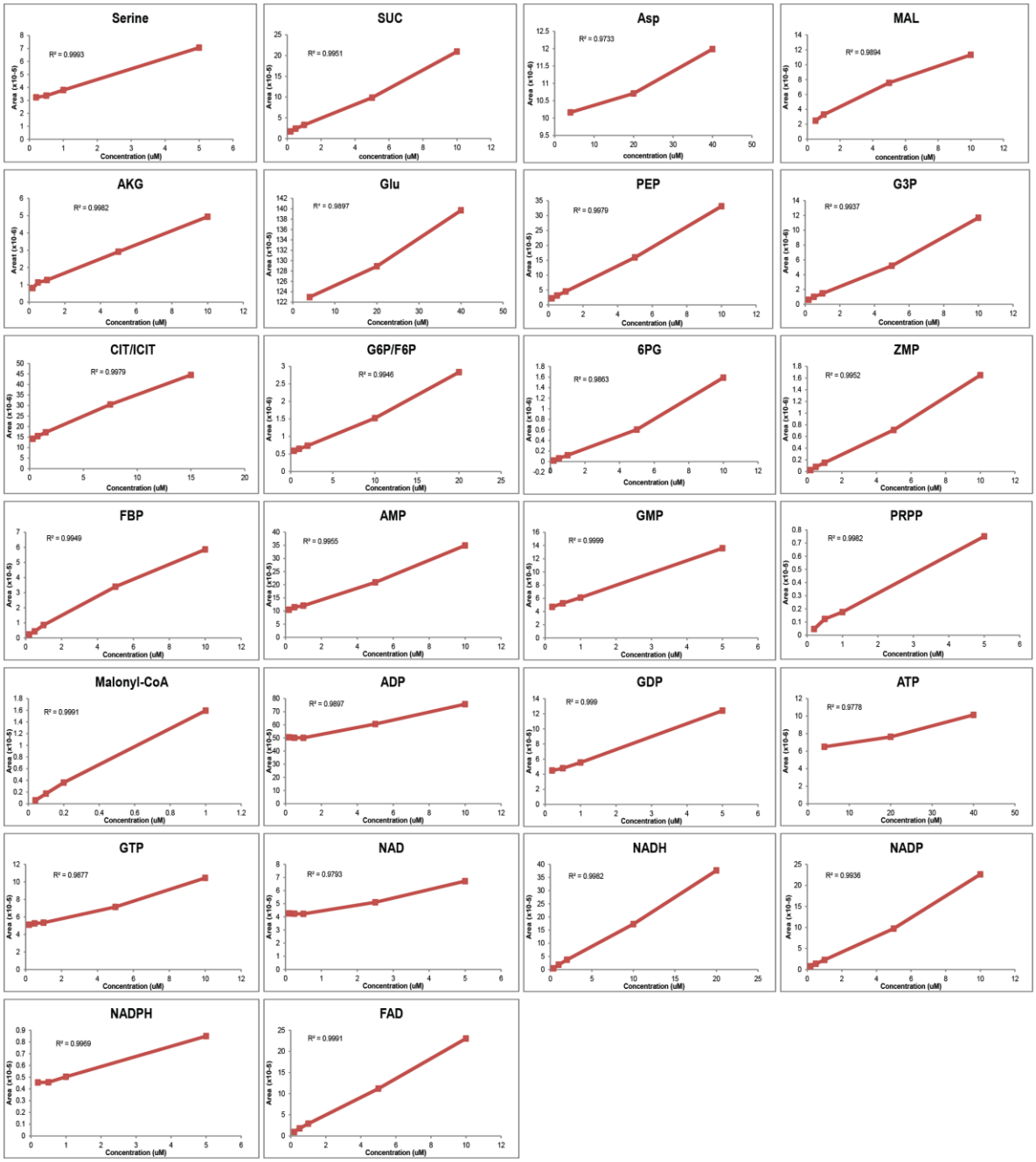

Figure S1. Results from standard addition experiment to determine linearity of response for 24 metabolites. An extract of INS-1 cells that had been incubated for 2 h in 0.5 mM glucose in KRB was divided into aliquots. The aliquots were spiked to create different concentrations of 24 metabolites and a constant final volume of extract. Each sample was analyzed by LC-TOF-MS and peak areas related to the spiked concentration (i.e., does not incorporate endogenous concentration). Analytes that have a smaller number of points in the lines have high concentrations so low concentration spikes were not used because they had undetectable effects on peak area. Each plot indicates the R2 value from linear regression analysis.

Chapter 4. METABOLIC REMODELING BY FATTY ACIDS AND ENHANCEMENT BY FFAR1/GPR40 AGONISTS DURING POTENTIATION OF INSULIN SECRETION

ABSTRACT

Acute fatty acid (FA) exposure potentiates GSIS in β-cells through metabolic and receptor mediated effects. We assessed the effect of fatty acids on the dynamics of the metabolome in INS-1 (832/3) cells following exposure to U-[^{13}C]glucose to assess flux through metabolic pathways. Metabolite profiling showed a fatty acid-induced increase in acyl-CoAs which were rapidly esterified with glucose-derived glycerol-3-phosphate to form lysophosphatidic acid, mono- and diacylglycerols and other glycerolipids, some implicated in augmenting insulin secretion. Glycolytic flux increased along with a reduction in the NADH/NAD$^+$ ratio, presumably by an increase in conversion of dihydoxyacetone phosphate to glycerol-3-phosphate. The fatty acid-induced increase in glycolysis also resulted in increases in tricarboxylic cycle flux and oxygen consumption. Inhibition of fatty acid activation of FFAR1/GPR40 by antagonist or siRNA knockdown decreased glycerolipid formation, attenuated fatty acid increases in glucose oxidation, and increased mitochondrial FA flux as evidenced by increased acyl-carnitine levels. Conversely, FFAR1/GPR40 activation in the presence of low FA, increased flux into glycerolipids and enhanced glucose oxidation. These results suggest that by remodeling glucose and lipid metabolism, fatty acid significantly increases the formation of both lipid- and TCA cycle-derived factors that augment insulin secretion.

INTRODUCTION

Glucose stimulated insulin secretion (GSIS) is mediated by a series of events that depend upon increases in glycolytic and tricarboxylic cycle (TCA) flux and the generation of metabolic coupling factors (1). Glycolytically derived ATP likely plays a role on the closure of K_{ATP} channels during the early phase of insulin secretion (1) and efficient glycolysis is dependent upon regeneration of NAD$^+$, at least in part via malate-aspartate and glycerol-3-phosphate shuttles (2). The TCA cycle is thought to participate in substrate cycling which allows the generation of NADPH and other proposed intermediates which participate in augmentation of insulin secretion (3).

Free fatty acids play an important role in regulating β-cell function under physiological and pathological conditions. Exposure to fatty acid is known to amplify glucose stimulated insulin secretion (GSIS) with optimal potentiation dependent upon both fatty acid metabolism within the β-cell (4, 5) and activation of the FFAR1/GPR40 receptor. Activation of this surface G protein coupled receptor has been shown to be responsible for ~ 50% of fatty acid potentiation effect of the second phase of GSIS in rat islets (6, 7). Both lipogenesis and lipolysis generate glycerolipids, such as DAG, which provides additional signals for potentiating GSIS (8). Fatty acids must be esterified to acyl-CoAs to function in GSIS potentiation; inhibition of lipogenesis by triascin C, an acyl-CoA synthase inhibitor, inhibited FFA potentiation of insulin secretion in rat islets (9). Long chain acyl-CoA can act as a lipid signal for insulin exocytosis (10, 11), increase intracellular free calcium, and modulate K_{ATP} (12) and calcium channels (13). Increased formation of malonyl-CoA via mitochondrial derived citrate reduces fatty acid oxidation and enhances lipogenesis (5), increasing the availability of acyl-CoAs for metabolism. In addition, inhibition of lipase decreased phase 2 insulin secretion in rat islets (14), indicating a role for lipolysis in potentiation of insulin secretion. The decrease was reversed by palmitic acid, suggesting that lipolysis can be substituted by de novo generation of signaling lipids.

To our knowledge, there are no large scale assessments of metabolite changes in response to acute fatty acid exposure in β-cells. In previous papers (15, 16), we have shown that assessment of metabolites in INS-1 cells, a robust model for studying GSIS, can provide detailed temporal and assessments of flux through multiple metabolic pathways. Using these techniques we assessed the changes in the INS -1 cell metabolome associated with fatty acid potentiation of GSIS. In addition to temporal changes in metabolites, we used both U-[^{13}C]glucose and U-[^{13}C]palmitate to follow remodeling of INS -1 cell metabolism in response to fatty acids and to synthetic FFAR1/GPR40 agonists and antagonists. The studies suggest that fatty acids enhance the flux of dihydroxyacetone phosphate to glycerol-3-phosphate, regenerating NAD^+, resulting in enhanced glycolytic and TCA cycle flux. We also provide evidence that FFAR1/GPR40 signaling enhances this flux, providing additional mechanisms for the positive pharmacological action FFAR1/GPR40 agonist (17, 18).

EXPERIMENTAL PROCEDURES

Materials. INS-1 832/3 cells (hereafter, INS-1) were kindly provided by Dr. Christopher Newgard (Duke University). All chemicals were purchased from Sigma-Aldrich unless otherwise noted.

Cell Culture and media. INS-1 cells were cultured in RPMI as described previously (16). Cells were incubated in RPMI supplemented with 3 mM glucose for ~6 h prior to experimentation. Free fatty acid solution was prepared by finely grinding fatty acid (sodium palmitate) using mortar and pestle and adding it to a warm solution of BSA (fatty acid free) dissolved in KRHB buffer (16). Leaving the palmitate solution to stir using magnetic stirrer for several hours at high speed yielded a homogenous suspension.

Glucose Stimulation. Palmitic or oleic acid (0.5 mM) was complexed with 0.5 % BSA (fatty acid free) solution in KRHB to achieve a 1:6 molar ratio of BSA to fatty acid. Cells were incubated for 30 min in glucose-free media with BSA or palmitate or oleate before stimulation with 16.6 mM [^{12}C] glucose or U-[^{13}C] glucose for time periods ranging from 5 to 60 minutes. At each time point, cells were snap frozen using liquid nitrogen and kept at -80° C until metabolite extraction as described previously (15). At each time point the media was also collected for insulin measurement.

Fatty acid metabolism. Cells were incubated with 500 µM U-^{13}C palmitic acid (Sigma), 500 µM U-^{13}C oleic acid (sigma) or 0.5 % BSA (fatty acid free) for 30 min in KRHB with 0 mM glucose before stimulation with 16.7 mM 12C-glucose for 60 min.

GPR40 activation and inhibition. Cells were incubated for 30 min with or without palmitate in the presence of either the FFAR1/GPR40 antagonist GW1100 (5 µM) or the FFAR1/GPR40 agonist Cay 10587 (10 µM) (Cayman Chemical, Ann Arbor, MI). Drugs were dissolved in DMSO which was added alone for control studies.

GPR40 Knockdown. INS-1 cells were cultured in 6 well plates and 150 pM of GPR40 siRNA (Invitrogen) or Non-targeting siRNA (Thermo) was added for48 hours cells after which cells were harvested for Western blot or for metabolomic profiles.

Oxygen consumption and extracellular acidification rate measurement. Measurements were performed using a Seahorse XF24 extracellular flux analyzer (Seahorse Bioscience) using 5x KHB as described by the manufacturer (555 mM NaCl, 23.5 mM KCl, 10 mM MgSO4 and 6 mM

Na2HPO4). Briefly cells were seeded in 24 sea horse plate in full RPMI. RPMI was replaced with low glucose RPMI 6 hours before the experiment. The cells were incubated at 37 °C in the absence of CO2 for 1 hr after which media was changed to KHB containing fatty acid or BSA before assay. After equilibration, measurements were taken for 10 minutes followed by the addition of 16.7 mM glucose for an additional 40 min for assessment of oxygen consumption.

Insulin measurement and Western blot. For insulin assay, a 100 µl aliquot of supernatant was assayed using a rat/mouse insulin ELISA kit (Millipore, Billerica, MA) after dilution with 1% BSA. Western blot for phospho-ACC, phospho-AMPK or β-actin (all from Cell Signaling, Danvers, MA) or GPR40 receptor (Novus Biologicals, Littleton, CO) was performed as described (16).

Metabolites Measurement. Metabolites were extracted using 90% (9:1 methanol: chloroform)/10% water. Polar metabolites were separated using Luna NH2, and lipids separated using Xbridge BEH C18 XP or Capcell C18 column (2 mm x 150 mm). Metabolites were detected by time of flight mass spectrometry in negative and positive mode as described previously (16). Untargeted analysis was performed using XCMS online (19) and metabolites were identified using accurate mass or authentic standards (if available) (16). Relative peak areas were used for relative quantification of identified metabolites (16).

Statistics. Data are expressed as mean ± 1 standard error (S.E). Statistical significance was determined when appropriate using unpaired, two-tailed Student's t test assuming equal variance or ANOVA using Tukey's post-hoc analysis using SPSS; p-values < 0.05 were considered significant.

RESULTS

Palmitic acid potentiates glucose stimulated insulin secretion (GSIS). INS-1 cells were preincubated with BSA or 500 µM palmitate complexed to BSA ('palmitate') for 30 min in 0 mM glucose followed by stimulation with 16.6 mM glucose. Media was collected for measurement of insulin secretion from 0 to 60 min after addition of glucose. Cell extracts were collected for determination of 69 metabolites by LC-MS prior to addition of BSA or palmitate (-30 min) or from the same cultures used to assess insulin secretion (0 to 60 min) (Figure 1). As previously demonstrated in islets (4), preincubation of INS-1cells with fatty acids potentiated GSIS by ~2-

fold, at each time point compared to BSA controls (Figure 2A). Heat maps of metabolite profiles (Figure 1) showed that 30 min of preincubation with either BSA or palmitate in glucose-free media resulted in lowering of the concentrations of most metabolites relative to preincubation levels with the exception of expected rises in nucleotide monophosphate levels.

As we (16) and others (20) have previously observed, palmitoyl-CoA rapidly decreased (~ 50%) following the addition of glucose in both BSA and palmitate pretreated cells (Figure 2B). This observation is despite the marked increase in palmitoyl-CoA concentration following preincubation with palmitate (Figure 2B). In addition, the concentration of palmitoyl-carnitine rapidly declined (Figure 2C), likely representing reduction in entry of palmitate into the mitochondria. The reduction in fatty acid entry into the mitochondria in β-cells has been ascribed to elevations in malonyl-CoA which inhibits CPT1 activity on the outer mitochondrial membrane (for review, see (21)). Indeed, in the absence of fatty acids, malonyl-CoA levels increase following glucose addition to INS-1 cells. However, in the presence of palmitate, the malonyl-CoA rise was blunted (Figures 2D and 1).

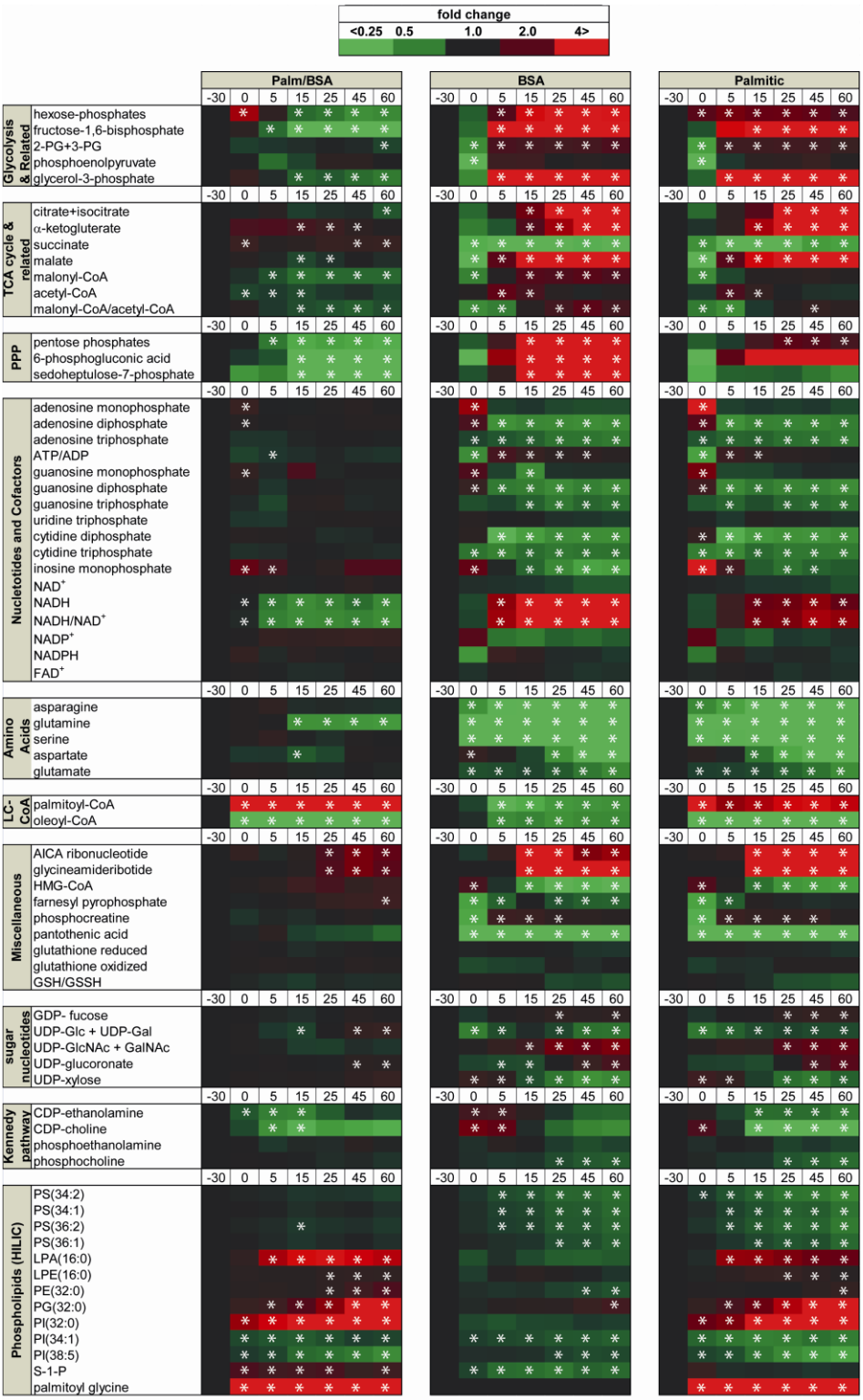

Figure 4-1. Temporal metabolites profile of INS-1/832/3 cells upon glucose stimulation in the presence or absence of palmitic acid. The heat map (middle and right) are showing the metabolites levels expressed as fold change of the (-30 min) time point. INS-1 cells were incubated in RPMI with 3 mM glucose for 6 hours (-30 time point) before incubation in KRHB for 30 minutes with no glucose in the presence or absence of 500 µM palmitate (0 time point). Cells were stimulated with 12C glucose for different time points (5 till 60 min). Asterisk indicates significant difference in peak area versus time -30 with p <

0.05. The heat map to the left is showing the fold change for metabolites in palmitate versus BSA treated cells, comparing each time point. Asterisk indicates significant difference in peak area of each time point of palmitate versus the corresponding BSA treated cell with p < 0.05. Statistics test used was ANOVA using Tukey's post-hoc analysis using SPSS software.

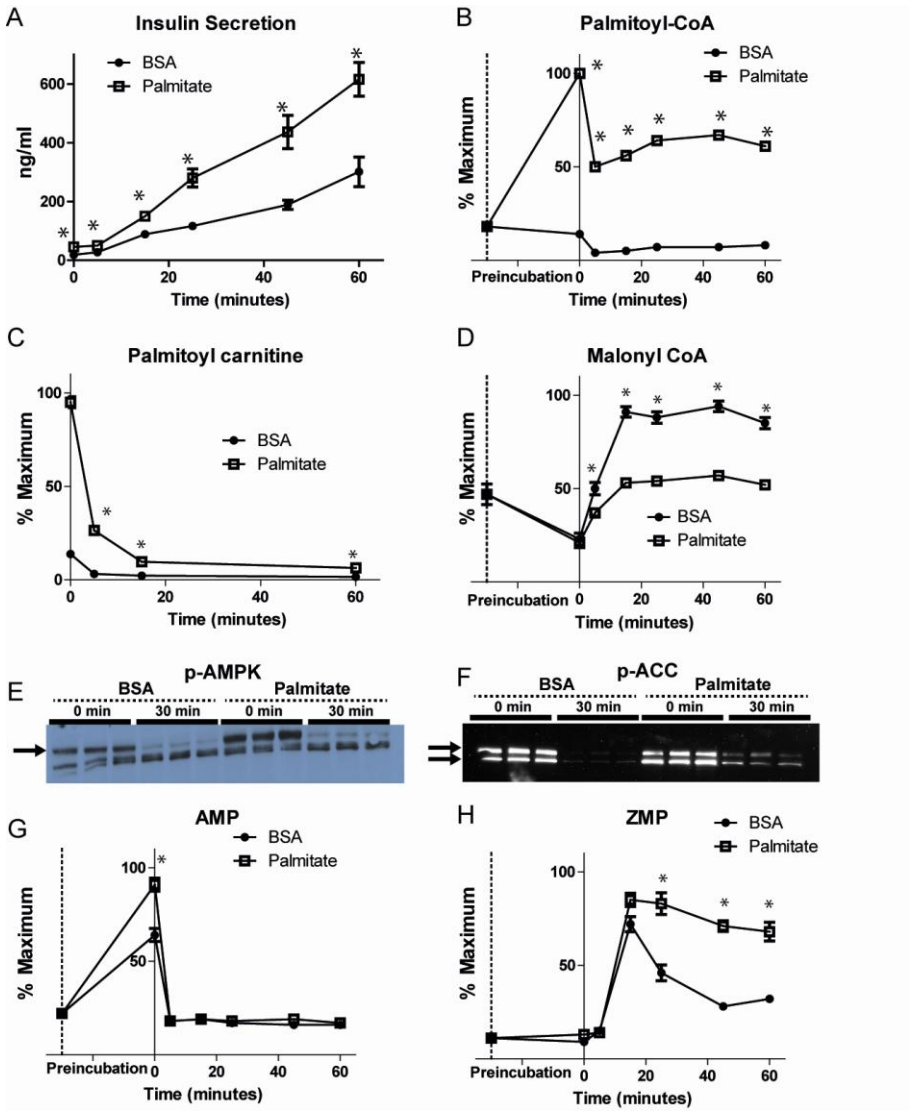

Figure 4-2.Palmitic acid incubation effect on GSIS, AMPK and related metabolites. Insulin levels after stimulation with 16.6 mM glucose for different time intervals in the presence or absence of 500 uM palmitate (A). Levels of palmitoyl-CoA (B) Palmitoyl-carnitine (C) Malonyl-CoA (D) AMP (G) ZMP (H) before and after 30 min incubation with 500 µM palmitate (time zero) and after stimulation with 16.6 mM glucose for different time points. Western blot for pAMPK (E) and pACC (F) before glucose addition (time zero) and after 30 min of glucose stimulation (30 min). * = p < 0.05 between BSA and palmitate at each time point. Error bars represent 1 S.E n= 3-4 per time point.

AMP-activated protein kinase (AMPK) is a known regulator the glycerolipids/free fatty acid cycle (22, 23) and generates malonyl-CoA by phosphorylating acetyl-CoA carboxylase

(ACC). We found that fatty acid addition increased the phosphorylation of AMPK and ACC (Figure 2E-F), increased AMP levels ~30% (Figure 2G), and resulted in a small, but persistent increase in p-ACC following glucose addition (Figure 2F). Interestingly, ZMP, an AMP analog known to activate AMPK, also increased after glucose addition with both BSA and fatty acid. However, ZMP remained elevated through the time course of insulin secretion in cells exposed to palmitate (Figure 2H), which may also contribute to the increased AMPK and ACC phosphorylation.

Fatty acid caused an increase in de novo-synthesized glycerolipids. To assess the effect of fatty acids on the formation of glycerolipids, we used LC-MS to quantify a series of lipid-associated metabolites in INS-1 during GSIS using U-[^{13}C]glucose to track de novo generation of glycerolipids containing palmitate. In the absence of added palmitate, a small rise was seen in the M+3 isotopologues of LPA, palmitic acid (PA), diacylglycerol (DAG), triglycerides (TG), phosphatidylglycerol (PG) and phosphatidylinositol (PI) and monoacylglycerol (MAG) (Figures 3A-H and Figure 1). In contrast, total levels and M+3 isotopologues rose significantly in cells pre-incubated with palmitate (Figure 3A-H) with the rise in LPA preceding that of the other lipids, demonstrating a significant increase in the esterification of U-[^{13}C]glycerol-3-phosphate (Go3P) (Figure 3A-H). In INS-1 cells, the increase in DAG, previously suggested to play an important role in GSIS (6, 9), was primarily due to increases in M+3 species, suggesting that the bulk of DAG is generated de novo during GSIS in INS-1 cells. We also observed increases in the labeling of phosphatidylcholine (PC), phosphatidyl ethanolamine (PE) and a parallel, rapid decrease in their precursor moieties, CDP-choline and CDP-ethanolamine, respectively (Figure 3, I-L). A mass shift of M+3 is detected for all these metabolites, except PG which shows M+6 mass shifts, presumably because of the incorporation of two [^{13}C]Go3P molecules into the lipid.

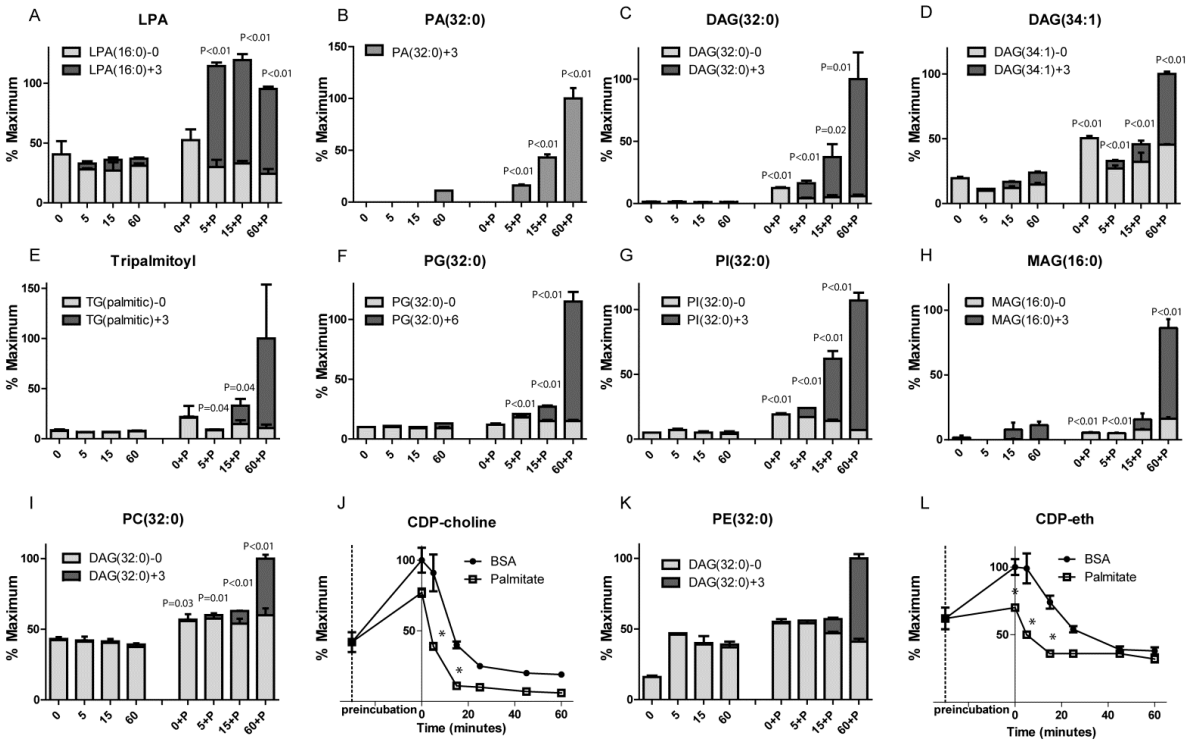

Figure 4-3.Palmitic acid effect on carnitines and glycerolipids metabolites. Glycerolipids levels before and after stimulation with 16.6 mM U-[13C]glucose with and without preincubation with 500 µM palmitate for 30 min (time 0) and after 5 or 15 or 60 min of glucose stimulation (A-I and K). CDP-choline (J) and CDP-eth (L) are measured after stimulation with 12C glucose. Error bars represent 1 S.E n= 3-4.

Fatty acid exposure increases Sphingosine-1-Phosphate and N-acyl amide levels. To further identify metabolites that could be implicated in fatty acid potentiation of GSIS, we used untargeted metabolomic profiling. We found significant increases in sphingosine-1-phosphate and two acyl amides; palmitoyl taurine and palmitoyl glycine (Figure 4A-C) whose identities were confirmed by accurate-mass and retention time matching with standards. Addition of taurine or glycine increased the levels of palmitoyl taurine and palmitoyl glycine, respectively, in the presence of palmitic acid (Figure 4, D and E). Although significant increases in the palmitoylated species were observed, minimal effect on basal or GSIS was found (Figure 3F). Despite recent studies that suggest that acyl-taurine species added exogenously to β-cells enhanced GSIS, we did not detect changes in insulin secretion following addition of taurine (not shown) and similarly, minimal effects of glycine.

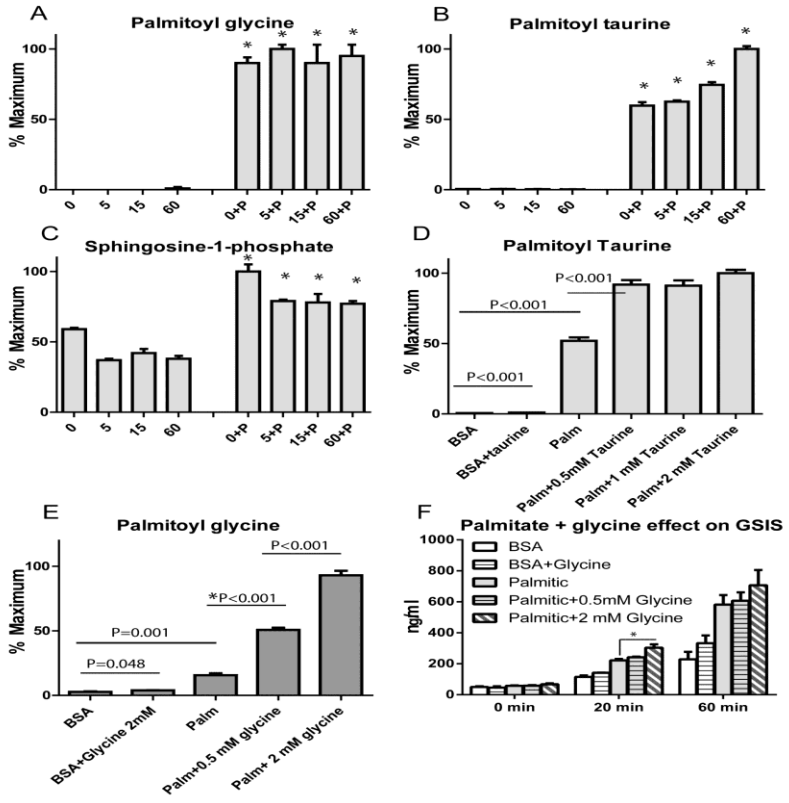

Figure 4-4.undirected analysis for metabolites changing with fatty acid treatment. levels of palmitoyl glycine, palmitoyl taurine and sphingosine phosphate after incubation with fatty acid for 30 min followed by stimulation with 16.6 mM U13C glucose for 5,15 or 60 min (A-C). Levels of palmitoyl taurine and palmitoyl glycine after the addition of increasing dose of their precursor amino acids in the presence or absence of palmitate (D-E). Insulin levels after incubation of cells with BSA or palmitic acid in the presence or absence of glycine (F). Media was collected before addition of glucose (0 minute) or after stimulation with 16.6 mM glucose for 20 or 60 min. Error bars represent 1 S.E n= 3-4.

Fatty acids increase glycolytic and TCA cycle carbon flux. Following the addition of glucose, glycolytic and pentose phosphate intermediates rose as expected in both BSA and palmitate treated cells (Figure 1); however, palmitate blunted this rise. By using U-[^{13}C]glucose, we found that the levels of fructose-bis-phosphate fell (Figure 5A) due to a reduction in ^{13}C-labeled intermediates (Figure 5B). Similar finding was observed other glycolytic intermediates (not shown) as well as in the pentose phosphate intermediates such as 6-phsophoglucanate and ribose+ribulose 5P (not chromatographically resolved) (Figure 5C-F). Similar changes were seen in Go3P levels (Figure 5G and H). Palmitate did not affect the glucose-induced rise in 2PG+3PG 2-phospho + 3-phosphoglycerate (2PG+3PG), which are not chromatographically resolved) or TCA cycle intermediates (Figure 5I-K and Figure 1).

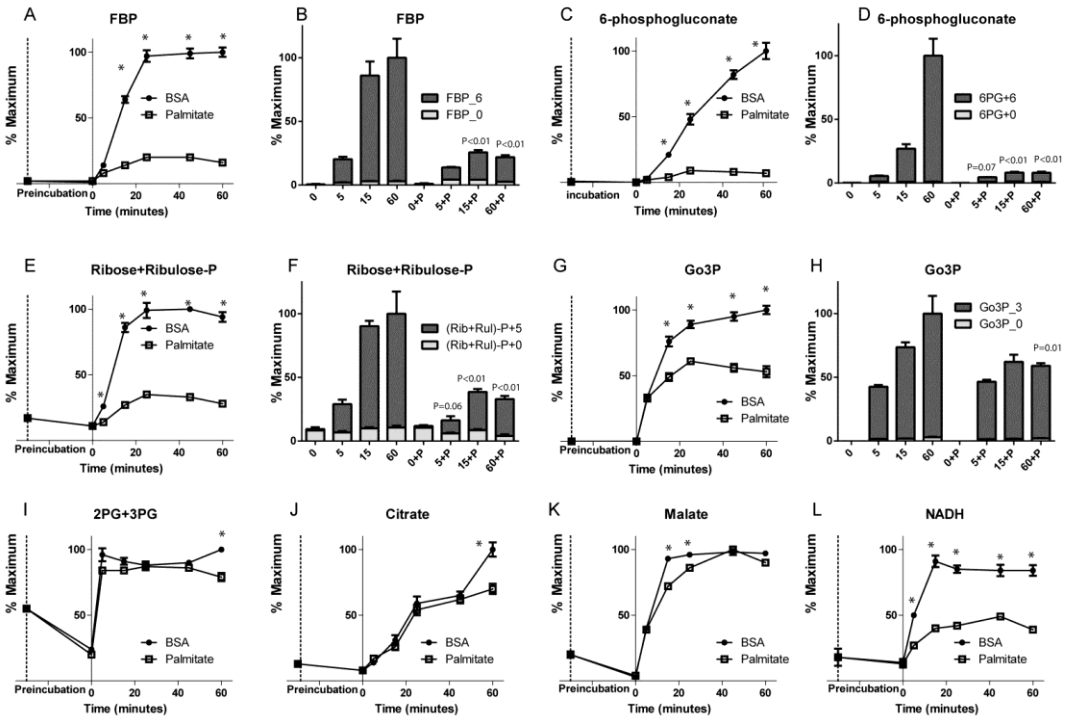

Figure 4-5.Palmitic acid effect on glycolysis, pentose phosphate metabolites and TCA cycle. Changes in levels of fructose bisphoshphate (A) phosphogluconate (C) ribose+ribulose-P (E), glycerol-3-phosphpate (G), 2PG+3PG (I), citrate (J), malate (K) and NADH (L) after stimulation with 16.6 mM 12C glucose in the presence or absence of 500 µM palmitate. Changes in total mass and 13C isotopologues after stimulation with 16.6 mM U13C glucose for fructose bisphosphate (B), phosphogluconate (D), ribose and ribulose-P (F) and glycerol-3-phosphate (H). Error bars represent 1 S.E n= 3-4 except for control at 60 minute using 13C glucose, where n=2, and the values were confirmed with n= 4 in separate experiment.

Because we found an increase in the flux of glucose into glycerolipids in the presence of palmitate, we hypothesized that the reduction in the glycolytic intermediates was due to their rapid consumption. The conversion of dihydroxyacetone phosphate to Go3P utilizes NADH and we observed a significant reduction the NADH levels in palmitate treated cells following the addition of glucose (Figure 5L) as well as reduction in the NADH/NAD^+ (Figure 1). To confirm increased glucose flux to Go3P by fatty acid treatment, we performed a pulse chase experiment in which a 15 min pulse of U-[^{13}C]glucose was chased for 2 min with unlabeled glucose in INS-1 pretreated with BSA or palmitate. The consumption of ^{13}C-labeled Go3P as well as the generation of unlabeled Go3P was faster in the presence of fatty acid (Figure 6A), confirming a rapid increase of Go3P consumption following palmitate treatment. Identical effects on metabolite flux were observed following preincubation of INS-1 cells with oleic acid (Supplemental Figure 1).

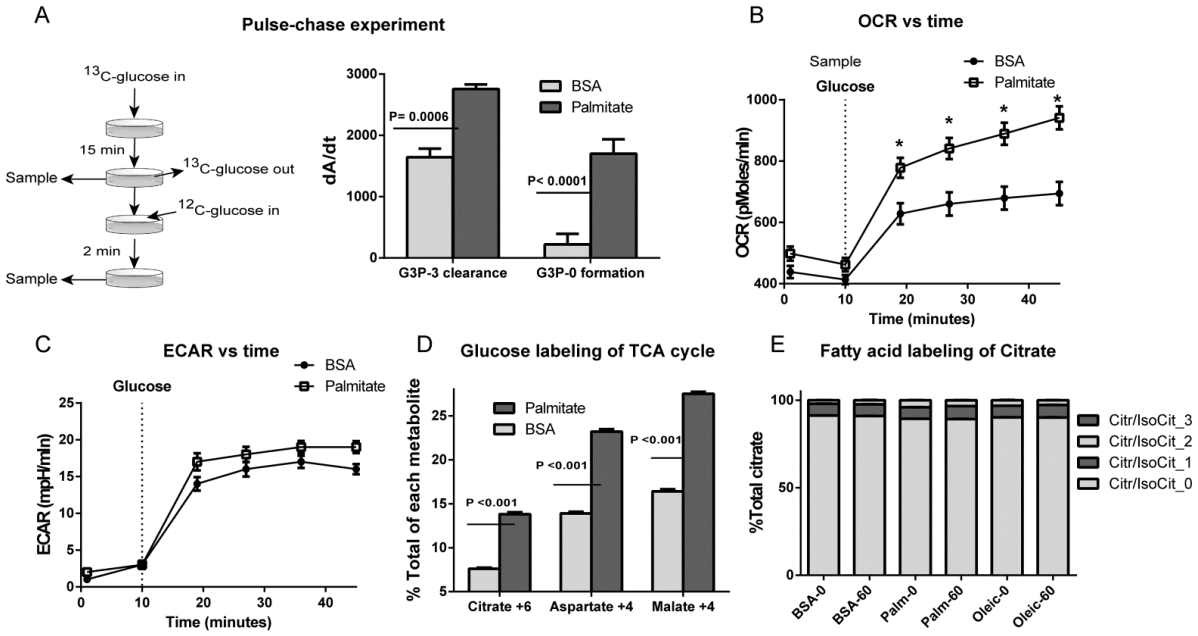

Figure 4-6.palmitic acid effect on glycolytic flux, fatty acid oxidation and oxygen consumption. For pulse-chase experiment, cells were stimulated with 16.7 mM U-13C glucose for 15 min (pulse) before the KRHB was replaced with the same media containing 16.7 mM 12C glucose for 2 min, after which the cells were quenched and the rate of consumption of labeled (Go3P) and the rate of formation of unlabeled (Go3P) in 2 min was plotted (A). Statistics was done by comparing the slope of linear regression lines (ANCOVA) using GraphPad prism. Oxygen consumption rate (OCR) and Extracellular acidification rate measured by sea horse system before and after the addition of 16.6 mM glucose (B and C). The percentage labeling of ultimate labeling of citrate, aspartate and malate after 1 hour treatment with U13C glucose (D). The % labeling of citrate after incubation of INS-1 cells with either BSA or U-[13C]palmitate or U-[13C]oleate for 30 min with no glucose (time zero) and after stimulation with 16.6 mM 12C glucose for 60 min (time 60) (E). Error bars represent 1 S.E with n= 3-4 for metabolites analysis and n= 10 for sea horse experiment.

As a consequence of regeneration of NAD^+ following palmitate treatment, an increase glucose flux into the TCA cycle would be expected. Thus, we measured oxygen consumption in INS-1 cells pretreated with BSA or palmitate for 30 min. As shown in Figure 6B, addition of palmitate produced a small increase in oxygen consumption rates (OCR) prior to the addition of glucose. In contrast, preincubation with palmitate increased OCR by ~66% following the addition of glucose, demonstrating an increase in glucose oxidation. Extracellular acidification rose following glucose addition, but was not affected by palmitate pretreatment (Figure 6C).

The rise in extra cellular acidification rate "ECAR", a measure of lactate production, was small, consistent with the low levels of lactate dehydrogenase in these cells (24). To further assess flux through the TCA cycle, cells were preincubated with BSA or palmitate and then for 60 min in the presence of U-[^{13}C] glucose. Measurement of the ratio of ^{13}C- isotopologues of

TCA intermediates revealed that fully labeled citrate (M+6), malate (M+4) and aspartate (M+4) were increased in the palmitate pretreated cells by approximately 35% (Figure 6D), supporting an increase of flux of glucose into the TCA cycle following palmitate treatment. Finally, the minimal contribution of palmitate to oxygen consumption in INS-1 cells was confirmed by the low levels of ^{13}C-carbon incorporation into citrate following exposure of cells to U-[^{13}C]palmitate or U-[^{13}C]oleate in the presence or absence of glucose (Figure 6E).

GPR40 receptor modulates FFA potentiation of GSIS and fatty acid esterification. We next examined the role of the free fatty acid receptor FFAR1/GPR40 on metabolic flux in INS-1 cells. We first preincubated cells with the FFAR1/GPR40 antagonist, GW1100, in the presence or absence of 250 µM palmitate and measured insulin secretion and metabolite levels in response to the addition of 16.6 mM U-[^{13}C]glucose for 30 min. GSIS was decreased significantly by GW1100 inhibition of GPR40 receptor, both in the absence and presence of palmitate (Figure 7A) as previously described (7, 25). Metabolite analysis showed that palmitate reduced the concentration of M+6 hexose phosphates as well as M+3 Go3P while GW1100-treated samples showed increased levels of M+6 hexoses (Figure 7B) as well as M+3 Go3P isotopologues (Figure 7C) following preincubation with palmitate. There was a parallel decrease in accumulation of M+3 isotopologues of LPA (Figure 7D) and various DAG species (Figure 7E and F) in antagonist treated cells following palmitate addition. Conversely, the FFAR1/GPR40 agonist, Cay 10587, increased the M+3 isotopologues of DAG, but only in the presence of 50 µM palmitate (Figure 7G).

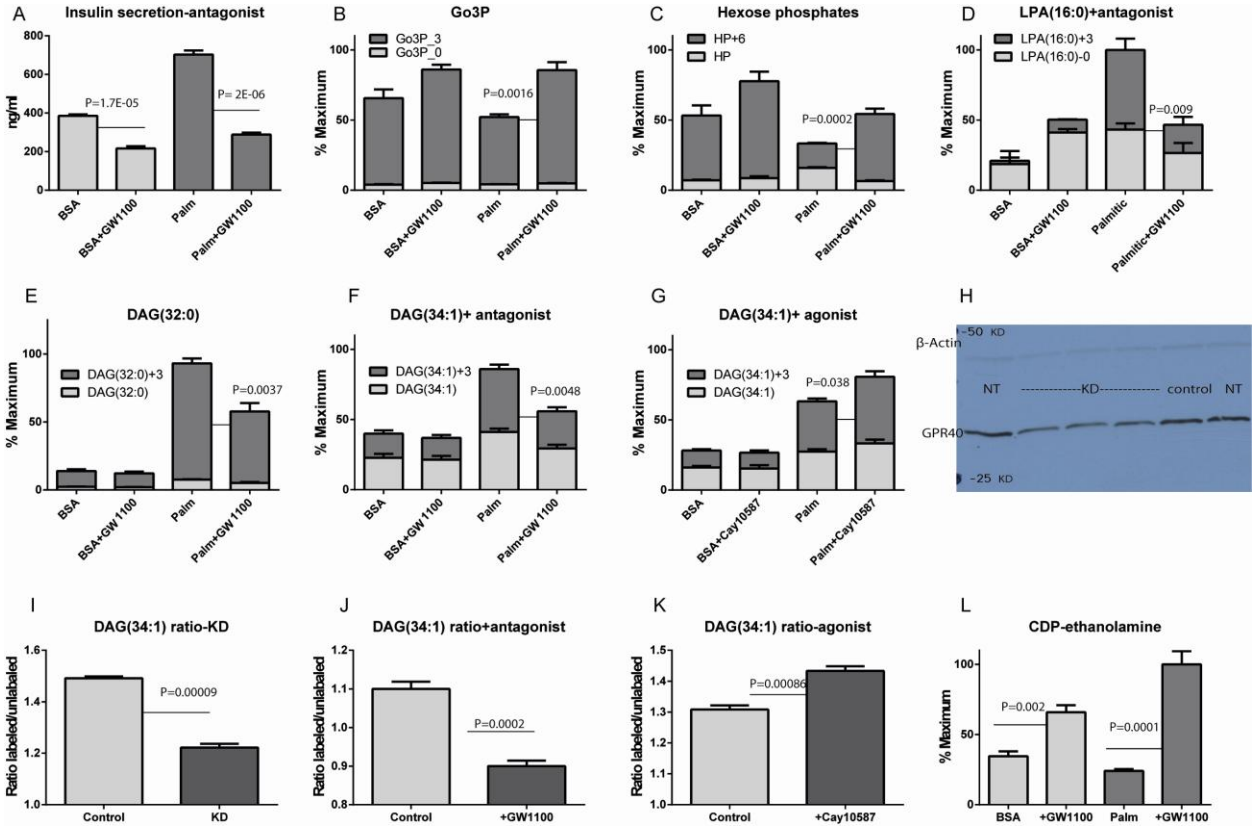

Figure4- 7: GPR40 role in palmitic acid induced metabolic changes. INS-1 cells were incubated with 250 µM palmitate or BSA in the presence or absence of 5 µM GPR40 antagonist (GW1100) for 30 min followed by stimulation with 16.6 mM U-[13C]glucose for 60 min. Using these conditions the following are measured : insulin levels (A), changes in total mass and 13C isotopologues of glycerol-3-phosphate (B), Hexose phosphates (C), LPA (16:0), DAG(32:0) (E), DAG (34:1) (F) and its isoptologue ratio (J), CDP-ethanolamine (L). INS-1 cells were incubated with 50 µM palmitate or BSA in the presence or absence of 10 µM Cay 10587 for 30 min followed by stimulation with 16.6 mM U-[13C] glucose for 60 min. Under these conditions, changes in total mass and 13C isotopologues of DAG(34:1) (G) and its isotopologues ratio (K) were measured. GPR40 was knocked down by siRNA and western blot is shown (H) for knocked down (KD) and non-transfected (control) or scrambled (non-targeting, NT). Under the knockdown conditions, INS-1 cells were incubated with 50 uM palmitate and 16.6 mM U-[13C] glucose for 30 min and the ratio of DAG (34:1) isotopologues was compared between knockdown (KD) and scrambled (control) samples. Error bars represent ± S.E n= 3-4.

To further confirm that these effects were GPR40 mediated, we were able to partially knockdown GPR40 receptor using siRNA (Figure 7H) and assess the M+3/M+0 isotopologues of DAG (34:1). GPR40 knocked down (KD) sample showed a significant decrease in the ratio of labeled/unlabeled DAG (34:1) (Figure 7I), similar to results seen in cells treated with the GPR40 antagonist (Figure 7J) and opposite to the effect mediated by GPR40 agonist (Figure 7K). CDP-ethanolamine increased in the presence of GPR40 antagonist (Figure 7L), which is in agreement with the decreased activity of the glycerolipids cycle (El Azzouny et al, in preparation)

Preincubation of INS-1 cells with GW1100 resulted in a ~2-fold increase in palmitoyl-carnitine levels, suggesting an increase in flux of palmitate into the mitochondria (Figure 8A), an effect was also found in FFAR1/GPR40 knockdown cells (Figure 8B). The FFAR1/GPR40 agonist had no effect on palmitoyl-carnitine levels when cells were incubated with low level (50 µM) palmitate (Figure 8C). These results suggest that flux into glycerolipids is the primary determinant of fatty acid entry into mitochondria. Neither antagonist (Figure 8D) nor agonist (Figure 8E) affected palmitoyl-CoA accumulation in the absence of glucose suggesting no effect of FFAR1/GPR40 receptors on fatty acid uptake or activation of the lipids by CoA synthase. To assess the effect of FFAR1/GPR40 activation on lipolysis, we incubated INS-1cells with U-[^{13}C]palmitate with or without agonist for 20 min in the absence of glucose. In the presence of agonist, there was an increase in the unlabeled DAG (34:1) and a decrease in the M+16/M+0 labeling ratio (Figure 8F), consistent with previous reports of phospholipase C activation by the receptor (26).

Finally, we assessed the effect of FFAR1/GPR40 receptor manipulation on palmitate-stimulated glucose oxidation in INS-1 cells. In the presence of agonist, there was a further increase in glucose oxidation in the presence of palmitate and Cay 10587 (Figure 8F). Conversely, the augmentation of glucose oxidation by palmitate was reduced by the antagonist (Figure 8G).

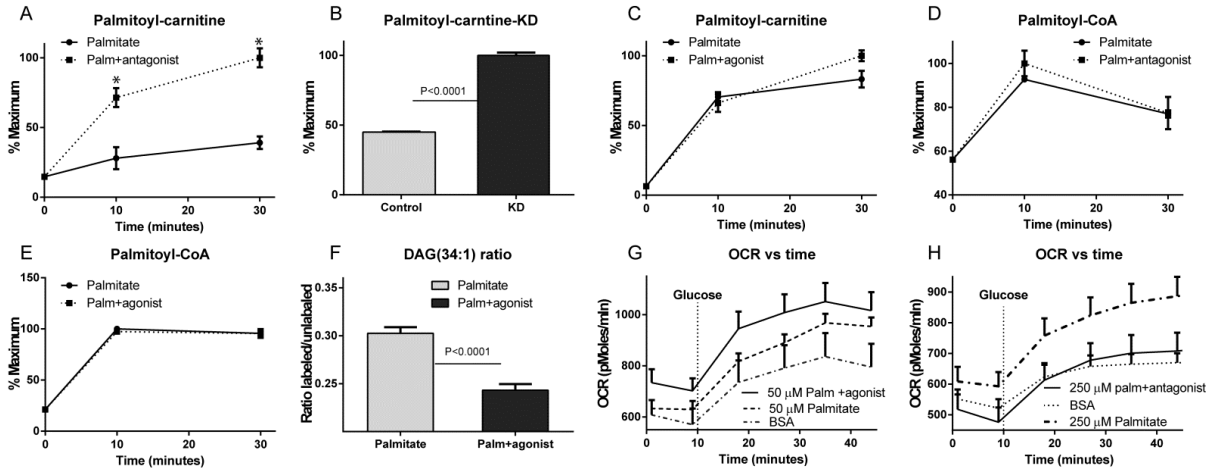

Figure 4-8.Metabolic changes with GPR40 modulation. INS-1 cells were incubated with 250 µM palmitate +/- 5 µM GW1100 in absence of glucose for 30 min and the levels of palmitoyl-carnitine (A) and palmitoyl-CoA (D) were measured at different

time points. Levels of palmitoyl carnitine in the GPR40 knockdown experiment described in figure 6 (B). INS-1 cells were incubated with 50 µM palmitate +/- 10 µM Cay10587 GPR40 agonist in absence of glucose for 30 min and the levels of palmitoyl-carnitine (C) and palmitoyl-CoA (E) were measured at different time points. INS-1 cells were incubated with 50 µM U-[13C] palmitate in the absence of glucose +/- agonist for 30 min and the ratio of labeled DAG(34:1)+16 to unlabeled DAG(34:1) was measured (F). Oxygen consumption rate in the presence or absence of agonist or antagonist (G and H). Error bars represent 1 S.E with n= 3 or 4 for metabolites analysis and n=6-7 for SeaHorse experiment

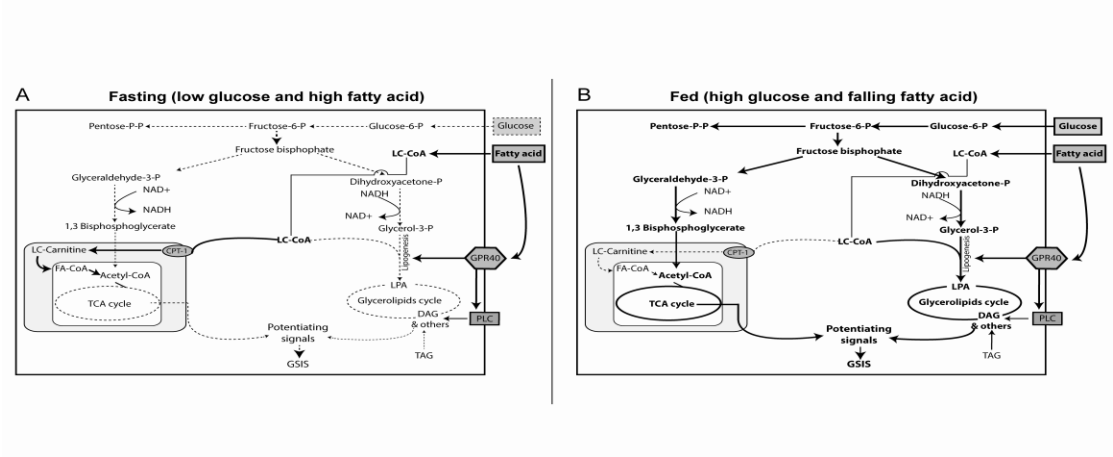

Figure 4-9.Proposed pathways for fatty acid potentiation of glucose stimulated insulin secretion. Metabolic remodeling of glucose flux due to fatty acids and FFAR1/GPR40 activation in β-cells.

DISCUSSION

The secretion of insulin is primarily regulated by the entry of glucose into the β-cell but is modulated by nervous system, hormonal, and nutritive inputs (27). Fatty acids augment insulin release in vivo and in vitro and its effects have been shown to be mediated via intracellular metabolism and through surface receptors (8). In this report we show that a 30 minute incubation of INS-1 cells with palmitate prior to addition of glucose results in a doubling of insulin release as seen previously in intact islets (4). Prior to glucose addition, palmitate exposure results in a ~7-fold increase in intracellular palmitoyl-CoA and a small increase in oxygen consumption, but little effect on basal insulin secretion and minimal changes in the majority of intracellular metabolites with the exception of a significant increase in the formation of palmitoyl-carnitine likely generated by the flux of fatty acid into the mitochondria. This suggests that despite a small increase in TCA cycle activity, there is minimal generation of factors necessary for insulin secretion. Following addition of U-[^{13}C] glucose, palmitoyl-CoA rapidly declines with the formation M+3 LPA and DAG isotopologues containing palmitate, directly demonstrating that acyl-CoAs are rapidly esterified to Go3P derived from extracellular

glucose. This effect is not limited to saturated fatty acids as identical changes are seen following preincubation of INS-1 cells with oleic acid (Supplemental Figure 1).

The esterification of fatty acids with Go3P has several effects that appear to contribute to their ability to augment insulin secretion. We identified an increased glycolytic flux towards Go3P (Figure 6A and B), reduced NADH levels, and a decrease in NADH/NAD^+ ratio following fatty acid addition (Figure 2 and 1). As previously suggested (28), we show directly that fatty acid addition increases glycolytic (Figure 5A) and TCA cycle (Figure 6D) flux, and glucose oxidation (Figure 6B). Each should result in the generation of additional stimulus-secretion coupling factors that have been suggested to arise from mitochondrial metabolism in β-cells (1). While fatty acids increased glucose oxidation, glucose addition reduced fatty acid entry and oxidation in mitochondria as indicated by the fall in C16 acyl-carnitine levels. The reduction in fatty acid mitochondrial uptake has been attributed to increases in malonyl-CoA inhibition of CPT-1. While malonyl-CoA levels rise with glucose, fatty acid addition results in a significant blunting of the rise in malonyl-CoA in INS-1 cells (Figure 2D). The reason for the reduction is not clear, but decreased export of citrate/isocitrate from the mitochondria or an increase in consumption for de novo lipogenesis may play a role. These results also suggest that the decrease in fatty acid oxidation following glucose addition may be primarily due to the redirection of acyl-CoA towards esterification rather than blocking influx to the mitochondria via CPT1 inhibition by malonyl-CoA. This is consistent with the results of Mulder et al. (29) who observed no effect on insulin secretion after reducing INS-1 malonyl-CoA levels by overexpression of a modified malonyl-CoA decarboxylase.

The increase in de novo lipogenesis resulted in the generation of a variety of lipid intermediates that have been described as candidate signals for insulin secretion (8). Lipogenesis is part of the larger glycerolipid-free fatty acid cycle which is activated by glucose in β-cells and there is evidence that both the lipogenic and lipolytic arms of the cycle supply important signaling molecules (21). In glucose-responsive INS-1 cells, we find that the majority of increases in whole cell lipid intermediates, including LPA, PA, DAG, PG, PI and MAG arise from the lipogenesis pathway as little increase in M+0 isotopologues are found even after 60 min of glucose stimulation. DAG has multiple potential roles in insulin secretion including

activation of Munc13-1, a receptor known to amplify insulin exocytosis (30, 31) and activation of phospholipase D1 (PKD1), which modulates the reorganization of the cortical actin network, perhaps playing a role in the second phase of insulin secretion (6). Recently, Prentki and colleagues have suggested that increases in MAG, generated by lipolysis of TAG in β-cells can be a better activator of Munc13-1 than DAG.

In addition to previously identified lipid species, we found marked increases in cellular content of various acyl-amides. These fatty acid derivatives have not been reported previously in β-cells and their effect is unknown. Acyl-amides have been found in neuronal tissue and reportedly possess various functions (32, 33) including modulation of calcium flux, nitric oxide generation (34), and TRP calcium channels (35). While, we were able to increase the intracellular concentration of those metabolites by increasing their amino acid precursor's levels, this did not result in alterations in insulin secretion. Interestingly, taurine has been suggested to restore β-cell insulin secretion following chronic fatty acid exposure. However this beneficial effect was attributed to its antioxidant ability (36).

The activation of the FFAR1/GPR40 receptor mediates about 50% of the augmentation of insulin secretion by fatty acid (7). As indicated above, FFAR1/GPR40 has been proposed to increase β-cell calcium and activate phospholipase C generating diacylglycerols which may tether PKD1 to the plasma membrane increasing its activity (6), though the latter has not been directly demonstrated in β-cells. We sought to determine whether acute modulation of FFAR1/GPR40 had an effect on the β-cell metabolome. Disrupting FFAR1/GPR40 activity by use of antagonist and knockdown of the receptor resulted in attenuation of the augmentation of de novo DAG synthesis (Figure 7E, F, I, J). In contrast, the FFAR1/GPR40 agonist, Cay10587 increased flux of a low concentration of palmitate (50 μM) into DAG (Figure 7G and K). In addition, GW1100 reduced oxygen consumption by INS-1 cells treated palmitate while agonist has an augmenting effect. These results suggest that FFAR1/GPR40 enhances the effect of fatty acids to remodel intermediary metabolism. This effect does not appear to be due to increased uptake or activation of fatty acid as disruption of FFAR1/GPR40 did not alter the levels of palmitoyl-CoA in the INS-1 cells. At present, it is unclear how the activity of the pathways

leading to de novo lipogenesis occurs following FFAR1/GPR40 activation, but modulation of GPAT activity may be a target, given the increased flux into the early steps of the lipogenic pathway.

In summary, our data are consistent with the idea that in the fasting state, plasma fatty acids increase, increasing long chain acyl-CoA levels in β-cells. There are both glucose and fatty acid oxidation, but no generation of coupling factors to increase insulin secretion (Figure 9A). As glucose levels rise after feeding, the presence of fatty acids increases esterification with glycerol-3-phosphate, resulting in an increased flux to glycolipids and the formation of lipid-derived factors important in insulin secretion (Figure 9B). The increased flux increases regeneration of NAD^+, accelerating glycolysis and flux into the TCA cycle above that which would occur following exposure to glucose alone. Our data also suggests that in addition to the previously described activation of the PLC-PKD1 pathway (6), FFAR1/GPR40 activation also enhances flux through the glycerolipid pathway, augmenting the formation of coupling factors. This may be important as fatty acid entry into the β-cell likely falls as plasma fatty acids decrease following a meal due to insulin-mediated reduction in lipolysis in fat cells. Thus, activation of the FFAR1/GPR40 receptor by fatty acids or receptor agonists (18) may ensure continued fatty acid esterification and the provision of signaling lipids for insulin secretion.

REFERENCES

1. Jitrapakdee, S., Wutthisathapornchai, A., Wallace, J.C., and MacDonald, M.J. (2010) Regulation of insulin secretion: role of mitochondrial signalling. *Diabetologia.* **53,** 1019-1032

2. Bender, K., Newsholme, P., Brennan, L., and Maechler, P. (2006) The importance of redox shuttles to pancreatic beta-cell energy metabolism and function. *Biochem.Soc.Trans.* **34,** 811-814

3. Jensen, M.V., Joseph, J.W., Ronnebaum, S.M., Burgess, S.C., Sherry, A.D., and Newgard, C.B. (2008) Metabolic cycling in control of glucose-stimulated insulin secretion. *Am.J.Physiol.Endocrinol.Metab.* **295,** E1287-97

4. Parker, S.M., Moore, P.C., Johnson, L.M., and Poitout, V. (2003) Palmitate potentiation of glucose-induced insulin release: a study using 2-bromopalmitate. *Metabolism.* **52,** 1367-1371

5. Nolan, C.J., Madiraju, M.S., Delghingaro-Augusto, V., Peyot, M.L., and Prentki, M. (2006) Fatty acid signaling in the beta-cell and insulin secretion. *Diabetes.* **55 Suppl 2,** S16-23

6. Ferdaoussi, M., Bergeron, V., Zarrouki, B., Kolic, J., Cantley, J., Fielitz, J., Olson, E.N., Prentki, M., Biden, T., MacDonald, P.E., and Poitout, V. (2012) G protein-coupled receptor (GPR)40-dependent potentiation of insulin secretion in mouse islets is mediated by protein kinase D1. *Diabetologia.* **55,** 2682-2692

7. Latour, M.G., Alquier, T., Oseid, E., Tremblay, C., Jetton, T.L., Luo, J., Lin, D.C., and Poitout, V. (2007) GPR40 is necessary but not sufficient for fatty acid stimulation of insulin secretion in vivo. *Diabetes.* **56,** 1087-1094

8. Prentki, M., and Madiraju, S.R. (2011) Glycerolipid/free fatty acid cycle and islet beta-cell function in health, obesity and diabetes. *Mol.Cell.Endocrinol.*

9. Roduit, R., Nolan, C., Alarcon, C., Moore, P., Barbeau, A., Delghingaro-Augusto, V., Przybykowski, E., Morin, J., Masse, F., Massie, B., Ruderman, N., Rhodes, C., Poitout, V., and Prentki, M. (2004) A role for the malonyl-CoA/long-chain acyl-CoA pathway of lipid signaling in the regulation of insulin secretion in response to both fuel and nonfuel stimuli. *Diabetes.* **53,** 1007-1019

10. Deeney, J.T., Gromada, J., Hoy, M., Olsen, H.L., Rhodes, C.J., Prentki, M., Berggren, P.O., and Corkey, B.E. (2000) Acute stimulation with long chain acyl-CoA enhances exocytosis in insulin-secreting cells (HIT T-15 and NMRI beta-cells). *J.Biol.Chem.* **275,** 9363-9368

11. Corkey, B.E., Deeney, J.T., Yaney, G.C., Tornheim, K., and Prentki, M. (2000) The role of long-chain fatty acyl-CoA esters in beta-cell signal transduction. *J.Nutr.* **130,** 299S-304S

12. Branstrom, R., Aspinwall, C.A., Valimaki, S., Ostensson, C.G., Tibell, A., Eckhard, M., Brandhorst, H., Corkey, B.E., Berggren, P.O., and Larsson, O. (2004) Long-chain CoA esters activate human pancreatic beta-cell KATP channels: potential role in Type 2 diabetes. *Diabetologia.* **47,** 277-283

13. Tian, Y., Corkey, R.F., Yaney, G.C., Goforth, P.B., Satin, L.S., and Moitoso de Vargas, L. (2008) Differential modulation of L-type calcium channel subunits by oleate. *Am.J.Physiol.Endocrinol.Metab.* **294,** E1178-86

14. Mulder, H., Yang, S., Winzell, M.S., Holm, C., and Ahren, B. (2004) Inhibition of lipase activity and lipolysis in rat islets reduces insulin secretion. *Diabetes.* **53,** 122-128

15. Lorenz, M.A., Burant, C.F., and Kennedy, R.T. (2011) Reducing time and increasing sensitivity in sample preparation for adherent mammalian cell metabolomics. *Anal.Chem.* **83,** 3406-3414

16. Lorenz, M.A., El Azzouny, M.A., Kennedy, R.T., and Burant, C.F. (2013) Metabolome Response to Glucose in the beta-Cell Line INS-1 832/13. *J.Biol.Chem.* **288,** 10923-10935

17. Burant, C.F. (2013) Activation of GPR40 as a Therapeutic Target for the Treatment of Type 2 Diabetes. *Diabetes Care.* **36 Suppl 2,** S175-9

18. Burant, C.F., Viswanathan, P., Marcinak, J., Cao, C., Vakilynejad, M., Xie, B., and Leifke, E. (2012) TAK-875 versus placebo or glimepiride in type 2 diabetes mellitus: a phase 2, randomised, double-blind, placebo-controlled trial. *Lancet.* **379,** 1403-1411

19. Tautenhahn, R., Patti, G.J., Rinehart, D., and Siuzdak, G. (2012) XCMS Online: A Web-Based Platform to Process Untargeted Metabolomic Data. *Anal.Chem.* **84,** 5035-5039

20. Prentki, M., Vischer, S., Glennon, M.C., Regazzi, R., Deeney, J.T., and Corkey, B.E. (1992) Malonyl-CoA and long chain acyl-CoA esters as metabolic coupling factors in nutrient-induced insulin secretion. *J.Biol.Chem.* **267,** 5802-5810

21. Prentki, M., Matschinsky, F.M., and Madiraju, S.R. (2013) Metabolic Signaling in Fuel-Induced Insulin Secretion. *Cell.Metab.*

22. Hardie, D.G. (2011) Sensing of energy and nutrients by AMP-activated protein kinase. *Am.J.Clin.Nutr.* **93,** 891S-6

23. Hardie, D.G. (2008) AMPK: a key regulator of energy balance in the single cell and the whole organism. *Int.J.Obes.(Lond).* **32 Suppl 4,** S7-12

24. Sekine, N., Cirulli, V., Regazzi, R., Brown, L.J., Gine, E., Tamarit-Rodriguez, J., Girotti, M., Marie, S., MacDonald, M.J., and Wollheim, C.B. (1994) Low lactate dehydrogenase and high mitochondrial glycerol phosphate dehydrogenase in pancreatic beta-cells. Potential role in nutrient sensing. *J.Biol.Chem.* **269,** 4895-4902

25. Briscoe, C.P., Peat, A.J., McKeown, S.C., Corbett, D.F., Goetz, A.S., Littleton, T.R., McCoy, D.C., Kenakin, T.P., Andrews, J.L., Ammala, C., Fornwald, J.A., Ignar, D.M., and Jenkinson, S. (2006) Pharmacological regulation of insulin secretion in MIN6 cells through the fatty acid receptor GPR40: identification of agonist and antagonist small molecules. *Br.J.Pharmacol.* **148,** 619-628

26. Mancini, A.D., and Poitout, V. (2013) The fatty acid receptor FFA1/GPR40 a decade later: how much do we know?. *Trends Endocrinol.Metab.*

27. Rorsman, P., and Braun, M. (2013) Regulation of insulin secretion in human pancreatic islets. *Annu.Rev.Physiol.* **75,** 155-179

28. Prentki, M., and Madiraju, S.R. (2008) Glycerolipid metabolism and signaling in health and disease. *Endocr.Rev.* **29,** 647-676

29. Mulder, H., Lu, D., Finley, J.,4th, An, J., Cohen, J., Antinozzi, P.A., McGarry, J.D., and Newgard, C.B. (2001) Overexpression of a modified human malonyl-CoA decarboxylase blocks the glucose-induced increase in malonyl-CoA level but has no impact on insulin secretion in INS-1-derived (832/13) beta-cells. *J.Biol.Chem.* **276,** 6479-6484

30. Kwan, E.P., Xie, L., Sheu, L., Nolan, C.J., Prentki, M., Betz, A., Brose, N., and Gaisano, H.Y. (2006) Munc13-1 deficiency reduces insulin secretion and causes abnormal glucose tolerance. *Diabetes.* **55,** 1421-1429

31. Sheu, L., Pasyk, E.A., Ji, J., Huang, X., Gao, X., Varoqueaux, F., Brose, N., and Gaisano, H.Y. (2003) Regulation of insulin exocytosis by Munc13-1. *J.Biol.Chem.* **278,** 27556-27563

32. Tan, B., O'Dell, D.K., Yu, Y.W., Monn, M.F., Hughes, H.V., Burstein, S., and Walker, J.M. (2010) Identification of endogenous acyl amino acids based on a targeted lipidomics approach. *J.Lipid Res.* **51,** 112-119

33. Tan, B., Yu, Y.W., Monn, M.F., Hughes, H.V., O'Dell, D.K., and Walker, J.M. (2009) Targeted lipidomics approach for endogenous N-acyl amino acids in rat brain tissue. *J.Chromatogr.B.Analyt Technol.Biomed.Life.Sci.* **877,** 2890-2894

34. Rimmerman, N., Bradshaw, H.B., Hughes, H.V., Chen, J.S., Hu, S.S., McHugh, D., Vefring, E., Jahnsen, J.A., Thompson, E.L., Masuda, K., Cravatt, B.F., Burstein, S., Vasko, M.R., Prieto, A.L., O'Dell, D.K., and Walker, J.M. (2008) N-palmitoyl glycine, a novel endogenous lipid that acts as a modulator of calcium influx and nitric oxide production in sensory neurons. *Mol.Pharmacol.* **74,** 213-224

35. Saghatelian, A., McKinney, M.K., Bandell, M., Patapoutian, A., and Cravatt, B.F. (2006) A FAAH-regulated class of N-acyl taurines that activates TRP ion channels. *Biochemistry.* **45,** 9007-9015

36. Oprescu, A.I., Bikopoulos, G., Naassan, A., Allister, E.M., Tang, C., Park, E., Uchino, H., Lewis, G.F., Fantus, I.G., Rozakis-Adcock, M., Wheeler, M.B., and Giacca, A. (2007) Free fatty acid-induced reduction in glucose-stimulated insulin secretion: evidence for a role of oxidative stress in vitro and in vivo. *Diabetes.* **56,** 2927-2937

SUPPLEMENTARY INFORMATION

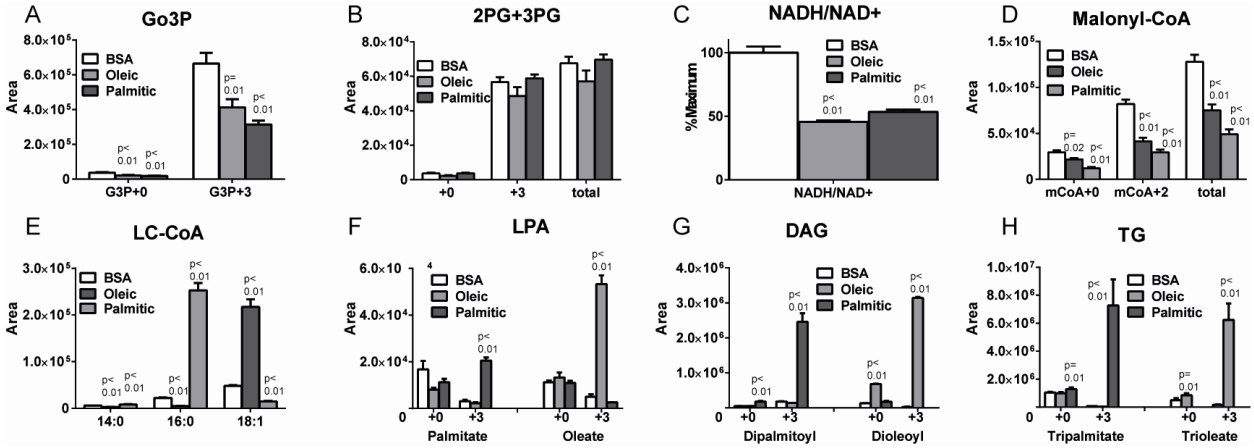

Figure S1: metabolites profiles of INS-1 cells after stimulation with 13C glucose in the presence or absence of BSA, oleate or palmitate.

Chapter 5. METABOLOMICS ANALYSIS REVEALS THAT AICAR AFFECTS GLYCEROLIPID, CERAMIDE AND NUCLEOTIDE SYNTHESIS PATHWAYS IN INS-1 CELLS

INTRODUCTION

Beta cells in islets of Langerhans secrete insulin in response to high glucose levels in blood. Glucose stimulated insulin secretion (GSIS) is mainly dependent on glucose metabolism to generate signals that trigger or amplify insulin secretion (1). Deterioration of beta cell function represents one of the factors responsible for development of metabolic syndrome and type 2 diabetes.

An energy sensor that is located in all cells (including beta cells) is AMP-activated protein kinase (AMPK). AMPK switches between promoting catabolic and anabolic cellular processes to ensure energy balance depending upon nutrient availability (2). Increased AMP during starvation activates AMPK and subsequent activation of catabolic processes and inhibition of anabolic processes (3), on the other hand, high levels of glucose deplete AMP causing AMPK deactivation and subsequent activation of anabolic processes and inhibition of catabolic processes.

Because of its effects on various metabolic pathways, AMPK is an interesting target for metabolic syndrome treatment. Pharmacological agents like 5-Aminoimidazole-4-carboxamide ribonucleotide (AICAR) have been developed to activate AMPK. AICAR is a pro-drug that is uptaken by the cell and metabolized intracellularly into AICAR monophosphate (ZMP) which is an AMP analog. AICAR has been used to probe the effects of AMPK on several tissues in vitro, as well as in vivo (4). Intravenous administration of AICAR to diabetic patients decreased their hepatic glucose output and lowered their blood glucose and free fatty acids (5).

Metabolic effects of AMPK activation varies from one tissue to another. In adipocytes, AMPK activation inhibits hormone sensitive lipase, inhibiting lipolysis. In heart and macrophages, AMPK activation activates phosphofructokinase B2 and B3 respectively, activating glycolysis. In muscles and liver AMPK activation inhibits glycogen synthase 1 and 2, respectively, inhibiting glycogen synthesis (6). AMPK activation also has general effects that

have been observed in multiple tissues, such as the inhibition of acetyl-CoA carboxylase 1 and 2 (ACC1 and ACC2), inhibiting fatty acid synthesis and increasing fatty acid oxidation respectively. AMPK activation also inhibits 3-hydroxy-3 methylglutaryl CoA reductase (HMGR), inhibiting cholesterol synthesis (6, 7).

AMPK activation effect on B-cell insulin secretion has been studied in islets or cell lines like (INS-1 cells) yielding conflicting results (8). AMPK over-expression in INS-1 cells significantly decreased glucose stimulated insulin secretion in the presence of fatty acid, this was attributed to the increased oxidation of fatty acid and the reduction in lipid signals involved in insulin secretion (9). The reduction in lipid messengers was the same reason AMPK activation by AICAR was able to rescue INS-1 beta cells from saturated acid induced toxicity (10). On the other hand, AMP activation by AICAR was shown to potentiate insulin secretion from rat islets and INS-1 cell lines at low glucose, with no significant effect at higher glucose levels (11).

Although AICAR's primary mode of action is thought to be as an AMP mimetic that causes AMPK activation, some effects of AICAR have been shown to be independent of AMPK activation. AICAR inhibited choline kinase and phosphatidyl choline synthesis in liver cells independent of AMPK (12). AICAR has also been shown to induce apoptosis in chronic lymophcytic leukemia cells independent of AMPK leading to clinical studies on this treatment (13). AMPK independent effects induced by AICAR were protective in animal models of human malignant hyperthermia from sudden death. This useful effect was suggested as a possible prophylactic treatment for the human disease (14).

In light of the widespread use of AICAR as an activator of AMPK for research purposes and the growing interest in use of AICAR as a treatment for certain human diseases, improved understanding of the molecular basis of its action is essential. As AICAR directly affects many aspects of cellular metabolism, metabolomics may be expected to provide valuable insight into the effects of AICAR. Global intracellular metabolite changes associated with AICAR treatment have been studied in human umbilical vein endothelial cells using NMR techniques (15). In hepatocytes, a few alterations in metabolite levels were reported, including a decrease in ATP as well as changes in phospholipid pathway metabolites (12, 16) . Global extracellular

metabolite changes were studied recently in T-cells using LC-MS and showed an increase in secreted purine and pyrimidine intermediates (17).

We have recently shown that ZMP is an endogenous metabolite that increases after glucose stimulation in INS-1 cells which could be a negative regulator for insulin secretion, however we did not investigate its role in detail (1). So a follow up experiment was performed to study the acute effect of ZMP on beta cell metabolism and insulin secretion using INS-1 832/13 cells. We applied metabolomics isotopic nutrients to investigate various pathways. We were able to identify different AMPK dependent and independent pathways as well as identifying metabolomics markers or fingerprint for AMPK activation in beta cell.

MATERIAL AND METHODS

Materials. INS-1 cells (18) were kindly provided by Dr. Christopher Newgard (Sarah W. Stedman Nutrition and Metabolism Center, Duke University, Durham, NC). All chemicals were purchased form Sigma-Aldrich (St. Louis, MO) unless otherwise noted. RPMI media, fetal bovine serum, 4-(2-hydroxyethyl)-1-piperazineethanesulfonic acid (HEPES), and penicillin-streptomycin were purchased from Invitrogen Corp, (Carlsbad, CA). Stable isotope labeled U-^{13}C glucose and ethanolamine were purchased from Sigma.

Cell culture.INS-1 832/13 cells were cultured in RPMI supplemented with 2 mM glutamine, 1 mM sodium pyruvate, 10% FBS, 10 mM HEPES, 100 U/mL penicillin, 100 µg/mL streptomycin, 250 ng/mL amphotericin B, and 50 µM β-mercaptoethanol. Cells were plated at a density of ~14 x 103 cells/cm2 and grown in 6 cm culture dishes at 37 °C and 5% CO2 in a humidified atmosphere to ~70% confluence. Krebs-Ringer-HEPES buffer (KRHB) was prepared containing 20 mM HEPES, 118 mM NaCl, 5.4 mM KCl, 2.4 mM CaCl2, 1.2 mM MgSO4, and 1.2 mM KH2PO4 and was adjusted to pH 7.4 with NaOH.

Experimentation. On the day experiments were performed, the cell culture medium was changed to KRHB containing 2 mM glucose +/- 250 uM AICAR for 60 min prior to addition of 10 mM ^{12}C or ^{13}C glucose from 1 M stock solution. Cell metabolism was quenched at different time points as described in each experiment. For the dose response curve of AICAR, cells were incubated with 10 mM glucose and serial concentration of AICAR (0, 25, 125,250 and 1250 uM) for 1 hour before quenching. For experiment showing the effect of starvation on

CDP-ethanolamine, cells were incubated in RPMI with 3 mM glucose or 10 mM glucose for 6 hours before quenching.

Glycerolipids pathway monitoring. For DAG and ceramide analysis, the INS-1 (832/13) clonal cell line was incubated with 2 mM glucose, 250 uM AICAR and 50 uM palmitic acid for 1 hour before stimulation with 13C glucose for 30 minutes. In the case of CDP-ethanolamine labeling, labeled ethanolamine was also added for the 1 hour pre-incubation period.

Insulin measurement and western blot. For insulin, aliquots of supernatant was diluted with 1% BSA and stored at +4 °C before being assayed using Rat/Mouse insulin ELISA Kit (Millipore, Billerica, MA). For western blot, cells were washed with cold PBS before the addition of lysis buffer (RIPA buffer supplied with complete protease inhibitor cocktail and phosphatase inhibitor cocktail (Roche diagnostics)). Anti-phospho-Acc, anti-phospho-HMGR antibodies were obtained from Cell signaling.) Blots were developed with ECL (Pierce) according to manufacturer's instructions.

Metabolite Measurement. Cell plates were rinsed, metabolism quenched, and metabolites extracted using the procedure described previously (1). Briefly, cell plates were rapidly rinsed with water and quenched with liquid nitrogen. Metabolites were extracted with 8:1:1 methanol: chloroform: water and assayed by high performance liquid chromatography with time-of-flight mass spectrometry (HPLC-TOF-MS). Chromatographic separations were performed with an Agilent Technologies (Santa Clara, CA) 1200 HPLC system equipped with a Phenomenex (Torrance, CA) Luna NH2 2.0 × 150 mm, 3 µm HPLC column and a 2.0 × 4 mm guard column using the following conditions: mobile phase A was 100% acetonitrile (ACN); mobile phase B was 100% 5 mm ammonium acetate pH 9.9 with ammonium hydroxide. Lipids were separated on a C18 Capcell column (2 mm bore by 150 mm long packed with 3 µm particles). Mobile phases and gradient are similar to that described in (19) . Detection was performed on an Agilent Technologies LC/MSD TOF using dual electrospray ionization (ESI) source in negative-ion mode for polar metabolites and both negative and positive mode for lipids.

Data analysis and statistics. Directed analysis was performed to measure Metabolites previously implicated in GSIS (e.g. glycolytic and TCA cycle intermediates). Those were

identified using standards, accurate mass, and isotope ratios to confirm peak assignments as described in (1)

Undirected analysis was performed using XCMS online (20). Hits with significant increase was manually checked for correct assignment. These metabolites were identified by searching both Human Metabolome Database and Metlin to match mass and comparing to standards. For relative quantification of identified metabolites, peak areas were used as described before.

For all studies, peak areas were measured from extracted ion chromatograms of [M-H]− metabolite ions with ± 70 ppm detection windows centered on the theoretical mass. [M-2H]2− ions were used for malonyl-CoA (mCoA) and other CoAs to improve sensitivity. Statics was performed using unpaired student-t test comparing different time points +/- AICAR, with significance value <0.05

RESULTS

AICAR effect on insulin secretion and metabolome of beta cell

The effect of 0 uM to 1250 uM AICAR treatment for 60 min on ZMP formation was tested. As shown in supplemental figure 1, ZMP increased linearly with AICAR concentration up to 250 uM where it began to level off. For all subsequent studies we used 250 uM which was within the linear range and generated a ZMP concentration that was ~150 times greater than the highest endogenous levels. This AICAR concentration is an intermediate value relative to previous studies, which used doses ranging from 100-1000 uM (12, 16).

The effect of AICAR on insulin secretion was evaluated by incubating INS-1/832 (13) cells in KRB with 2 mM glucose for 60 minutes in the presence or absence of 250 uM AICAR. This pretreatment was intended to allow the uptake of AICAR and its conversion into the active form before stimulation with 10 mM glucose. Insulin secretion was measured after the incubation period at low glucose (time zero) and after 60 minutes of high glucose. At low glucose, AICAR substantially increased insulin secretion; however, after stimulation with elevated glucose the total amount of insulin secreted was unaffected by AICAR. Because of the difference in basal secretion, the stimulation index was significantly reduced in the presence of AICAR (Figure 1). These results were reproduced in a different cell line (INS-1 832/3) as shown in supplemental

figure 2. These results are also consistent with our previous study that showed that if 10 mM glucose and 25 uM AICAR were applied simultaneously to a cell, insulin secretion was slightly reduced at 45-60 min.

To determine the effect of AICAR on the INS-1 cell metabolome, metabolism was quenched and metabolites extracted for LC-MS analysis at different times before and after glucose treatment. LC-MS analysis of cell extracts allowed monitoring of 66 identified metabolites. The relative change in metabolite concentration between AICAR treated sample and control at different times during glucose treatment is summarized in figure 1. The results show that AICAR affected many metabolites involved in a variety of pathways. Some of these pathways are known to be associated with AMPK activation, while others are not. Results from different metabolites and follow up studies are discussed below.

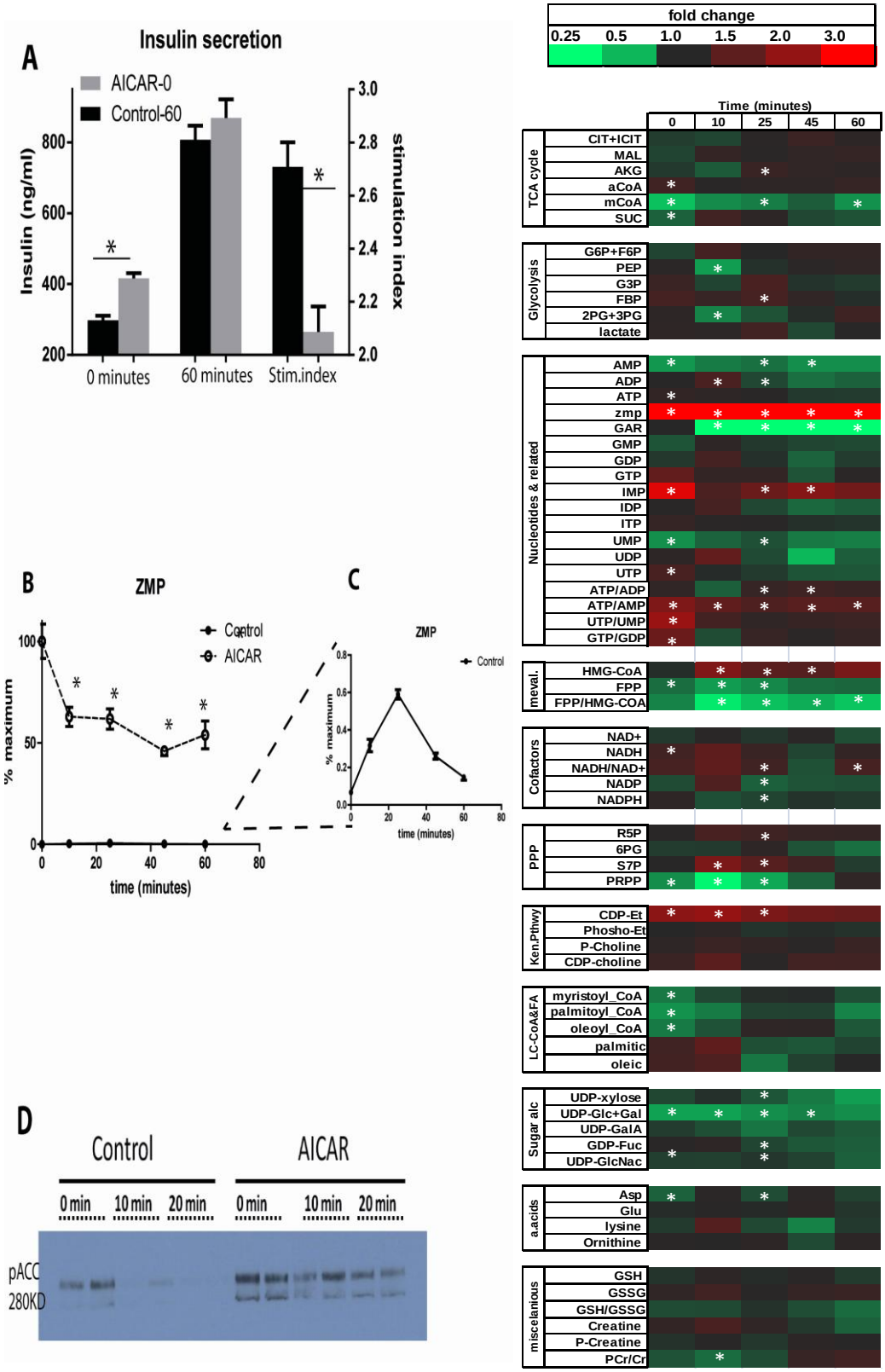

Figure 5-1.insulin and metabolites changes with AICAR incubation (a) insulin level after AICAR incubation and after glucose stimulation for 60 minutes.(b) formation of ZMP with AICAR incubation (C) phosphoACC after AICAR incubation and after

glucose treatment for 10 and 20 minutes. (D) Heat map showing fold change of metabolites with AICAR treatment. Significantly different values are highlighted with asterisk. Student t-test was performed on each time points comparing the control and AICAR treated samples.

AICAR decreased malonyl CoA and long chain CoA levels.

Incubation of cells with AICAR increased ZMP levels after the incubation period, that decreased after glucose addition (figure 1b) ($p < 0.05$).In the absence of AICAR, glucose increased ZMP ~ 5 fold, as we have shown previously (1), but still far below that evoked by AICAR alone (Figure 1B, C).

ZMP is known to activate AMPK which in turn phosphorylates and deactivates ACC. We confirmed this effect by determining ACC1 phosphorylation using western blot. Phospho-ACC increased with AICAR treatment, but then decreased with glucose stimulation (figure 1). These results indirectly show that the AICAR treatments used can modulate AMPK activity and that elevated glucose opposes the effect, mirroring the changes in intracellular ZMP. A key metabolic marker of this effect is malonyl CoA, the product of ACC. Malonyl CoA increases with glucose treatment, but AICAR lowered the concentration throughout the glucose treatment (Figure 2A). The substrate of ACC, acetyl CoA, was unaffected by AICAR suggesting other regulation of its steady state concentration. This was expected because Acetyl CoA was previously shown to be stable (1).

The ratio of malonyl CoA to acetyl CoA more clearly shows the apparent effect of ACC phosphorylation evoked by AICAR (Figure 2C). Malonyl CoA inhibits CPT-1 and fatty acid oxidation with a consequence of increasing availability of long chain CoA in cytosol. As expected, AICAR reduced long chain CoAs at low glucose (time 0 in Figure 2B). Interestingly, glucose treatment without AICAR also decreases long chain CoAs. We have shown that this is due to consumption by reaction with glycerol phosphate, which dramatically increases with glucose treatment, to produce glycerolipids. While AICAR reduces long chain CoAs at low glucose, its effect is not additive with glucose so that at high glucose the effect of AICAR is nil on long chain CoAs (figure 2B).

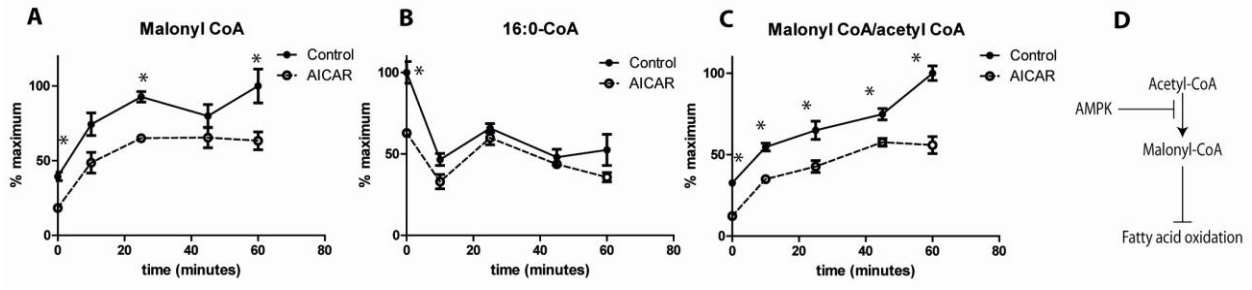

Figure 5-2.metabolites affected by ACC deactivation. (a) Malonyl-CoA. (b) palmitoyl CoA. (c) ratio of malonyl CoA/acetyl CoA.(d) AMPK effect on malonyl-CoA formation. Cells were incubated with/without AICAR for 1 hour, followed by stimulation with 12C glucose for different time points.

AICAR increased HMG-CoA and decreased farnesyl pyrophosphate

AMPK also phosphorylates and deactivates HMG-CoA reductase. We found that phospho-HMG-CoA was increased by AICAR treatment (Figure 3D), again indirectly showing that the AICAR concentrations used activate AMPK. The substrate of HMG-coA reductase, HMG-CoA, decreases substantially with glucose treatment. AICAR did not affect the initial concentration but did blunt the decrease evoked by glucose (Figure 3A). Farnesyl pyrophosphate, a downstream product of HMG-CoA, was also not strongly affected at low glucose, but its increase induced by glucose was blunted by AICAR (Figure 3B). The combined effects, plotted as the ratio of FPP/HMG-CoA suggest that AICAR deactivation of HMG-CoA reductase lowers flux through this pathway and reduces net concentration of downstream products even with elevated glucose (Figure 3C). This would lie in agreement with AICAR reduction of cholesterol accumulation in myotubes(21) and macrophages(22).

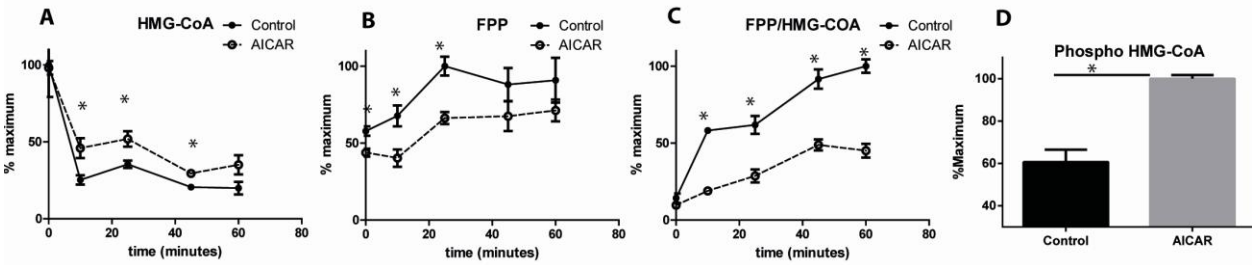

Figure 5-3. Metabolites affected by HMGR deactivation. (a) HMG-CoA, (b) Farnesyl pyrophosphate (c) ratio of Farnesyl pyrophophate/ HMG-CoA. Cells were incubated with/without AICAR for 1 hour, followed by stimulation with 12C glucose for different time points.(d) Phospho-HMGR levels after cells incubation in the presence or absence of AICAR for 1 hour. (e) AMPK effect on mevalonate pathway.

AICAR did not affect glycolysis or TCA metabolites

Glucose stimulation is known to increase flux into glycolytic pathway and TCA cycle that cause a consequent increase ATP/ADP ratio. To investigate if central carbon metabolism

pathways are affected by AICAR, key metabolites involved in glycolysis and the TCA cycle were analyzed and did not show significant differences (figure 1). ^{13}C labeling of fructose bisphosphate and citrate after exposure of cells to $U^{13}C$ glucose for 30 minutes was analyzed as representative measure of flux in glycolysis and TCA cycle, respectively, but no significant effects of AICAR were detected (figure 4).This was consistent with the lack of effect on the ratio of ATP/ADP at early time points (figure 1). However, AICAR slightly increased ATP/ADP ratio after 25 minutes of glucose treatment, which was mainly because of the decrease in ADP concentration (described below).

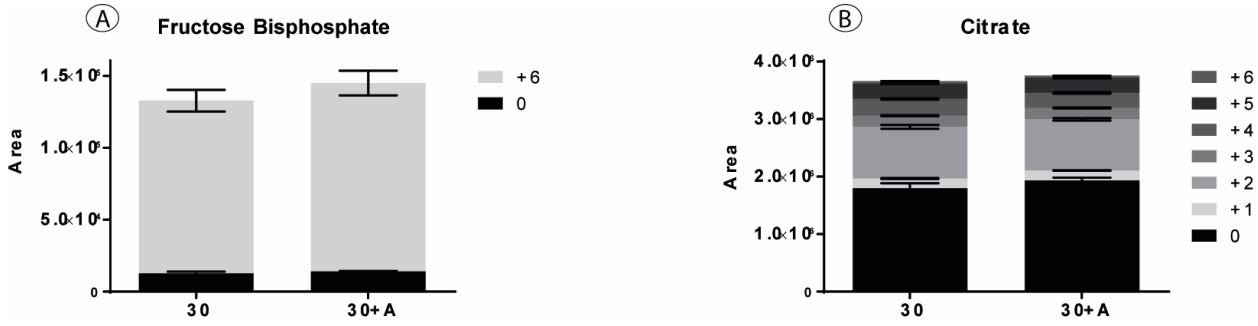

Figure 5-4.Effect of AICAR on TCA cycle and glycolysis: levels of the different isopotomers (a) Fructose bisphosphate (b) Citrate

AICAR decreased GAR and PRPP with slight change in pentose phosphate shunt metabolites and decreased glucose flux in the purine and pyrimidine pathway.

Our metabolomic analysis also showed significantly lower levels of glycinamide ribonucleotide (GAR) and phosphoribosyl pyrophosphate (PRPP) after glucose treatment (figure 1). PRPP is a metabolite that links the pentose phosphate pathway with the purine and pyrimidine synthesis pathway. Glycinamide ribonucleotide (GAR) is one of the metabolites in the early steps of the purine synthesis pathway (figure 5G). Both PRPP and GAR increase significantly in control cells after glucose stimulation (1); however, AICAR incubation significantly blunted this increase (figure 5A, B) suggesting decreased activity in this pathway. In accordance with this finding, the substrate pentose phosphates increased slightly with AICAR incubation (figure 1 and Figure 5C).

To further understand the effect of AICAR on GAR and PRPP concentration, we used uniformly ^{13}C labeled glucose to monitor the flux of glucose in the purine and pyrimidine pathway. Using uniformly ^{13}C labeled glucose, newly synthesized ATP and UTP could be measured by LC-MS, by observing the 5 Dalton mass increases caused by addition of a $^{13}C_5$-labeled ribose sugar to adenine or uridine. The levels of 5 labeled ATP or UTP decreased significantly in the presence of AICAR (Figure 5E). The labeling of pentose phosphate metabolites did not show significant differences (Figure 5F).

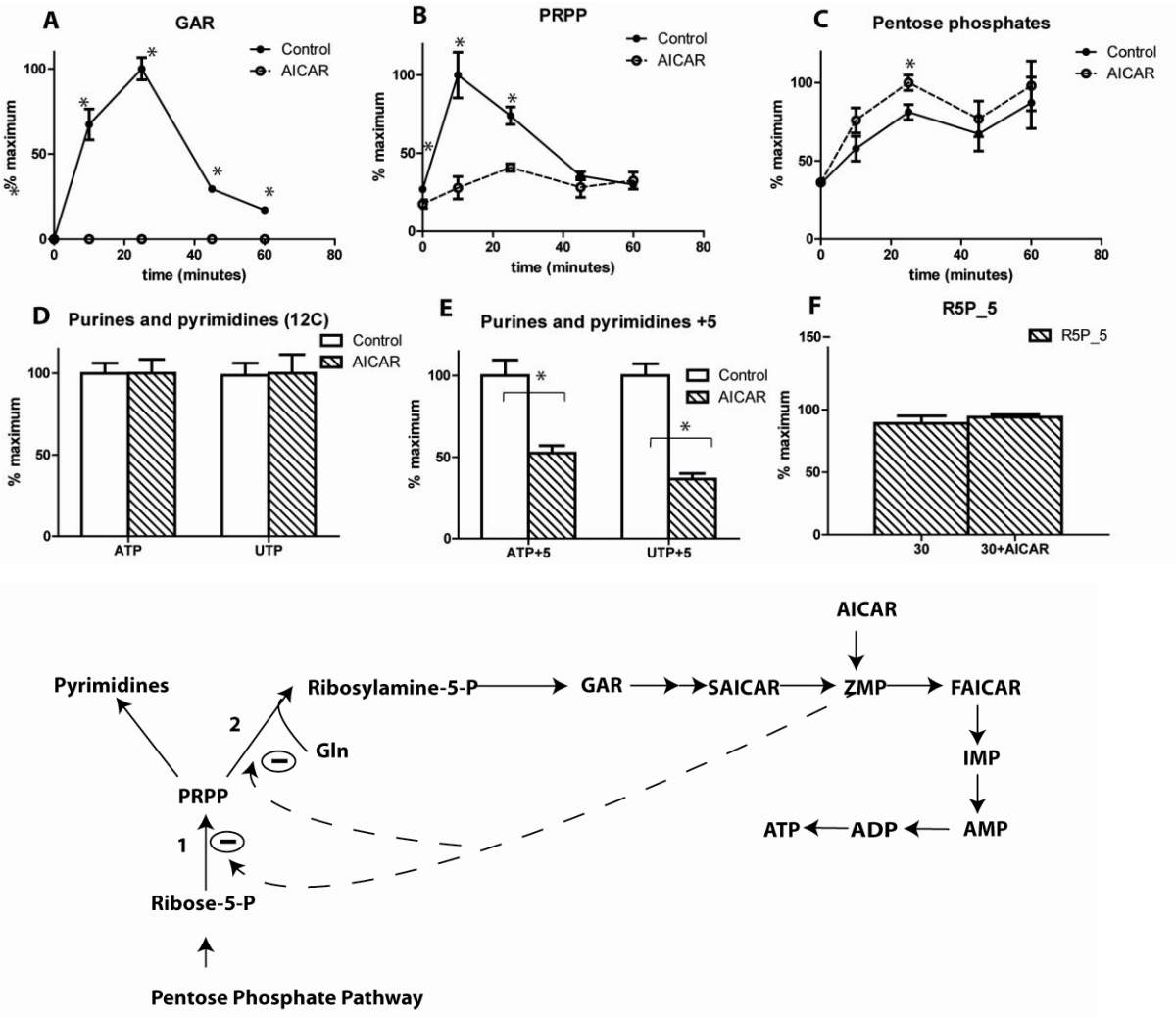

Figure 5-5.Effect of AICAR on pentose phosphate and purine pathway metabolites: (a) GAR (b) PRPP (C) pentose phosphates (d) +5 labeled pentose phosphates. (e) Unlabeled ATP and UTP levels (f) +5 labeled ATP and UTP. Cells were incubated with/out AICAR for 1 hour, followed by stimulation with 12C glucose for different time point (a-c) or using 13C glucose for 30 minutes (d-f). The percentage of maximum was calculated based on the maximum of each species.(e) the purine and pyrimdine pathway (1) PRPP synthase (2) PRPP amidotransferase

AICAR affected Kennedy pathway of phosphatidyl ethanolamine synthesis and decreased flux of glucose in glycerolipids pathway and decreased ceramides

Undirected metabolomic analysis of polar metabolites revealed an increase in CDP-ethanolamine with AICAR incubation (figure 6A and supplemental figure 2). According to the Kyoto Encyclopedia of Genes and Genomes (KEGG) (23, 24), CDP-ethanolamine is used only in de novo phospholipid synthesis (Kennedy pathway) (Figure 7E). This increase is in agreement with previous data showing an increase of CDP-ethanolamine in hepatocytes with AICAR treatment (16). The AICAR induced increase in CDP-ethanolamine was also induced by low glucose (figure 6 B), which suggests that the increase in CDP-Et is AMPK dependent. To confirm the peak assignment (since no authentic standard is available for this metabolite) and to understand the reason for this increase of CDP-ethanolamine, we incubated cells with 2-^{13}C labeled ethanolamine in the presence or absence of AICAR. Labeled CDP-ethanolamine was formed and co-eluted with the unlabeled form, confirming correct peak assignment (figure 6 D, E, G). Both the labeled and the unlabeled CDP-ethanolamine increased with AICAR treatment (figure 6C) suggesting inhibition of consumption of CDP-enthanolamine rather than an increase in synthesis which would have preferentially increased the labeled form.

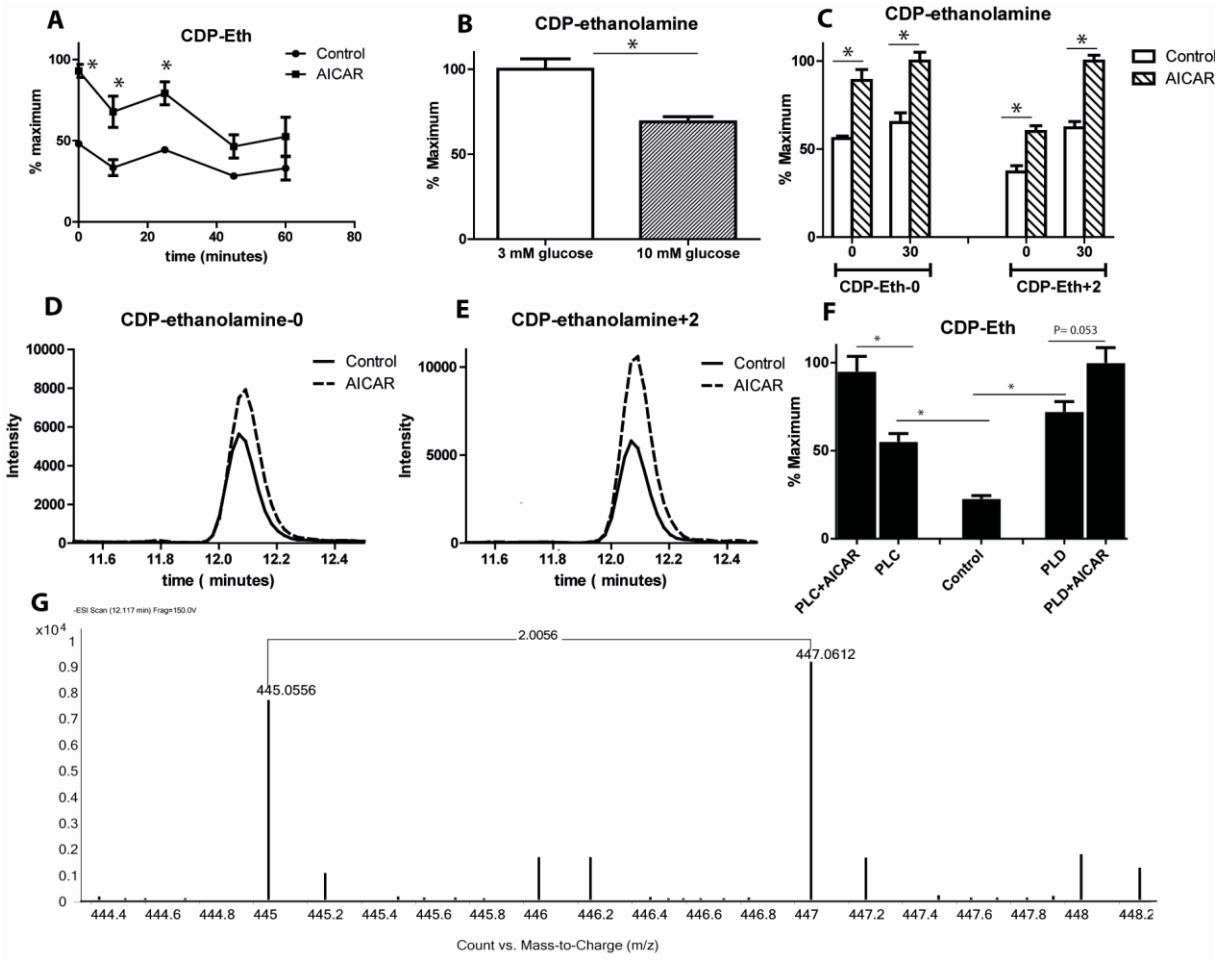

Figure 5-6.Effect of AICAR on metabolites in the Kennedy pathway for PE: (a) CDP-ethanolamine after incubation with/without AICAR for 1 hour followed by stimulation with glucose for different time points (b) CDP-ethanolamine levels after starvation for 6 hours at low glucose (c) levels of labeled and unlabeled CDP-ethanolamine-after incubation with +2 ethanolamine for 1 hour and stimulation with glucose for 30 minutes. (D, E, G) EIC and mass spectrum of labeled and unlabeled CDP-ethanolamine-after incubation with +2 ethanolamine for 1 hour before glucose treatment for 30 minutes (f) Levels of CDP-ethanolamine after phospholipase inhibition. Cells were incubated at 2 mM glucose for 60 minutes +/- AICAR +/-phospholipase C (PLC) inhibitor (U-73122) 20 uM or +/- phospholipase D inhibitor Cay10593 (60 uM).

In the Kennedy pathway, CDP-enthanolamine is consumed by condensation with diacylglycerol (DAG) to form Phosphatidyl ethanolamine (PE). To confirm that flux of DAG into PE formation is reduced, we incubated cells with 50 uM palmitic acid for 1 hour before the addition of $U^{13}C$ glucose to allow lipogenesis and formation of $^{13}C_3$-labeled glycerolipids (figure 7). By observing the labeling ratio (+3 labeled/unlabeled glycerolipids) it is evident that AICAR induced a consistent decrease of glucose flux into the glycerolipids pathway. This was also coupled with an accumulation of Go3P as shown in supplementary figure 3. The decrease in glucose flux in the glycerolipids pathway was true in DAG and PC but surprisingly not in PE. This discrepancy in PE formation has been seen before (25), in that over expression of the ECT

enzyme in the Kennedy pathway did not change PE levels. This was attributed to a balance between formation of PE and phospholipase activity that results in maintenance of PE pools at steady-state levels regardless of alterations in flux.

To confirm the existence of this equilibrium between lipolysis and lipogenesis we attempted to inhibit phospholipase C or D using previously described inhibitors (U-73122 and Cay10593 respectively(26, 27)). We observed a significant increase in CDP-ethanolamine that was augmented by the addition of AICAR (figure 6F). This accumulation of CDP-ethanolamine would imply less flux into PE in response to phospholipase inhibition. This flux was further inhibited by AICAR, which caused even more accumulation of CDP-ethanolamine. This would support the hypothesis of continuous PE formation and breakdown by phospholipases, keeping PE at steady-state levels. Based on these data, we conjecture that decreased formation of PE from DAG is partially due to reduced availability of the substrate (DAG), but also because of the inhibition of EPT enzyme. This suggestion is supported by the fact that CDP-ethanolamine accumulated mainly under low glucose conditions where there is low glucose flux and low lipogenic activity.

To detect other possible effects of AICAR on lipids, untargeted metabolomics analysis was applied to the previous experiment using 50 uM palmitic acid and U-13C glucose. The most prominent identified changes were ceramides, which decreased significantly with AICAR treatment (figure 7D).

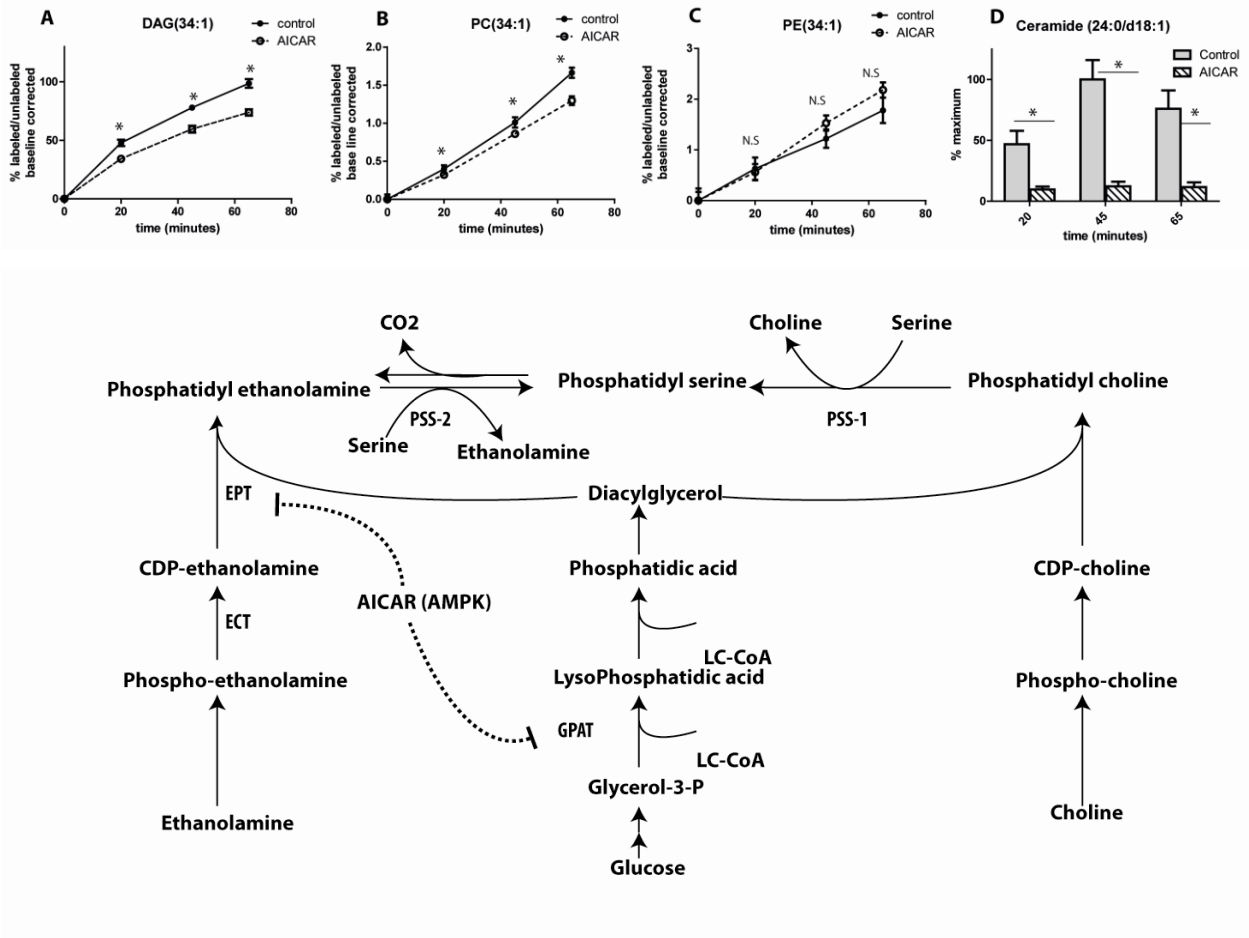

Figure 5-7.effect of AICAR on Ceramides and glycerolipids synthesis pathway: (a-c) ratio of +3 labeled DAG,PC or PE(34:1) (d) Ceramides levels. INS-1 cells incubated with 50 uM palmitic acid with or without AICAR 250 uM for 1 hour before stimulation with U-13C glucose for different time points (e) Kennedy pathway for phospholipid synthesis: ECT-ethanolamine phosphate cytidylyltransferase, EPT-ethanolamine phosphotransferase, GPAT-glycerol-3-phosphate O-acyltransferase, PSS-1 and PSS-2: phosphatidylserine synthase 1 and 2

DISCUSSION

We used an LC-MS based metabolomics method to probe the metabolic effect of AICAR on the β-cell line INS-1. The effects of AICAR treatment on β-cell lines were observed in a diverse range of metabolic pathways and appear to be mediated by both AMPK-dependent and independent processes. These pathways appear to be relevant to the β-cell secretory function as well as the cancerous nature of the cell line. These pathways might represent novel targets for future development of treatments for diabetes and cancer.

Effect of AICAR on GSIS related pathways.

The metabolomics method allows us to evaluate the effect of AICAR on several key metabolites involved in GSIS. We have shown before that ATP/ADP ratio increases after within

5 min of glucose stimulation as expected to trigger first phase insulin secretion (1). AICAR did not affect ATP/ADP ratio at early time points, but evoked a slight increase after 25 minutes. This increase in ATP/ADP ratio is because of a decrease in ADP concentration presumably because of the ZMP induced inhibition of purine synthesis (figure 1 and 5).

AICAR modulated the long chain coA pathway, presumably through activation of AMPK and its effects on ACC. AICAR lowered the levels of long-chain CoAs which is known to have several roles in GSIS. Long-chain CoAs can potentiate opening Katp so that decreases in long-chain CoA's may be stimulatory to GSIS (1). Consistent with this idea, we and others have found that glucose lowers the long chain CoA concentration (28). AICAR lowered the long-chain CoA concentration at low glucose, but did not significantly lower it further with glucose stimulation. These results are consistent with elevated basal insulin secretion that does not increase substantially with glucose.

The succinate pathway proposed to enhance GSIS involves the formation of HMG-CoA through HMG-CoA reductase (HMGR) (29). The inhibition of HMGR by statin drugs has shown to inhibit glucose stimulated insulin secretion (29). Supporting the potential importance of this pathway, we have previously shown that glucose increases flux through HmgCoA yielding net a decrease in HmgCoA and an increase in FPP, a downstream metabolite that is involved in prenylation of proteins (1). Such modifications may promote exocytosis. AICAR blunted the effects of glucose resulting in higher HmgCoA and lower FPP. Such results are consistent with inactivation of HmgCoa reductase by AICAR through AMPK and could explain some of the inhibitory effects on GSIS.

Glycerolipid synthesis pathway is believed to be involved in promoting and sustaining GSIS (30). Products like DAG may be proximal metabolites in exocytosis while pathways supporting production of these compounds are critical for providing a supply at the proper time for GSIS. AICAR evoked a number complex changes, including a decrease in DAG, that may be linked to its net inhibitory effect on GSIS. The decrease in glucose flux in the glycerolipids cycle, would suggest that this decrease in DAG is probably due to reduced glycerol-3-phosphate and LC-CoA esterification by GPAT This is in agreement with the idea that GPAT enzyme could be a target of AMPK (31). Although Go3P did not accumulate in the preliminary metabolites

screening (Figure 1), it accumulated in the presence of 50 uM palmitic acid (supplementary figure 3) because of increased flux in the glycerolipids pathway. Similar accumulation of Go3P was seen before in myoloma cell (32). Although we suggest GPAT inhibition by AICAR we cannot exclude the possibility that the reduced esterification could be due to decreased LC-CoA levels.

The reoxidation of NADH to NAD+ is critical to maintaining glycolytic flux into the mitochondria and for GSIS (33). The formation of Go3P from dihydroxyacetone phosphate (DHAP) by cytosolic glycerol-3-phosphate dehydrogenase utilizes NADH to regenerate NAD+, allowing continuing flux through glycolysis (1). The ratio of NADH/NAD+ slightly increased with AICAR, indicative of less esterification of Go3P with LC-CoA which might also explain some of the inhibitory effect on GSIS.

ZMP effect on survival pathways

The results point to several ways that AICAR may mediate survival or growth of cells. AICAR decreased the denovo synthesis of purine and pyrimidine metabolites by decreasing glucose flux through these pathways. Slight accumulation of pentose phosphate metabolites was seen, which would suggest that AICAR caused an inhibition in enzymes that links the pentose phosphate pathway with the purine and pyrimidine pathway. These enzymes could be PRPP synthase, the enzyme responsible of formation of PRPP and/or PRPP amido transferase which catalyzes the conversion of PRPP and glutamine to ribosyl amine-5 phosphate which forms GAR (figure 5E). Interestingly, both enzymes are known to be inhibited by metabolites in the purine synthesis pathway, like AMP, ADP, GMP and GDP (34, 35). This inhibition could be mediated by ZMP, which is an AMP analog based on being a purine derivative and probably not through AMPK. These observations and conclusions would support a plausible explanation for the decrease in ATP seen before in hepatocytes (the main site for purine synthesis) after AICAR treatments (12).This effect might also put AICAR in the category of an anti-metabolite therapy for cancer treatment. Interestingly it was shown recently that AICAR induced apoptosis in cancer cells independent of AMPK activation (13). Indeed, it has recently been shown that AICAR was able to induce apoptosis in multiple myoloma cells independent of AMPK (32). The cytotoxic effect was suggested to be due to inhibition of enzymes in the pyrimidine pathway,

mainly UMP synthase, which would agree with another published data (17). Although the metabolites measurements was done at 8 hours compared to our 60 minutes, but they observed a decrease in PRPP as we have shown.

Another metabolic change that is highly relevant to β- cells is the significant decrease in ceramides seen with AICAR incubation. Ceramides are suggested to be a lipid second messenger responsible for β- cell death after its exposure to saturated fatty acid (36). This decrease in ceramides agrees with other work showing that showed that AMPK activation by AICAR inhibited serine palmitoyl transferase II (SPT II) and lowered palmitate induced ceramide formation in skeletal muscle (37). Serine levels decreased in a dose dependent manner after the addition of a range of concentrations of AICAR as shown in supplemental figure 2. This inhibition of SPT II could then be a consequence of less substrates availability, mainly palmitoyl CoA and serine. The two findings of decreased flux in the glycerolipids synthesis pathway and decreased ceramides synthesis in β- cells could help explain the finding that AICAR decreased palmitic acid induced apoptosis in INS-1 cells (10).

Metabolic markers for enzyme activities

An LC-MS run for a metabolomics study could provide plenty of information for enzyme activities and act as confirmation for immunoassay studies. It might also act as the sole marker for enzyme activity if no antibodies are available. Malonlyl CoA could be a useful marker for ACC activity as we have shown. Even better ratio would be the ratio of malonyl-CoA to acetyl-CoA that would benefit from the stable levels of acetyl-CoA and help normalizing metabolites for any variation in cell mass, extraction or instrumental sensitivity, a major concern in metabolomics. HMG-CoA accumulation and the reduction of FPP levels would also provide a "finger print" for HMGR inhibition, and the ratio of HMG-CoA to FPP would also help normalizing the variation and provide a sensitive marker for HMGR activity.

CDP-ethanolamine metabolite is an interesting metabolite marker that is readily detectable and involved only in the glycerolipids pathway. The current study showed that this polar metabolite can act as a simple probe for perturbation in lipogenesis and lipolysis.

CONCLUSION

Metabolomic profiling revealed alterations in numerous biochemical pathways, which provide insight into the response of β- cells to a simulated "starvation" condition. Stable isotope labeled glucose provided more detailed information regarding metabolic flux in pathways of interest. We highlighted metabolomic markers that act as a metabolic fingerprint of AMPK activation and confirm immunoassay measurements. U- ^{13}C-glucose treatment revealed a decrease in glucose flux in the purine and pyrimidine pathway, suggesting an inhibition in PRPP synthase and/or PRPP amidotransferase enzyme by ZMP. Using labeled ethanolamine, we showed that AICAR may inhibit EPT via an AMPK dependent process. We also showed the fine equilibrium in lipogenesis and lipolysis that can be probed by CDP-ethanolamine levels. Using U- ^{13}C glucose and the ratio of labeled/unlabeled DAG we showed a decrease in glucose flux in the glycerolipid synthesis pathway suggesting an inhibition of GPAT enzyme. Undirected metabolomics showed a decrease in ceramides that might help to explain the protective role of AMPK in decreasing fatty acid induced toxicity in β- cells.

REFERENCES

1. Lorenz, M.A., El Azzouny, M.A., Kennedy, R.T., and Burant, C.F. (2013) Metabolome Response to Glucose in the beta-Cell Line INS-1 832/13. *J.Biol.Chem.* **288,** 10923-10935

2. Hardie, D.G. (2011) AMP-activated protein kinase: a cellular energy sensor with a key role in metabolic disorders and in cancer. *Biochem.Soc.Trans.* **39,** 1-13

3. Salt, I.P., Johnson, G., Ashcroft, S.J., and Hardie, D.G. (1998) AMP-activated protein kinase is activated by low glucose in cell lines derived from pancreatic beta cells, and may regulate insulin release. *Biochem.J.* **335 (Pt 3),** 533-539

4. Bosselaar, M., Smits, P., van Loon, L.J., and Tack, C.J. (2011) Intravenous AICAR during hyperinsulinemia induces systemic hemodynamic changes but has no local metabolic effect. *J.Clin.Pharmacol.* **51,** 1449-1458

5. Boon, H., Bosselaar, M., Praet, S.F., Blaak, E.E., Saris, W.H., Wagenmakers, A.J., McGee, S.L., Tack, C.J., Smits, P., Hargreaves, M., and van Loon, L.J. (2008) Intravenous AICAR administration reduces hepatic glucose output and inhibits whole body lipolysis in type 2 diabetic patients. *Diabetologia.* **51,** 1893-1900

6. Hardie, D.G., Ross, F.A., and Hawley, S.A. (2012) AMP-activated protein kinase: a target for drugs both ancient and modern. *Chem.Biol.* **19,** 1222-1236

7. Suzuki, T., Bridges, D., Nakada, D., Skiniotis, G., Morrison, S., Lin, J., Saltiel, A., and Inoki, K. (2013) Inhibition of AMPK Catabolic Action by GSK3. *Mol.Cell.* **50,** 407-419

8. Fu, A., Eberhard, C.E., and Screaton, R.A. (2013) Role of AMPK in pancreatic beta cell function. *Mol.Cell.Endocrinol.* **366,** 127-134

9. Eto, K., Yamashita, T., Matsui, J., Terauchi, Y., Noda, M., and Kadowaki, T. (2002) Genetic manipulations of fatty acid metabolism in beta-cells are associated with dysregulated insulin secretion. *Diabetes.* **51 Suppl 3,** S414-20

10. El-Assaad, W., Buteau, J., Peyot, M.L., Nolan, C., Roduit, R., Hardy, S., Joly, E., Dbaibo, G., Rosenberg, L., and Prentki, M. (2003) Saturated fatty acids synergize with elevated glucose to cause pancreatic beta-cell death. *Endocrinology.* **144,** 4154-4163

11. Gleason, C.E., Lu, D., Witters, L.A., Newgard, C.B., and Birnbaum, M.J. (2007) The role of AMPK and mTOR in nutrient sensing in pancreatic beta-cells. *J.Biol.Chem.* **282,** 10341-10351

12. Jacobs, R.L., Lingrell, S., Dyck, J.R., and Vance, D.E. (2007) Inhibition of hepatic phosphatidylcholine synthesis by 5-aminoimidazole-4-carboxamide-1-beta-4-ribofuranoside is independent of AMP-activated protein kinase activation. *J.Biol.Chem.* **282,** 4516-4523

13. Santidrian, A.F., Gonzalez-Girones, D.M., Iglesias-Serret, D., Coll-Mulet, L., Cosialls, A.M., de Frias, M., Campas, C., Gonzalez-Barca, E., Alonso, E., Labi, V., Viollet, B., Benito, A., Pons, G., Villunger, A., and Gil, J. (2010) AICAR induces apoptosis independently of AMPK and p53 through up-regulation of the BH3-only proteins BIM and NOXA in chronic lymphocytic leukemia cells. *Blood.* **116,** 3023-3032

14. Lanner, J.T., Georgiou, D.K., Dagnino-Acosta, A., Ainbinder, A., Cheng, Q., Joshi, A.D., Chen, Z., Yarotskyy, V., Oakes, J.M., Lee, C.S., Monroe, T.O., Santillan, A., Dong, K., Goodyear, L., Ismailov, I.I., Rodney, G.G., Dirksen, R.T.,

and Hamilton, S.L. (2012) AICAR prevents heat-induced sudden death in RyR1 mutant mice independent of AMPK activation. *Nat.Med.* **18,** 244-251

15. Martinez-Martin, N., Blas-Garcia, A., Morales, J.M., Marti-Cabrera, M., Monleon, D., and Apostolova, N. (2012) Metabolomics of the effect of AMPK activation by AICAR on human umbilical vein endothelial cells. *Int.J.Mol.Med.* **29,** 88-94

16. Houweling, M., Klein, W., and Geelen, M.J. (2002) Regulation of phosphatidylcholine and phosphatidylethanolamine synthesis in rat hepatocytes by 5-aminoimidazole-4-carboxamide ribonucleoside (AICAR). *Biochem.J.* **362,** 97-104

17. Paglia, G., Hrafnsdottir, S., Magnusdottir, M., Fleming, R.M., Thorlacius, S., Palsson, B.O., and Thiele, I. (2012) Monitoring metabolites consumption and secretion in cultured cells using ultra-performance liquid chromatography quadrupole-time of flight mass spectrometry (UPLC-Q-ToF-MS). *Anal.Bioanal Chem.* **402,** 1183-1198

18. Hohmeier, H.E., Mulder, H., Chen, G., Henkel-Rieger, R., Prentki, M., and Newgard, C.B. (2000) Isolation of INS-1-derived cell lines with robust ATP-sensitive K+ channel-dependent and -independent glucose-stimulated insulin secretion. *Diabetes.* **49,** 424-430

19. Sato, Y., Nakamura, T., Aoshima, K., and Oda, Y. (2010) Quantitative and wide-ranging profiling of phospholipids in human plasma by two-dimensional liquid chromatography/mass spectrometry. *Anal.Chem.* **82,** 9858-9864

20. Tautenhahn, R., Patti, G.J., Rinehart, D., and Siuzdak, G. (2012) XCMS Online: A Web-Based Platform to Process Untargeted Metabolomic Data. *Anal.Chem.* **84,** 5035-5039

21. Habegger, K.M., Hoffman, N.J., Ridenour, C.M., Brozinick, J.T., and Elmendorf, J.S. (2012) AMPK enhances insulin-stimulated GLUT4 regulation via lowering membrane cholesterol. *Endocrinology.* **153,** 2130-2141

22. Li, D., Wang, D., Wang, Y., Ling, W., Feng, X., and Xia, M. (2010) Adenosine monophosphate-activated protein kinase induces cholesterol efflux from macrophage-derived foam cells and alleviates atherosclerosis in apolipoprotein E-deficient mice. *J.Biol.Chem.* **285,** 33499-33509

23. Kanehisa, M., and Goto, S. (2000) KEGG: kyoto encyclopedia of genes and genomes. *Nucleic Acids Res.* **28,** 27-30

24. Kanehisa, M., Goto, S., Sato, Y., Furumichi, M., and Tanabe, M. (2012) KEGG for integration and interpretation of large-scale molecular data sets. *Nucleic Acids Res.* **40,** D109-14

25. Bleijerveld, O.B., Klein, W., Vaandrager, A.B., Helms, J.B., and Houweling, M. (2004) Control of the CDPethanolamine pathway in mammalian cells: effect of CTP:phosphoethanolamine cytidylyltransferase overexpression and the amount of intracellular diacylglycerol. *Biochem.J.* **379,** 711-719

26. Smith, R.J., Sam, L.M., Justen, J.M., Bundy, G.L., Bala, G.A., and Bleasdale, J.E. (1990) Receptor-coupled signal transduction in human polymorphonuclear neutrophils: effects of a novel inhibitor of phospholipase C-dependent processes on cell responsiveness. *J.Pharmacol.Exp.Ther.* **253,** 688-697

27. Scott, S.A., Selvy, P.E., Buck, J.R., Cho, H.P., Criswell, T.L., Thomas, A.L., Armstrong, M.D., Arteaga, C.L., Lindsley, C.W., and Brown, H.A. (2009) Design of isoform-selective phospholipase D inhibitors that modulate cancer cell invasiveness. *Nat.Chem.Biol.* **5,** 108-117

28. Prentki, M., Matschinsky, F., and Madiraju, S.R. . Metabolic Signaling in Fuel-Induced Insulin Secretion. *Cell Metabolism.*

29. Fahien, L.A., and MacDonald, M.J. (2002) The succinate mechanism of insulin release. *Diabetes.* **51,** 2669-2676

30. Straub, S.G., and Sharp, G.W. (2002) Glucose-stimulated signaling pathways in biphasic insulin secretion. *Diabetes Metab.Res.Rev.* **18,** 451-463

31. Muoio, D.M., Seefeld, K., Witters, L.A., and Coleman, R.A. (1999) AMP-activated kinase reciprocally regulates triacylglycerol synthesis and fatty acid oxidation in liver and muscle: evidence that sn-glycerol-3-phosphate acyltransferase is a novel target. *Biochem.J.* **338 (Pt 3),** 783-791

32. Bardeleben, C., Sharma, S., Reeve, J.R.,Jr, Bassilian, S., Frost, P.J., Hoang, B., Shi, Y., and Lichtenstein, A. (2013) Metabolomics identifies pyrimidine starvation as the mechanism of 5-aminoimidazole-4-carboxamide-1-beta-riboside (AICAr) induced apoptosis in multiple myeloma cells. *Mol.Cancer.Ther.*

33. Jitrapakdee, S., Wutthisathapornchai, A., Wallace, J.C., and MacDonald, M.J. (2010) Regulation of insulin secretion: role of mitochondrial signalling. *Diabetologia.* **53,** 1019-1032

34. Chen, S., Tomchick, D.R., Wolle, D., Hu, P., Smith, J.L., Switzer, R.L., and Zalkin, H. (1997) Mechanism of the synergistic end-product regulation of Bacillus subtilis glutamine phosphoribosylpyrophosphate amidotransferase by nucleotides. *Biochemistry.* **36,** 10718-10726

35. Champe, P.C., Harvey, R.A., and Ferrier, D.R. (2008) *Lippincott's illustrated reviews : biochemistry,* , Wolters Kluwer/Lippincott Williams & Wilkins, Philadelphia

36. Boslem, E., Meikle, P.J., and Biden, T.J. (2012) Roles of ceramide and sphingolipids in pancreatic beta-cell function and dysfunction. *Islets.* **4,** 177-187

37. Erickson, K.A., Smith, M.E., Anthonymuthu, T.S., Evanson, M.J., Brassfield, E.S., Hodson, A.E., Bressler, M.A., Tucker, B.J., Thatcher, M.O., Prince, J.T., Hancock, C.R., and Bikman, B.T. (2012) AICAR inhibits ceramide biosynthesis in skeletal muscle. *Diabetol.Metab.Syndr.* **4,** 45

SUPPLEMENTARY INFORMATION

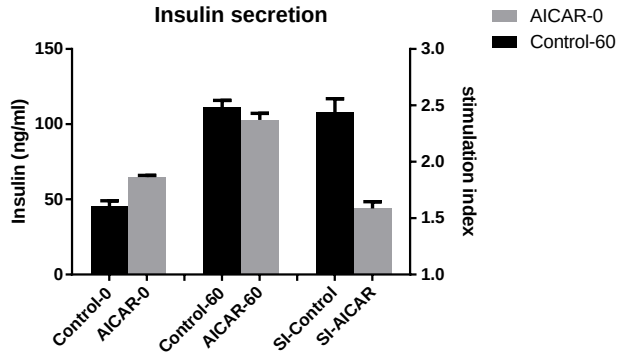

Figure S1: insulin secretion levels in INS-1 (832/3) after AICAR incubation.

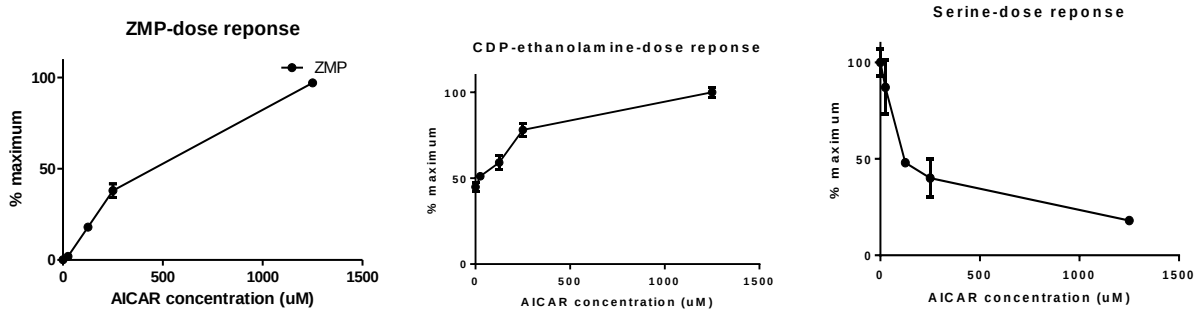

Figure S2: dose response curve: levels of ZMP, CDP-ethanolamine and serine after increasing dose of AICAR.

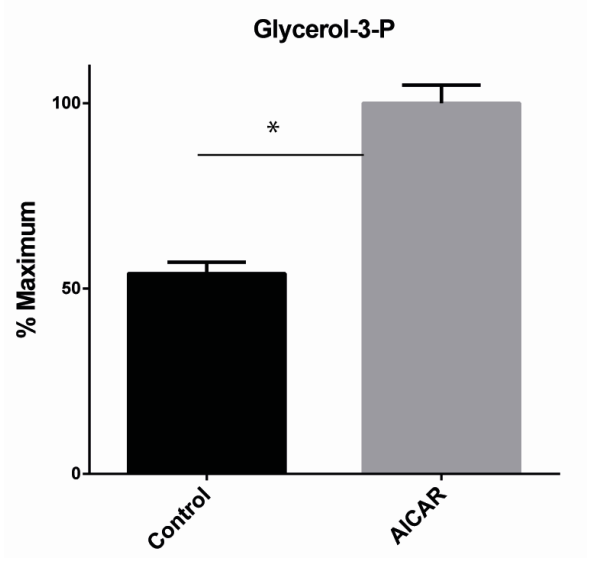

Figure S3: levels of G3P after incubation of INS-1 cells with 50 uM Palmitic acid, 2 mM glucose and ethanolamine +/- 250 uM AICAR for 1 hour.

Chapter 6. SUMMARY AND FUTURE PLANS

SUMMARY

We developed and optimized a method for non polar metabolite extraction and analysis using LC-MS. Different stationary phases were investigated including HILIC and reverse phase. As expected, HILIC separated lipids into classes based on its head group, while reverse phase separated lipids based on their chain length. HILIC provided superior separation for some low abundant lipid classes such as phosphatidyl serine, while reverse phase separation provided better separation for the rest of lipid classes. Different reverse phase stationary phases with various chain lengths were evaluated, such as C8, C18 and C30. The compromise chain length of C18 was more suitable for global lipid separation than the C8 or C30. We evaluated the impact of temperature and mobile phase pH on lipids separation and detection. Different extraction solvents were screened to evaluate its efficiency for lipid extraction. The final method for non polar metabolites analysis was combined with a HILIC based method for polar metabolites analysis, providing an analytical platform for global metabolites analysis. Using different metabolic tracers, this analytical platform enabled flux monitoring in different metabolic pathways such as glycerolipids pathway and central carbon metabolism.

We were able to successfully apply this developed analytical platform for several biological questions, with main focus on beta cell and its ability to secrete insulin in response to different stimuli. The first question was to understand metabolic changes during glucose stimulated insulin secretion. Using $U^{13}C$ glucose we were able to probe metabolic changes that took place in the first 10 minutes of insulin secretion. We showed that U-^{13}C glucose induced an increase in several metabolites, such as those involved in glycolysis and TCA cycle. This increase in metabolite levels was mainly derived from newly added glucose. We showed that malate was exception for this observation, where the glucose induced increase was mainly derived from aspartate, presumably through the aspartate malate shuttle. By blocking the aspartate-malate shuttle; we reduced this glucose induced increase in malate and confirmed the importance of this shuttle in insulin secretion. Using $U^{13}C$ glucose, we monitored glucose flux in the glycerolipids pathway and explained the rapid decrease in long chain coAs upon glucose

stimulation. Those novel findings are important to understand how glucose regulate insulin secretion and what are metabolic pathways involved in glucose stimulated insulin secretion.

The second biological question was to understand why fatty acids can potentiate glucose stimulated insulin secretion. This is representative of the hyperinsulinemia condition, which precedes the development of type 2 diabetes. We showed that fatty acids increase glucose oxidation, while being minimally oxidized by beta cell. Most fatty acids were esterified with glycerol-3-phosphate, derived from glucose and forming several glycerolipids signals that are known to facilitate insulin exocytosis. The increased glucose flux into glycerolipids pathway and the increased glucose oxidation are novel findings that were not reported before that would help understanding this potentiation mechanism. We also applied undirected metabolomics analysis and we found novel lipid signals that increased with fatty acid treatment such as palmitoyl glycine and palmitoyl taurine. The role of those acylamides is yet to be investigated.

Although the potentiation of fatty acid for insulin secretion appeared to be mainly mediated by the metabolism of fatty acid, the effect of free fatty acid receptor was reported to contribute to this potentiation mechanism. We were able to block and knockdown GPR40 receptor and study metabolic changes associated with the inhibition of this receptor. Interestingly metabolic changes induced by fatty acid were partially reversed after GPR40 inhibition. Inhibition of GPR40 led to the divergence of fatty acid away from esterification and towards oxidation in the mitochondria. These data suggest for the first time a role of GPR40 in glucose and fatty acid metabolism. This data would also justify the current development of GPR40 agonist drugs towards the treatment of type 2 diabetes.

We further investigated the effect of AMPK activation on beta cells and GSIS. We used a pharmacological agent (AICAR) which is known to activate AMPK. AMPK is metabolic master switch that activated by AMP and is known to regulate many metabolic pathways. AICAR was developed as an AMP analog, capable of activating AMPK and was suggested to be used in the treatment of type 2 diabetes. We showed that AICAR reduced insulin secretion stimulatory index, this was parallel with a reduction in glucose flux in several metabolic pathways that are

known to contribute to the GSIS response. These attenuated pathways include the glycerolipids and mevalonate synthesis pathway. We showed also the danger of using AICAR as a purine analog for AMPK activation, because this would lead to the inhibition of the purine and pyrimidine synthesis pathway, which might lead to cell apoptosis on the long term. We also showed that AICAR decreased ceramides levels, which are known signals for beta cell apoptosis. Those novel findings would further augment importance of glycerolipids and mevalonate pathway in insulin secretion and would rise a concern on the usage of AICAR clinically.

FUTURE DIRECTIONS

Glucolipotoxicity

Acute exposure of beta cells to fatty acid will potentiate GSIS as described in chapter 4 while the chronic exposure to fatty acids and glucose will lead to beta cell toxicity. This toxicity is named "glucolipotoxicity" because it is induced by the synergistic effect of fatty acids and glucose, leading to impairment of insulin secretion and expression as well as beta cell apoptosis (1, 2). The decline in beta cell function plays a central role in the development of type-2 diabetes. To understand and find a treatment for type-2 diabetes, the mechanism of the glucolipotoxicity needs to be well understood. Several intermediates have been suggested to play a role in the glucolipotoxicity process. Lipids in the glycerolipids pathway, ceramides and cholesterol intermediates have been suggested to be candidates' signals for inducing cell toxicity (2-4). Free radical generation was also suggested as a part of the glucolipotoxicity effect on beta cells (3).

Recently a glucolipotoxicity study using INS-1 cells showed changes in the expression of many genes, increase in lipid synthesis as well as changes in TCA cycle intermediates (5). This research interestingly showed that glucose induced increase in TCA cycle intermediates is attenuated in the lipotoxic model (5). These results were similar to the results obtained in our lab, were a lipotoxic model of INS-1 cells showed lower glucose flux in TCA cycle (unpublished data). Our lab data showed several metabolomics changes induced by glucolipotoxicity, among these changes is the reduction in aspartate levels. Following glucose stimulation, the increase

in malate induced by aspartate through the asp-mal shuttle was significantly attenuated, suggesting a defect in this shuttle.

Aspartate plays an important role in insulin secretion (6) since it acts as an anaplerotic substrate for TCA cycle and provides enough malate for TCA cycle through the asp-mal shuttle. The defect in asp-mal shuttle in lipotoxic models could be due to the interaction of fatty acid with proteins in this shuttle. An interesting hypothesis is that fatty acids modify proteins involved in GSIS thus affecting their function. Fatty acids like palmitic acid can covalently attach to proteins through a thio-ester bond in a process called palmitoylation. It was recently shown that many proteins including those involved in the asp-mal shuttle are palmitoylated (7, 8) and this palmitoylation can be inhibited by 2-bromopalmitate (9). Dynamic palmitoylation is reversed by enzymes named lysophospholipase 1 and 2 (LYPLA1 and LYPLA2), which can depamitoylate proteins (10, 11) . The extensive palmitoylation of proteins suggested its important role in obesity related diseases (8) and it was recently shown that inhibition of palmitoylation using bromopalmitate reduced palmitate induced toxicity in beta cells (12).

LYPLA inhibitors were recently developed to treat some forms of cancers (11) and at the same time prevent the depalmitoylation step. As a preliminary data, we tested on some of these LYPLA inhibitors on INS-1 cells and interestingly the changes detected were mainly in the malate and aspartate levels (figure 1). Therefore a future work would suggest testing the hypothesis that palmitoylation of asp-malate shuttle is involved in the defect of GSIS in lipotoxicity model. Future work should also involve the inhibition of palmitoylation by bromopalmitate (figure 1)

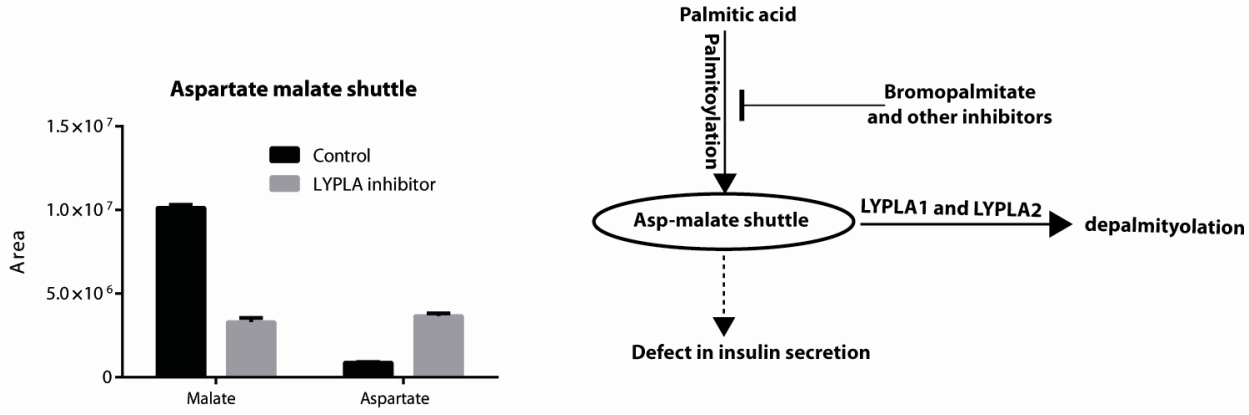

Figure 6-1: showing the effect of palmitoylation inhibitors on metabolites levels in INS-1 cells (left) and a proposed hypothesis for the effect of fatty acid on aspartate malate shuttle (right).

We have shown in chapter 4, that fatty acid increase the TCA cycle activity and glucose oxidation. Thus, the decrease in asp-shuttle activity could also arise from the depletion of aspartate, which is being consumed to feed the "very active" TCA cycle. Thus a supply of aspartate could restore the beta cell secretory function and its response to glucose. Interestingly, increasing glutamate conversion into α-Ketoglutarate by BCH decreased cell death in glucolipotoxic cell model (13). This would confirm our suggestion for the importance of TCA cycle in mediating the effect of glucolipotoxity.

Other secretagogues

As described in chapter 1, different secretagogues like leucine, α-ketoisocaproate (KIC) and monomethyl succinate (MMS) can stimulate insulin secretion. Addition of KIC alone will not stimulate insulin secretion but the addition of KIC with MMS will stimulate insulin secretion in INS-1 cells. Some metabolic couplers are being generated from these secretagogues that stimulate insulin secretion. Although the mechanisms for different secretagogues were described in chapter 1, there are still many unanswered question. Among these questions are: What are the metabolic couplers or pathways that are activated by MMS addition to KIC and leads to insulin secretion? Why is leucine less effective than glucose in stimulating insulin secretion? What pathways are being activated by glucose but not by leucine?

Preliminary data were obtained comparing U-^{13}C glucose vs U-^{13}C KIC or U-^{13}C KIC+ MMS. U-^{13}C glucose increased the unlabeled malate (coming from aspartate) (figure 2) as we have shown before in chapter 3. KIC did not induce this increase; however the addition of MMS increased the unlabeled Malate. The increase in unlabeled Malate could be coming from the MMS itself, by supplying succinate to the TCA cycle, since aspartate levels did not change (figure 3).

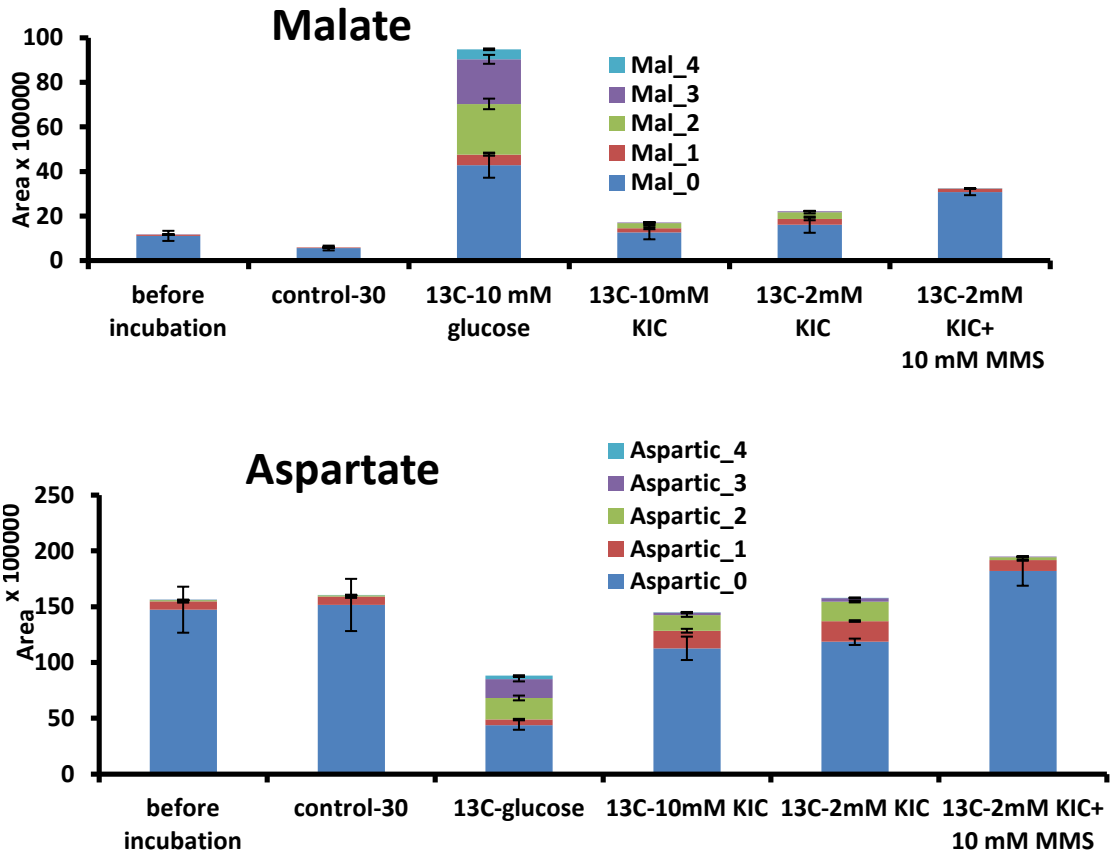

Figure 6-2: Isotope distribution of aspartate and malate after stimulation with U^{13}C-labeled glucose or KIC.

This would suggest that although KIC could not stimulate the asp-mal shuttle, addition of MMS acted as anaplerotic substrate rather than aspartate. However KIC+MMS were not as efficient as glucose in increasing malate or reducing aspartate.

Away from the asp-mal shuttle, glucose was also able to increase flux in the mevalonate pathway, which reduced the level of HMG-CoA significantly (figure 3 and chapter 3-5). This mevalonate

pathway was suggested to play a role in insulin secretion (14). Interestingly KIC alone did not increase the flux in this pathway, while the addition of MMS increased the flux (figure 3), suggesting a novel role for these combination of nutrients.

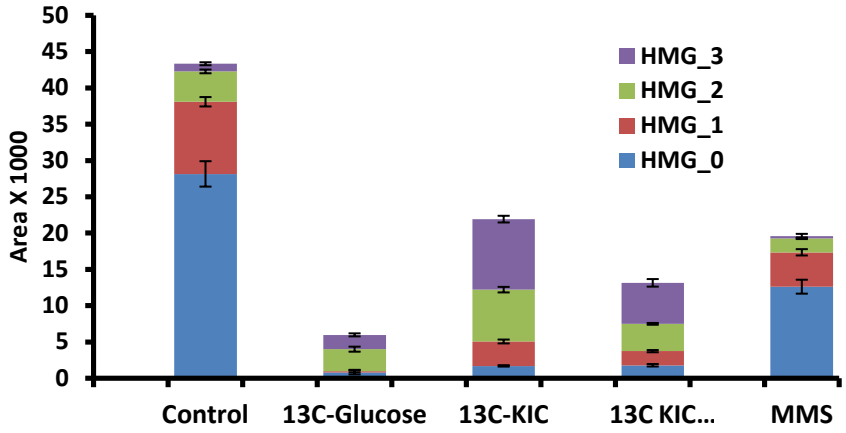

Figure 6-3: HMG-CoA isotope distribution after INS-1 stimulation with different nutrients.

Finally, these preliminary data would provide a novel insight on the mechanism of these secretagogues. Further follow up experiments are required to investigate the importance of the mevalonic pathway in mediating the insulin secretion response for these secretagogues combination.

Human beta cell lines

Human beta cell lines were successfully generated in different labs (15, 16). This development will open the doors towards the treatment of insulin dependent diabetic patients. The novel human beta cell lines were shown to be responsive to glucose and other secretagogues (16). Glucotoxicity (17) and lipotoxicity (18) were studied on this novel cell line and cells showed impairment of GSIS similar to what was shown before in rodent cell lines and islets. Changes in gene expression and increase in cell apoptosis was shown in those cells when exposed to high glucose or fatty acid (17, 18).

So far, there is no metabolomics study that has studied these cell lines. It is important to compare metabolites changes between human and rodents' cell lines during insulin secretion, since this comparison will reveal any species differences in the regulation of insulin secretion.

This comparison is also important during glucolipotoxicity stages to discover new therapies that can restore human beta cell function.

Islets from human and rodents

Islets from human or from rodents represent a more physiological model for studying metabolic signaling during insulin secretion. Drawbacks of using islets are mentioned in chapter 1. A recent published metabolomics study performed on rat islets (19) using 240 islets for each time points. They were able to identify 31 metabolites changing with glucose stimulation, while in INS-1 cells we have monitored changes in ~70 metabolites during GSIS, without including glycerolipids species. The low number of identified islets metabolites in the previous study can be attributed to sample preparation and analysis. For sample preparation, extraction solvent for islets can be optimized to avoid sample dilution and increase the metabolites signal to noise ratio. For analysis, LC-MS can be used rather than the GC-MS used in this published study since the latter suffer from several drawbacks described in chapter 1. LC-MS can be further improved by using UPLC and nano ESI for the small and precious islets sample as described in the next section and in chapter 1.

UPLC and nano electrospray

As described in chapter 1, electrospray ionization is the most widely used ionization technique using in mass spectrometer. ESI provides the widest coverage of metabolome compared to other ionization techniques. However, one of the major drawbacks of ESI that low abundant metabolites are prone to ionization suppression from more abundant metabolites. The ideal scenario to avoid the ionization suppression is to have 1 ion per droplet sprayed into the mass spec. Nano flow LC coupled to nano spray ESI try to achieve flow rates of ~ 200 nl/minute to gain this improvement in sensitivity. UPLC provide a complementary increase in sensitivity by achieving better separation and narrower peaks. As described in chapter 1, narrower peaks will increase signal to noise ratio and allow the detection of many hidden metabolites. It is worth mentioning that the NH2 column is ideal for polar metabolites analysis as well as some lipid classes, but it suffers from column bleeding in high pH and hence very short column life compared to a reverse phase column. Hence improvement of the stationary phase stability represents a general need for metabolomics researchers.

REFERENCES

1. Prentki, M., and Madiraju, S.R. (2011) Glycerolipid/free fatty acid cycle and islet beta-cell function in health, obesity and diabetes. *Mol.Cell.Endocrinol.*

2. Poitout, V., Amyot, J., Semache, M., Zarrouki, B., Hagman, D., and Fontes, G. (2010) Glucolipotoxicity of the pancreatic beta cell. *Biochim.Biophys.Acta.* **1801,** 289-298

3. El-Assaad, W., Joly, E., Barbeau, A., Sladek, R., Buteau, J., Maestre, I., Pepin, E., Zhao, S., Iglesias, J., Roche, E., and Prentki, M. (2010) Glucolipotoxicity alters lipid partitioning and causes mitochondrial dysfunction, cholesterol, and ceramide deposition and reactive oxygen species production in INS832/13 ss-cells. *Endocrinology.* **151,** 3061-3073

4. El-Assaad, W., Buteau, J., Peyot, M.L., Nolan, C., Roduit, R., Hardy, S., Joly, E., Dbaibo, G., Rosenberg, L., and Prentki, M. (2003) Saturated fatty acids synergize with elevated glucose to cause pancreatic beta-cell death. *Endocrinology.* **144,** 4154-4163

5. Malmgren, S., Spegel, P., Danielsson, A.P., Nagorny, C.L., Andersson, L.E., Nitert, M.D., Ridderstrale, M., Mulder, H., and Ling, C. (2013) Coordinate changes in histone modifications, mRNA levels, and metabolite profiles in clonal INS-1 832/13 beta-cells accompany functional adaptations to lipotoxicity. *J.Biol.Chem.* **288,** 11973-11987

6. Lorenz, M.A., El-Azzouny, M.A., Kennedy, R.T., and Burant, C.F. (2013) Metabolome Response to Glucose in the β-cell line INS-1 832/13. *Journal of Biological Chemistry.*

7. Li, Y., Martin, B.R., Cravatt, B.F., and Hofmann, S.L. (2012) DHHC5 protein palmitoylates flotillin-2 and is rapidly degraded on induction of neuronal differentiation in cultured cells. *J.Biol.Chem.* **287,** 523-530

8. Kostiuk, M.A., Corvi, M.M., Keller, B.O., Plummer, G., Prescher, J.A., Hangauer, M.J., Bertozzi, C.R., Rajaiah, G., Falck, J.R., and Berthiaume, L.G. (2008) Identification of palmitoylated mitochondrial proteins using a bio-orthogonal azido-palmitate analogue. *FASEB J.* **22,** 721-732

9. Davda, D., El Azzouny, M.A., Tom, C.T., Hernandez, J.L., Majmudar, J.D., Kennedy, R.T., and Martin, B.R. (2013) Profiling targets of the irreversible palmitoylation inhibitor 2-bromopalmitate. *ACS Chem.Biol.* **8,** 1912-1917

10. Tom, C.T., and Martin, B.R. (2013) Fat chance! Getting a grip on a slippery modification. *ACS Chem.Biol.* **8,** 46-57

11. Adibekian, A., Martin, B.R., Speers, A.E., Brown, S.J., Spicer, T., Fernandez-Vega, V., Ferguson, J., Cravatt, B.F., Hodder, P., and Rosen, H. (2010) Optimization and characterization of a triazole urea dual inhibitor for lysophospholipase 1 (LYPLA1) and lysophospholipase 2 (LYPLA2)

12. Baldwin, A.C., Green, C.D., Olson, L.K., Moxley, M.A., and Corbett, J.A. (2012) A role for aberrant protein palmitoylation in FFA-induced ER stress and beta-cell death. *Am.J.Physiol.Endocrinol.Metab.* **302,** E1390-8

13. Choi, S.E., Lee, Y.J., Hwang, G.S., Chung, J.H., Lee, S.J., Lee, J.H., Han, S.J., Kim, H.J., Lee, K.W., Kim, Y., Jun, H.S., and Kang, Y. (2011) Supplement of TCA cycle intermediates protects against high glucose/palmitate-induced INS-1 beta cell death. *Arch.Biochem.Biophys.* **505,** 231-241

14. Alarcon, C., Wicksteed, B., Prentki, M., Corkey, B.E., and Rhodes, C.J. (2002) Succinate is a preferential metabolic stimulus-coupling signal for glucose-induced proinsulin biosynthesis translation. *Diabetes.* **51,** 2496-2504

15. Ravassard, P., Hazhouz, Y., Pechberty, S., Bricout-Neveu, E., Armanet, M., Czernichow, P., and Scharfmann, R. (2011) A genetically engineered human pancreatic beta cell line exhibiting glucose-inducible insulin secretion. *J.Clin.Invest.* **121,** 3589-3597

16. McCluskey, J.T., Hamid, M., Guo-Parke, H., McClenaghan, N.H., Gomis, R., and Flatt, P.R. (2011) Development and functional characterization of insulin-releasing human pancreatic beta cell lines produced by electrofusion. *J.Biol.Chem.* **286,** 21982-21992

17. Vasu, S., McClenaghan, N.H., McCluskey, J.T., and Flatt, P.R. (2013) Cellular responses of novel human pancreatic beta-cell line, 1.1B4 to hyperglycemia. *Islets.* **5,**

18. Vasu, S., McClenaghan, N.H., McCluskey, J.T., and Flatt, P.R. (2013) Effects of lipotoxicity on a novel insulin-secreting human pancreatic beta-cell line, 1.1B4. *Biol.Chem.* **394,** 909-918

19. Spegel, P., Sharoyko, V.V., Goehring, I., Danielsson, A.P., Malmgren, S., Nagorny, C.L., Andersson, L.E., Koeck, T., Sharp, G.W., Straub, S.G., Wollheim, C.B., and Mulder, H. (2013) Time-resolved metabolomics analysis of beta-cells implicates the pentose phosphate pathway in the control of insulin release. *Biochem.J.* **450,** 595-605

Appendix -Flux in metabolic pathways using labeled nutrients.

Metabolic tracers:

a) U-^{13}C Glucose:

Glucose can be used to monitor several pathways, including glycolysis, TCA cycle, pentose phosphate pathway, purine and pyrimidine pathways as well as glycerolipids synthesis pathway. Using ^{13}C glucose is very useful in beta cell studies, since glucose is the most powerful stimulant for insulin secretion and it allows the monitoring of different pathways involved in insulin secretion.

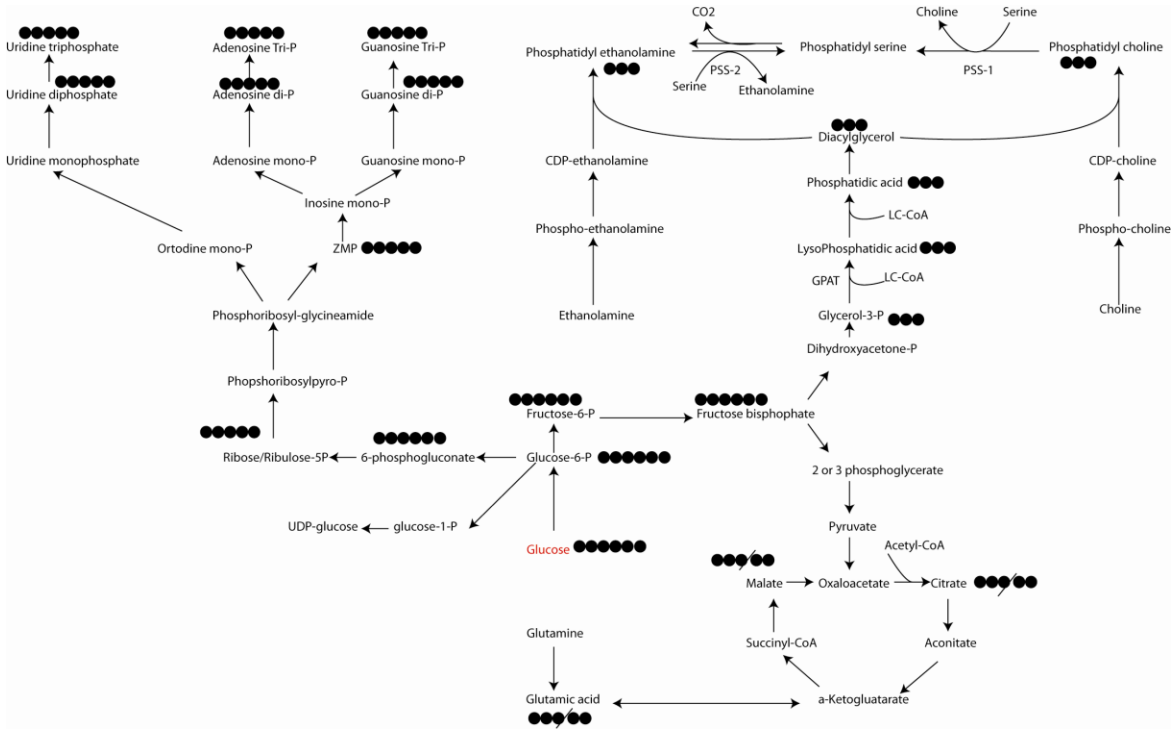

Figure A-1: Some of the metabolic pathways that can be probed using U-13C glucose.

Experimental conditions

- INS-1 cells were incubated at low glucose for several hours (~ 6 hours) before completely depriving them of glucose for 30 minutes. This treatment ensures the best uptake of the U-^{13}C glucose, without being diluted by any other unlabeled glucose.
- To avoid the utilization of nutrients other than glucose, experiments were performed in a salt solution (typically KRHB) instead of RPMI.

U^{13}C Glutamine

Glucose can probe several pathways as described in the previous section; however some nutrients, such as amino acids can be used to probe specific pathways. One of the widely used amino acids is glutamine which acts as an anaplerotic substrate and is widely used to probe flux in the TCA cycle (1) (figure 2).

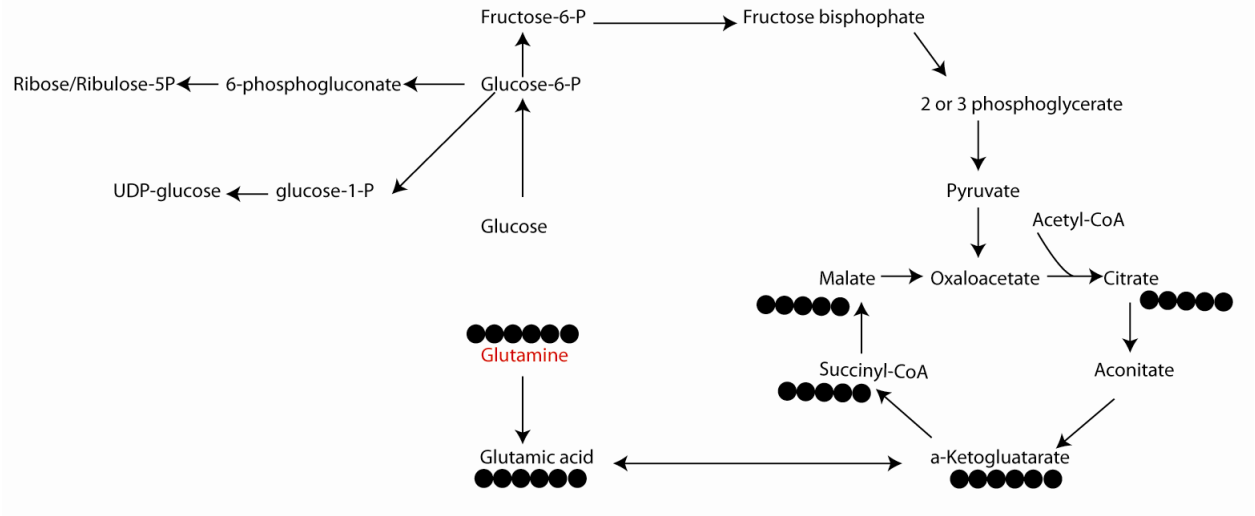

Figure A-2: metabolic pathways that can be probed using U-13C glutamic acid

Experimental conditions:

- INS-1 cells were starved from glutamine for 6 hours (at 3 mM glucose), before the addition of 2 mM labeled glutamine for 30 minutes in KRHB and no glucose. This treatment resulted in ~ 50% labeled glutamate, aspartate and malate. Addition of unlabeled glucose increased the uptake of labeled glutamic acid into the TCA cycle (figure 3).

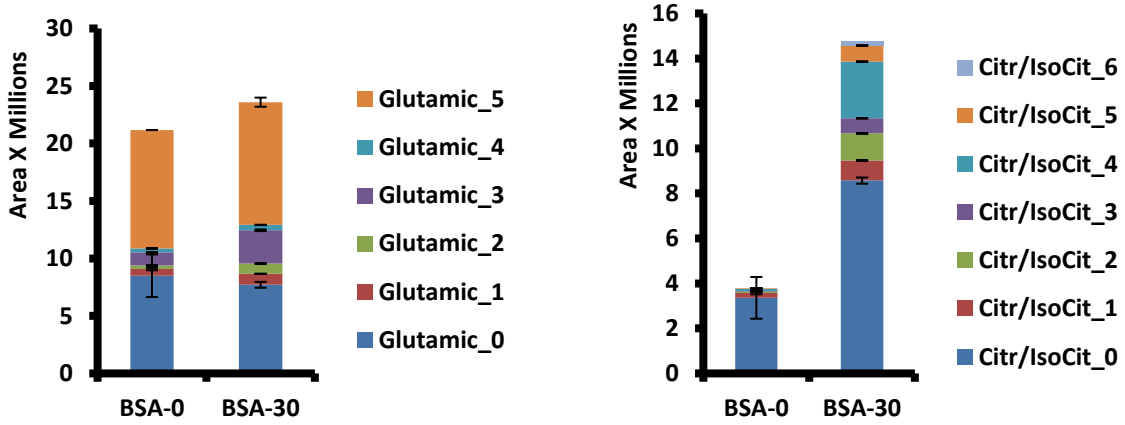

Figure A-3: glutamic and citrate labeling using U-13C glutamine.

Ethanolamine

Ethanolamine can be used to monitor flux in the Kennedy pathway of phosphatidylethanolamine synthesis (figure 4). Phosphoethanolamine and CDP-ethanolamine are polar metabolites that can be monitored using the HILIC method, while phosphatidylethanolamine can be monitored using a lipid separation method.

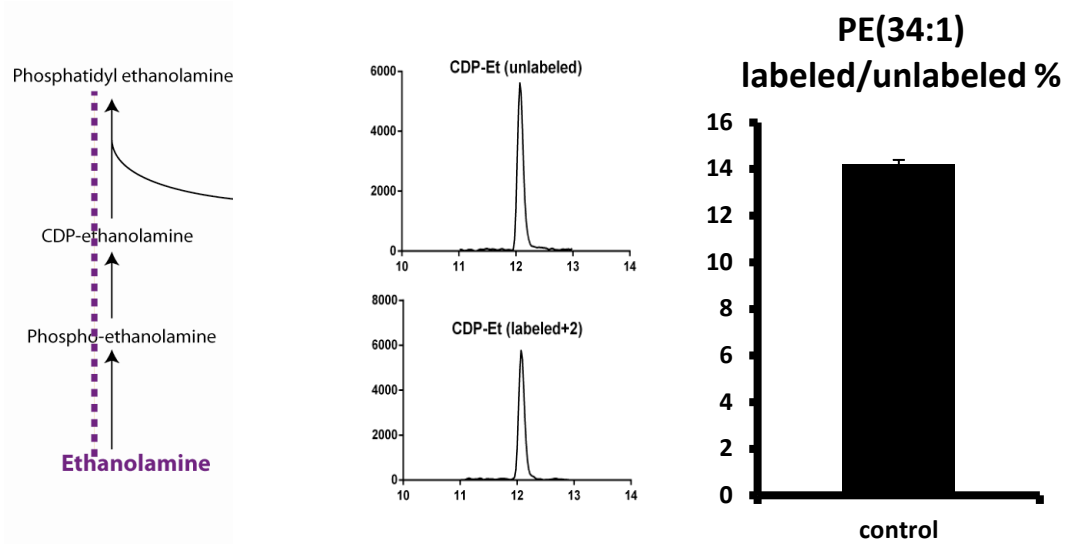

Figure A-4: metabolic pathways that can be probed using labeled ethanolamine. Left: Kennedy pathways for PE synthesis. Middle: chromatogram showing the intensity of labeled and unlabeled CDP-ethanolamine. Right: The ratio of labeled PE to unlabeled PE after 1 hour incubation with labeled ethanolamine.

<u>Experimental conditions:</u>

- The concentration of ethanolamine used in the experiment was 160 µM which is ~ 8 times the concentration originally used in advanced RPMI media (~ 20 µM). INS-1 cells could be incubated in RPMI or in KRHB during the experiment; however, glucose presence is crucial to allow for lipogenesis.
- One hour incubation with 160 µM ethanolamine achieved 50% labeling in CDP-Et (figure 4) and achieved 14 % labeling in PE (34:1) (figure 4)

***Note**: ethanolamine is an ion pairing agent that can change RPC column binding affinity; however the most dramatic effect will be seen in the mass spec in the positive mode, where a large peak of the ethanolamine will be seen in the background of subsequent runs. Washing the LC-MS system with IPA and acetonitrile is recommended to clean the system.*

Choline

Choline can be used to monitor flux in the Kennedy pathway of PC synthesis (figure 5). Phosphocholine and CDP-choline are polar metabolites that can be monitored using the HILIC method, while PC should be monitored using a lipid separation method. Phosphocholine and CDP-choline can be ionized in the negative mode by monitoring the M-H ion, but also by observing the acetate adduct formed due to the presence of the choline group.

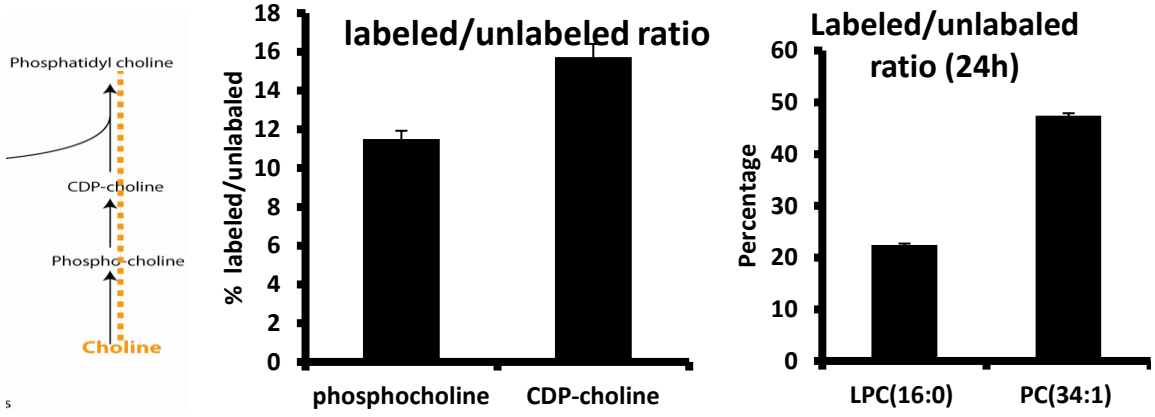

Figure A-5: metabolic pathways that can be probed using labeled choline. Left: Kennedy pathway for PC synthesis. Middle: the percentage labeling in polar fraction after 1 hour incubation with labeled choline. Right: labeling ratio of PC and LPC after 24 hour incubation in labeled choline in RPMI.

Experimental conditions:

- D_9-choline chloride was used in the range of 200 µM - 1000 µM which is approximately 10- 50 times the concentration used in normal RPMI media (20 µM). INS-1 cells could be incubated in RPMI or in KRHB during the experiment; however, glucose presence is crucial to allow for lipogenesis.
- One hour of incubation with 200 µM choline chloride resulted in approximately 12 and 15 % of labeling in phosphocholine and CDP-choline. This low percentage is because of the endogenous large pool of those metabolites. Incubation of cells in RPMI supplied with 1000 µM D_9-choline for 24 hours achieved approximately 50 % labeling in major PC forms like PC (34:1) and 20% in LPC (16:0).

Note: *Deuterated compounds are unstable compared to ^{13}-C carbon labeled compounds, they can exchange with the hydrogen present in the media, causing loss of labeling.*

Serine

Serine can be used to monitor flux into phosphatidyl serine. There are no polar intermediates except serine in this pathway. PS can only be generated indirectly in mammalian cells from PC or PE by PS synthase 1 or 2 (PSS-1 and PSS-2) respectively. Owing to the large pool of PC and PE, it is hard to anticipate which form of PS will be formed. This makes HILIC, which separates lipids based on their head group, an ideal option for PS measurements.

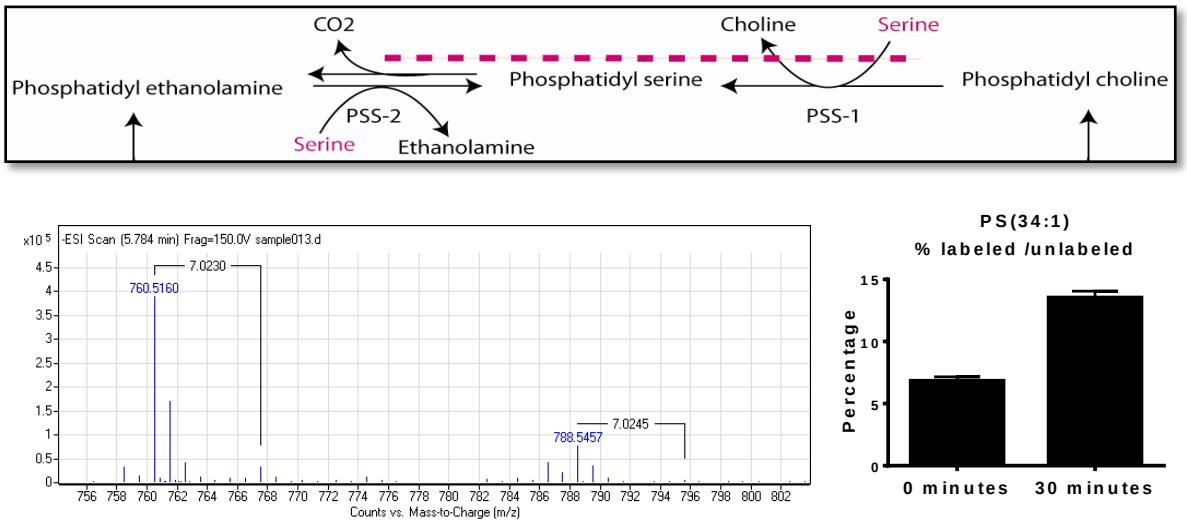

Figure A-6: metabolic pathways that can be monitored using serine. Upper: PS synthesis pathway from PE and PC. Lower left: mass spectrum showing the labeling in PS (34:1) and PS (36:1). Lower right: ratio of labeled to unlabeled PS after 1 hour incubation with labeled serine.

<u>Experimental conditions</u>

- The concentration of +7 serine (C_3, D_3, ^{15}N) serine used in the experiment was 1 mM which is 5 times the concentration originally used in RPMI (~ 200 µM). INS-1 Cells could be incubated in RPMI or KRHB during the experiment, however, KRHB was be preferred to avoid any dilution from unlabeled serine in the RPMI media.
- INS-1 cells were incubated in KRHB with the +7 serine and low glucose (2 mM) for 1 hour before stimulation with 10 mM glucose for 30 minutes. This treatment resulted in ~ 10 % labeling in PS (34:1) (figure 6). The most abundant forms seen in INS-1 cells were PS (34:1) and PS (36:1) (figure 6).

Fatty acids

Labeled fatty acids can be used to monitor flux into all phospholipid classes at short time points, except for PS, which needs extensive labeling in PE and PC first before it can be detected in PS. Lipid species formed are dependent on the fatty acid precursor added, for example, the addition of palmitic acid (16:0) will form the palmitoyl species of carnitine and LPA, while forming the dipalmitoyl species of PA, PE,PI,DAG,PC,PE. These forms will be in addition to the formation of oleic and palmitoyl combinations (18:1, 16:0) or (34:1).

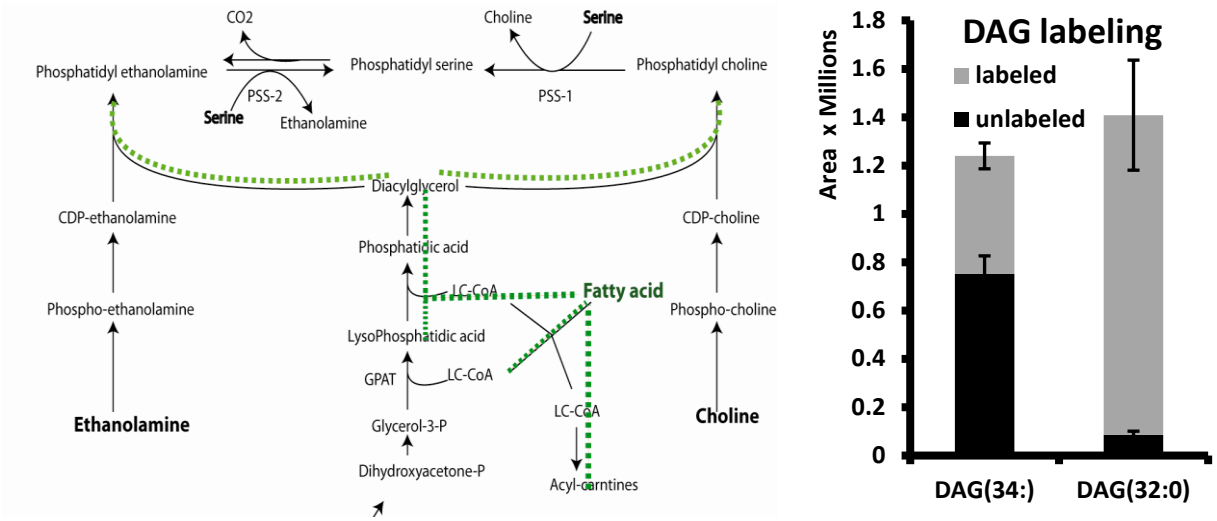

Figure A-7: Metabolic pathways of fatty acid. Left: diagram showing the pathway of fatty acid. Right: the levels of DAG (34:1) or DAG (32:0) after incubation with 100 µM +16 fatty acid with 10 mM glucose for 30 minutes.

<u>Experimental conditions:</u>

- The concentration of labeled fatty acid used ranged from 10 µM to 500 µM. The usage of U-^{13}C palmitate or U-^{13}C Oleate results in +16 or +18 mass shift for each fatty acid added in the lipid respectively. Glucose presence depends on the goal of experiment. Glucose will provide the glycerol back bone needed to synthesize glycerolipids; however this will consume long chain CoAs and reduces their intracellular levels. Fatty acid oxidation will be reduced in the presence of glucose, thus reducing the level of acyl-carnitines.
- Incubation of INS-1 cells with 100 µM of U-^{13}C palmitic acid with 10 mM glucose for 30 minutes resulted in 40% labeling in the abundant DAG (34:1) and 95 % labeling in the less abundant DAG (32:0) (figure 7).

Summary and conclusion

We have described the application of different metabolic tracers to probe different metabolic pathways. Metabolic tracers described here include glucose, glutamine, choline, ethanolamine, serine and fatty acids. The culture conditions and concentration used for those metabolic tracers were described, together with the expected results within a specific time frame. Depending on the goal of the experiment, these metabolic tracers can be used in the absence or presence of glucose. The applications of the previously mentioned metabolic tracers are summarized in figure 8.

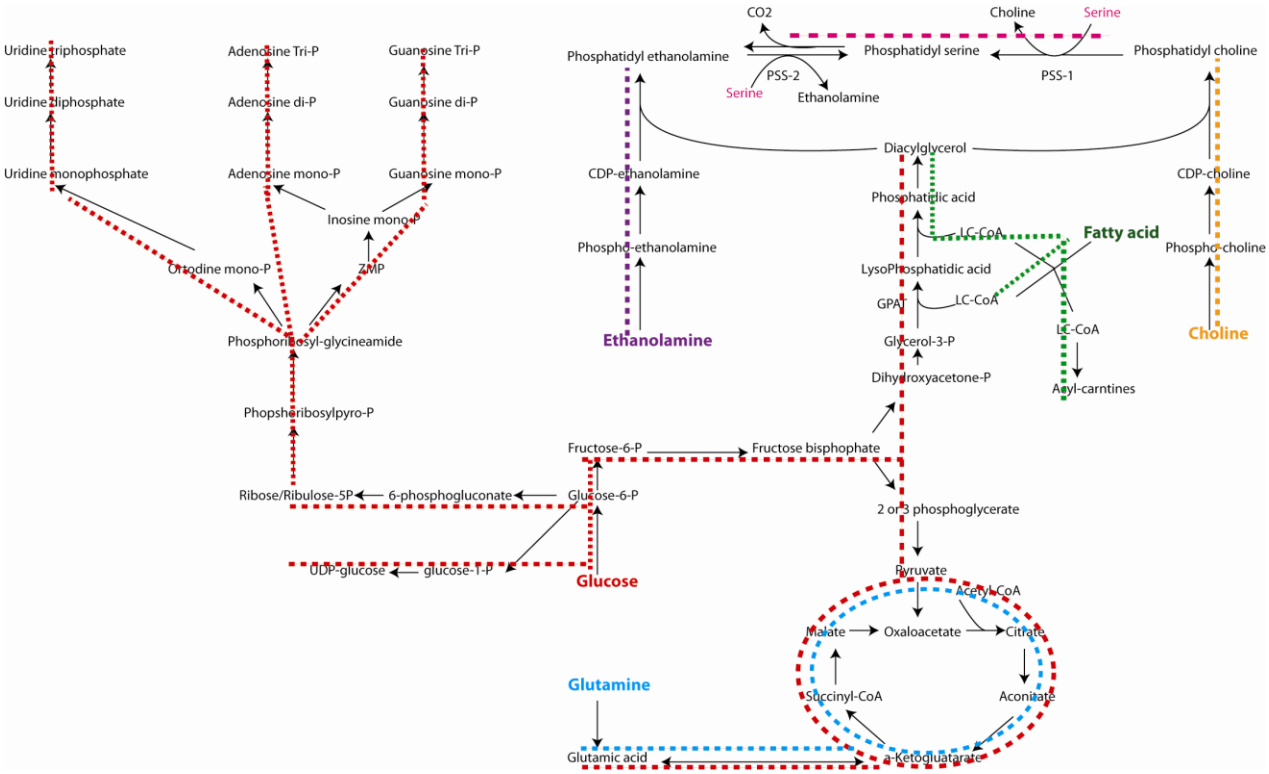

Figure A-8: General metabolic pathways and possible metabolic tracers.

References

1. Crown, S.B., and Antoniewicz, M.R. (2013) Parallel labeling experiments and metabolic flux analysis: Past, present and future methodologies. *Metab.Eng.* **16,** 21-32